Casting and Analysis of Squeeze Cast Aluminium Silicon Eutectic Alloy

Matthew Smillie

A thesis presented in partial fulfilment
of the requirements for the degree of
Doctor of Philosophy
in
Mechanical Engineering
at the
University of Canterbury,
Christchurch, New Zealand.

2006

Figure 1 Squeeze cast aluminium silicon eutectic alloy, differential interference contrast illumination at 50x magnification. A combination of small, hard crystals of primary silicon, partially modified aluminium silicon eutectic, and soft primary aluminium dendrites are shown by the contrast in polishing relief revealed using differential interference contrast illumination.

ABSTRACT

Squeeze casting is the practise of solidifying metals under mechanically applied pressure via a slow displacement of a die volume. It has been shown that squeeze casting enhances the mechanical properties of cast metals. Research into other high integrity casting processes has shown that using techniques that enhance melt quality can further increase the mechanical properties. Therefore a bottom-tapped, bottom-fed squeeze casting machine was designed and built around a pre-existing squeeze casting die designed for uniaxial pressure application. This was used to obtain quantitative metallurgical and microstructural information on the squeeze castings produced, including the effects of common micro-alloying additions of strontium modifier and titanium modifier on the microstructure and hardness of a commercial aluminium silicon eutectic alloy. These were examined using a Taguchi design of experiments approach. It was found that squeeze casting reduced porosity and secondary dendrite arm spacing and increased hardness, and reduced or eliminated increases in porosity and secondary dendrite arm spacing associated with micro-alloying addition. The size of possibly deleterious iron-rich precipitates was reduced, and the morphology of such precipitates changed to a possibly less deleterious form without further alloy additions of manganese. It was also found that melt control and handling is essential for consistent quality of castings in the production of small volume squeeze castings, such as the ones produced in this experimental work.

For my wife, Fleur.

ACKNOWLEDGEMENTS

The author would like to acknowledge the following:

Dr John Smaill and Dr Milo Kral: For their supervision, instruction and advice.

Julian Philips, Ken Brown, Paul Wells, Scott Amies, Bruce Sparks and Otto Bolt: For the fabrication of the many parts, and replacements thereof, of the experimental casting rig.

Kevin Stobbs, Mike Flaws and Hugh Mobbs: For their help in the Materials Laboratory, the foundry and the Microscope Laboratories.

CWF Hamilton & Company Limited: For the supply of commercial LM6 alloy and alloy additions used in this research.

New Zealand Aluminium Smelters Limited: For their financial support in the form of the New Zealand Aluminium Smelters Limited Research Scholarship in 1996 and 1997.

Andrew Lintott, Rodney Elliot, Janna van Hasselt, and especially Charlotte Overton: For their friendship and support.

CONTENTS

LIST OF FIGURES

LIST OF TABLES

NOMENCLATURE

γ	Surface tension.
μ	Distribution mean.
μm	Micrometre.
π	Pi.
σ	Standard deviation.
A_i	Distribution area.
g	Acceleration due to gravity, 9.81m/s^2
p	Distribution proportion.
p_f	Furnace pressure.
p_{fs}	Furnace system pressure.
P_i	Infiltration pressure.
P_p	Point count percentage.
$r_{1,2}$	Radii of curvature of infiltration front.
V_v	Volumetric percentage.
x	Distribution value.
AA	Aluminum Association.
AC	Alternating current.
AFS	American Foundrymen's Society.
API	American Petroleum Institute.
AS	Australian Standard.
ASM	American Society for Metals.
ASTM	American Society for Testing and Materials.
BS	British Standard.
°C	Degrees Celsius.

EBSD	Electron back-scatter diffraction.
EDS	Energy dispersive spectroscopy.
FEA	Finite element analysis.
DAS	Dendrite arm spacing.
DOF	Degree of freedom.
HRC	Rockwell hardness, C scale.
HV	Vickers hardness.
HV(0.1)	Vickers hardness, applied load 0.1kg.
ISO	International Organization for Standardization.
kg	Kilogram.
kN	Kilonewton.
kPa	Kilopascal.
kW	Kilowatt.
MMC	Metal matrix composite.
MPa	Megapascal.
NB	Nominal bore.
OA	Orthoganal array.
Pa	Pascal.
PDF	Probability distribution function.
PID	Proportional-integral-derivative.
ppi	Pores per inch.
SEM	Scanning electron microscope.
UNS	Unified Numbering System for Metals and Alloys.
V	Volts.

GLOSSARY

B

Billet A casting used as an intermediate stage in the production of alloy components, upon which subsequent machining, rolling or forging is performed.

Binary alloy An alloy consisting of only two metals, with negligible further alloy content.

Blistering Large scale porosity near the surface of a casting can form undesirable blisters on the surface, especially after subsequent heating.

Bottom filling The filling of the die from the bottom. This allows excess air to escape via the top of the die, reducing porosity. It also reduces turbulence during the filling of the die, thereby reducing oxide contamination.

Bottom tapping Obtaining the molten metal for the casting from near the bottom of the holding furnace. This avoids excess oxide contamination near the surface of the melt.

C

Castability A qualitative term describing the casting behaviour of a metal or alloy (can cover such factors as melting point, fluidity, reactivity and solidification range).

Chill zone The area at or near the casting surface with fine grain structure. This results from increased nucleation sites on the mold wall and the initial high heat transfer rates leading to rapid solidification.

Cold shuts Incomplete fusion in the body of the casting due to premature solidification in the body of the casting.

D

Dendrite A branched primary phase, formed preferentially in an undercooled liquid due to increased heat transfer at protuberances on a nucleating solid.

Die soldering An undesirable mechanical bond occurring between the casting and the die surface.

E

Eutectic A three phase reaction in which one liquid phase solidifies to produce two solid phases. Also refers to the alloy composition and temperature at which this occurs.

F

Feeding The act of the molten metal flowing into the die cavity. Feeding parameters such as velocity and geometry can affect shrinkage, oxide inclusions and porosity.

Fluidity A qualitative term describing the viscosity of a molten metal or alloy. Higher fluidity is preferred when casting.

Freezing range The difference between the initial solidification and final solidification in alloys. This effects the castability of the alloy and its susceptibility to segregation.

G

Grain refinement Processes or additions designed to promote a fine grain (crystal) structure within a casting. A decrease in grain size is associated with an increase in tensile strength and ductility.

H

Hot isostatic pressing A post-casting process subjecting an item to a hot, pressurised atmosphere to reduce porosity via plastic deformation.

Hot tearing Tearing or cracking of a cast component during cooling, where the thermal stresses exceed the hot strength of the material.

I

Infiltration Movement of liquid metal through a fibrous reinforcement structure.

L

Liquidus The point at which solidification starts when cooling, or melting finishes when heating.

M

Melt A term covering the molten metal or alloy that solidifies to produce a casting.

Modification The effect on the morphology of the eutectic structure.

P

Porosity A void within the body of the casting. There are two main sources for porosity. Shrinkage porosity is formed by the contraction of the casting during solidification. Avoiding shrinkage

porosity is normally a function of die geometry and casting technique. Gas porosity occurs when gas (usually hydrogen) is rejected from the solidifying melt and is trapped within the solid form or when atmospheric gasses are trapped by turbulent feeding. It can be reduced by a number of degassing techniques and/or careful consideration of the feeding parameters.

Primary phase The first phase to solidify in a region of cooling liquid alloy.

S

Segregation A difference in alloy composition due to non-equilibrium cooling or a wide freezing range. Segregation can occur on a gross scale, e.g. a difference in composition between the surface of a casting and the core. This is known as "macrosegregation". Segregation occurring on a smaller scale, e.g. across the width of a dendrite, is known as "microsegregation".

Shrinkage The contraction of a casting during solidification.

Sludge Accumulation of insoluble intermetallic particles in molten aluminium alloys, generally as a result of iron contamination.

Stringer A long, tangled oxide inclusion, resulting from a surface oxide layer.

T

Teem To pour out or empty.

U

Undercooling A cooling of the liquid metal below the liquidus due to the energy requirements of forming stable solid nuclei. Higher undercooling leads to higher nucleation rates and a subsequent finer grain structure.

W

Wetting The ability of the molten metal to cover and bond with surfaces (molds surfaces/reinforcements) during handling and solidification.

Whiskers Short reinforcing fibres used in composites, generally with an aspect ratio of 50 to 100.

Chapter 1

INTRODUCTION

1.1 RATIONALE FOR RESEARCH

Pressure applied to molten metal during and after solidification has been shown to improve the material properties of the resulting component. Such pressure can be applied in number of ways, such as high pressure die casting, hot isostatic pressing or squeeze casting. Squeeze casting is held to provide the highest mechanical properties of the three[1]. Previous work in the Department of Mechanical Engineering of the University of Canterbury by Shilvock [2] had focused on the quantitative effects of micro-alloying additions to a eutectic aluminium silicon alloy. Research into the effect of the casting parameters on the alloy, such as pressure and casting temperature, would complement the extensive research into the composition parameters.

In 1995, a undergraduate project completed by Brown[3] involved the design and manufacture of a simple squeeze casting die, in which molten aluminium would be teemed into a circular cavity and pressure was to be applied to the solidifying metal by a hydraulic press. In research undertaken by Wakefield[4], it was indicated that the advantages of high integrity forming processes can be masked by high levels of oxide inclusions generated from the pouring and turbulent movement of the molten metal during casting. This indicated that investigation of squeeze casting would require attention to this aspect of the process.

Prior investigations into squeeze cast aluminium silicon eutectic alloys[5, 6] had used a simple top teemed casting die. Improving the melt quality by bottom tapping the melt, and bottom filling the die to improve the casting

quality could show an improvement over the previous results. These improvements to the casting methods were then included as part of the design requirements for the redesign of Brown's apparatus. The research will concentrate on the microstructural properties, such as defect distribution and especially upon any surface segregation present in the castings. Quantitative metallography techniques will be used to identify significant changes in characterisation of the alloy.

1.2 AIM OF RESEARCH

The aim of this research is twofold:

- That the existing die designed by Brown[3] be adapted into a bottom tapped, bottom fed casting rig suitable for the production of squeeze cast aluminium alloys.
- After the manufacture and commissioning of the squeeze casting machine, that it be used to investigate the effect of squeeze casting at varying pressures on the macrostructure, microstructure, porosity and mechanical properties of a commercial aluminium silicon eutectic alloy with varying amounts of common alloy additions.

1.3 THESIS OUTLINE

The thesis is split into four major chapters:

- Chapter 2 contains a review of the aluminium silicon eutectic alloy and common alloying additions and their effects, and a discussion of squeeze casting theory and applications and selected published results. A summary of the review shows the positive effect of squeeze casting on the mechanical properties of cast aluminium alloys, with the overwhelming majority of tensile testing results showing an increase in strength over permanent mold/gravity cast alloys. Squeeze casting generally increased measured elongation values, however more variability was shown, with decreases in elongation being more common, although still in a minority of results.

- Chapter 3 discusses the design, manufacture and commissioning of the experimental squeeze casting machine. This chapter reviews published designs of squeeze casting machines and related casting methods. From this review, conceptual designs were examined and a machine layout was selected. The final design of the experimental casting rig is shown.The chapter concludes with an analysis of the operation of the equipment and recommendations for further development.

- Chapter 4 contains details of the experimental methods used in the production and analysis of the squeeze castings. It briefly covers the Taguchi design of experiments approach used in this research and covers the development of semi-automated quantitative metallography techniques used in the analysis of specimens produced by the squeeze casting apparatus.

- Chapter 5 reports and discusses the results obtained from the analysis of the castings. It covers examination of the cast specimens for macro-porosity, macro-segregation, secondary dendrite arm spacing, and microhardness testing of the eutectic and aluminium dendrites. Included are a large number of micrographs, used to illustrate the discussions in this chapter.

The conclusions and recommendations arising from this experimental work are in Chapter 6. The raw experimental numerical data is held in the Appendices, along with manufacturing drawings, MATLAB^{TM} scripts used in the analysis of cast specimens, and a operations guide for the equipment.

Chapter 2

BACKGROUND THEORY

2.1 ALUMINIUM

2.1.1 Aluminium Production

Pure aluminium is a soft, lightweight metallic element. Although the third most common element in the Earth's crust, it has only been widely produced from its abundant oxide in since the late 19th century, when Charles Hall and Paul Héroult separately developed what came to be known as the Hall-Héroult process (see Figure 2.1). The Hall-Héroult process used the reduction of aluminium oxide by carbon anodes in a cryolite/fluoride salt bath. This allowed the commercial production of aluminium metal in large quantities for the first time. The Hall-Héroult process is still the only method by which aluminium is produced commercially.

The costs involved in producing aluminium are high compared to steel production[1], as the energy requirements to reduce the metal from the oxide is much higher. However, due to the higher specific strength of aluminium alloys, a comparative higher corrosion resistance due to the formation of a stable oxide layer and ease of working results in aluminium alloys being competitive with ferrous alloys in engineering applications.

[1]Cold rolled steel prices in April 2004 were approximately US$644 per tonne according to the Dow Jones Steel Index, whereas aluminium prices in June 2004, according to the London Metal Exchange were quoted at US$1716 per tonne for aluminium and US$1540 per tonne for aluminium alloys.

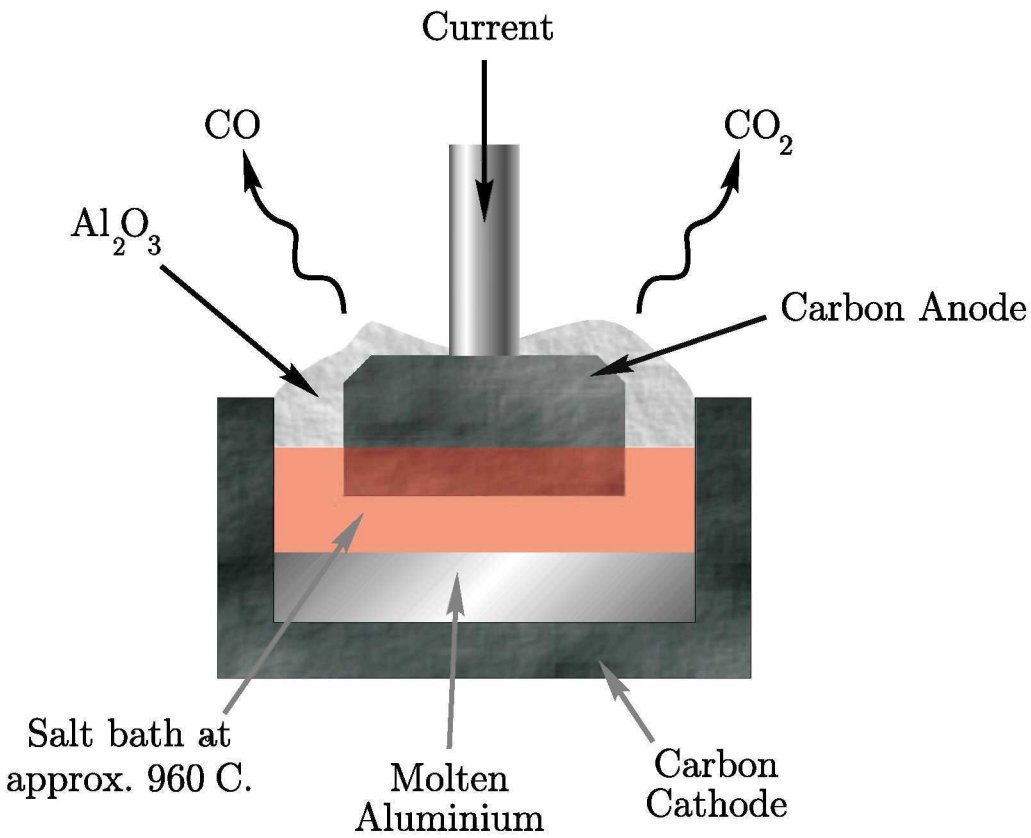

Figure 2.1 Schematic diagram of the Hall-Héroult process.

2.1.2 General Aluminium Designations

All aluminium is initially cast from the molten metal removed from Hall-Héroult cells. After suitable alloying has taken place, the aluminium billets are either used as *casting alloys* or worked (e.g. rolled, pressed, forged) as *wrought alloys*. This division provides the major identification for aluminium alloys. There are many designation systems for aluminium alloys, dependant on the country, time frame and application. Aluminium alloys are often described using the Aluminum Association (AA) system. The AA designation consists of a single 4 digit number, such as 2024, to identify wrought alloys and a single 3 digit number with a decimal value, such as 356.0, to identify cast alloys, with the decimal value indicating composition limits. The AA standard originated in the United States of America, but is now commonly used throughout the world. The numerical value of the designations are used to indicate the presence and relative content of the primary alloy additions, as shown in Table 2.1.

There is international agreement on the standard notation and description of wrought alloys, based on either the Aluminium Association system (International Alloy Designation System), a Unified Numbering System (UNS) numbering system developed by the Society of Automotive Engineers and the American Society for Testing of Materials (ASTM), or a descriptive system developed by the International Organisation for Standardisation (ISO). However for casting alloys, the ASM Specialty Handbook: Aluminium and Aluminium Alloys reports:

> "[for casting and foundry alloys]There is no similar international accord for these aluminium or aluminium alloy products."[1, p19]

Other designations applied to aluminium alloys include if the alloy is heat treatable; the state of heat treatment; and the state of strain hardening/work hardening of the alloy. Heat treatable, or more specifically, age-hardenable aluminium alloys are Al-Cu and Al-Mg-Si wrought alloys, and Al-Cu, Al-Mg-Zn, Al-Sn and some Al-Si-Mg-Cu cast alloys[7]. The state of heat treatment and the state of strain hardening (i.e. amount of

work) are indicated by suffixes to the designation number. The basic temper designations are:

F, as fabricated. This is used to described components which have had no special heat treatment or working applied to them.

O, annealed. The annealed state is nominally the lowest strength, highest ductility state.

H, strain hardened. This applies to wrought products that have undergone strain hardening, with or without heat treatment.

W, solution heat treated. This is the initial stage of the age hardening treatment. The **W** designation is applied to alloys which do not reach their stable condition for a long duration.

T, solution heat treated. This differs from the **W** designation in that the alloys reach a stable condition in a short duration (e.g. a few weeks) naturally or artificially (i.e. at an elevated temperature).

The temper designations also have one or two digit suffixes to indicate more specific detail about the treatment. For example, an alloy may be labelled *2024 T4*. This indicates an aluminium copper alloy that has been solution heat treated and naturally aged at room temperature to a stable condition. An alloy labelled *2024 T6* alloy has been solution heat treated and artificially aged at 190 °C.

Wrought Alloys		**Cast Alloys**	
1xxx	$\geq$ 99% pure Aluminium	1xx.x	$\geq$ 99% pure Aluminium
2xxx	Aluminium-Copper	2xx.x	Aluminium-Copper
3xxx	Aluminium-Manganese	3xx.x	Aluminium-Silicon-Copper-Magnesium
4xxx	Aluminium-Silicon	4xx.x	Aluminium-Silicon
5xxx	Aluminium-Magnesium	5xx.x	Aluminium-Magnesium
6xxx	Aluminium-Magnesium-Silicon	7xx.x	Aluminium-Zinc
7xxx	Aluminium-Zinc	8xx.x	Aluminium-Tin alloys
8xxx	Aluminium-Other elements	9xx.x	Aluminium-Other elements

Table 2.1 The AA designation system for aluminium alloys.

2.1.2.1 Other Casting Designations

As mentioned previously, there is no international agreement on the designation and specification for casting alloys. Other than the AA designation system, the casting alloy designations used will follow BS 1490 - "Aluminium and Aluminium Alloy Ingots and Castings for General Engineering Purposes " (e.g. LM6, LM20, LM24), AS 1874 - "Aluminium and Aluminium Alloys - Ingots and Castings" (e.g. EA401) or a descriptive designation based on the ISO alphanumeric designation system for wrought alloys (e.g. Al12Si). When these designations are used, they will be referenced to an alloying description and/or a suitable AA equivalent.

2.1.3 Aluminium Silicon Casting Alloys

Aluminium alloys are widely used in castings, as they possess many desirable qualities for casting. These include high fluidity, low melting points, light weight, rapid heat transfer and good surface finish[1, 8]. Alloy additions are used to enhance these properties, with silicon being the most common addition. The addition of silicon increases fluidity, decreases the melting point and reduces hot tearing during solidification. The amount of silicon added can depend on the casting process being used. Slow cooling processes such as sand and investment casting can use alloys with silicon compositions of 5% to 7%, while fast cooling processes, such as die casting, utilise silicon contents of 8% to 12%. The latter alloy has a higher fluidity and lower melting point than the former. The higher silicon content, approaching the eutectic composition of 12.6%, decreases the freezing range of the alloy, reducing the the chance of cold shuts and incomplete filling in the faster cooling processes, when cast at the same temperature. These advantages result in most common commercial casting alloys containing a significant proportion of silicon.

Other alloying additions are made to improve the mechanical properties of the casting, or are present as impurities, either arising from the casting process or are present in the raw material. A list of other common elements present in aluminium silicon alloys and their effects follows. The prime sources are Shilvock's extensive work on micro-alloying additions in eutectic

aluminium silicon alloys[2] and a summary of the information present in the ASM Aluminum and Aluminum Alloys Handbook[1].

Copper. The addition of copper increases the as-cast and heat-treated mechanical properties through solution strengthening and precipitation strengthening, respectively. Copper additions also reduce corrosion resistance, decrease castability and slightly reduce ductility[1, p90].

Magnesium. In small additions, up to 0.1%, magnesium causes increases in tensile and fatigue strength, and large decreases in ductility and impact strength. The reduction in ductility and impact properties involves the formation of Mg_2Si precipitates in the bulk metal. In addition, Shilvock found that the presence of magnesium detrimentally affected the modification of LM6 (Al12Si) alloys[2, p232].

Sodium. Sodium is used in aluminium silicon alloys as a modifier of the eutectic phase. By refining the coarse plates of eutectic silicon into a finely dispersed fibrous structure, sodium additions, in small quantities, can greatly improve mechanical properties of cast aluminium silicon alloys. Excess sodium modification results in over-modification, reducing the gains in strength and ductility achieved from the eutectic refinement. Over-addition of sodium has been shown to decrease tensile strength and elongation from the peak values. Sodium has a high rate of loss in the melt due to the high vapour pressure of liquid sodium. The window for an acceptable level of modification of a eutectic aluminium-silicon alloy by sodium is short compared to strontium, e.g. approximately 20 minutes[1, p535] to 50 minutes[9].

Iron. Iron is usually present in aluminium alloys as an impurity. Its presence decreases the mechanical properties of the alloy above a concentration of 0.6%, due to formation of phases such as $FeAl_3$ and βAlFeSi[2]. Iron increases hot tear resistance and reduces die soldering but decreases flowability and feeding characteristics.

[2]The β phase is the label associated with plate-like precipitates containing aluminium, silicon and iron. The stoichiometry quoted is often variable, and can contain significant amounts of manganese as well[10].

Zinc. Zinc is added to aluminium alloys to create heat treatable systems, often in conjunction with magnesium and copper[2]. Small additions up to 2.0% have been found to have limited effect on aluminium-silicon casting alloys.

Titanium. Titanium is added to aluminium-silicon casting alloys to achieve grain refinement. Small particles of titanium compounds act as nucleants for primary aluminium solidification.

Manganese. Manganese, when present in casting alloys, often arises due to its presence in recycled scrap wrought alloys. Manganese, by itself, is reported to have little to no effect on the mechanical properties of cast aluminium silicon alloys[1, p91]. However, Shilvock reports a number of conflicting studies which show that, in the absence of iron, manganese will either slightly increase or decrease tensile strength and decrease ductility[2, p80]. Shilvock concludes that tensile strength gains from manganese are only seen when strontium is used as a modifier, and the presence of manganese is detrimental to ductility in all cases. In the presence of significant iron (>0.5%) manganese is added to create αAl(Mn,Fe)Si "Chinese script" precipitates instead of more embrittling βAlFeSi plates[3][11, 12].

Strontium. Strontium is used as a modifier, similar to sodium. It has been noted to be a less effective modifier than sodium, but is less sensitive to over-modification. Excess strontium does not lead to a largely over-modified structure and the resultant drop in mechanical properties is smaller. Small precipitates of Al_2SrSi_2 have been noted when excess strontium is added[2, 9] and could be associated with a noted drop in tensile strength and ductility when excess strontium is added[2, p207]. Strontium is also retained longer in the melt than sodium, for up to a total of approximately 4 hours[9]. This allows strontium modified alloy to be remelted without the requirement for further modification alloy additions.

[3] Again, the published stoichiometry is variable for these phases, but the morphologies are generally consistent.

Boron. Boron is used as a nucleant to promote grain refinement and to remove titanium, vanadium, chromium and zirconium from high purity aluminium. It has been noted that boron has a detrimental effect on strontium modification[2].

Aluminium silicon eutectic alloys are defined in the AA413.x specification and in the British Standard 1490-LM6 specification. There are other alloys, such as AA336, AA339, AA384, AA385 and LM20 which contain the eutectic 11%-13% silicon content, but differ in that they contain significant quantities of other alloying elements, so are not considered an effectively binary aluminium-silicon system. The composition limits for AA413.0 and LM6 are described in Table 2.2.

The LM6 specification is more restrictive than the AA413 specification in terms of allowable impurity limits, having appreciably lower allowable copper, iron, nickel and zinc content. It should be noted that the AA413.2 specification is acceptable under the LM6 specification, as AA413.2 has lower limits on the impurity content than the base AA413.

2.1.3.1 Mechanical Properties

There are a number of factors to be considered when examining the physical properties of aluminium silicon casting alloys. The mechanical properties are affected by the casting method, eutectic modification, and grain refinement. Based upon similar casting parameters, casting methods and micro-alloying additions that promote fine grain structure (e.g. rapid undercooling due to high heat transfer rates, and the addition of titanium or boron) and peak modification of the silicon structure in the eutectic (i.e. the addition of sodium or strontium) give the best mechanical properties. For sand castings, Shilvock found that low impurity content castings (i.e. tending towards pure binary eutectic content) will have low strength[2, p.249]. Shilvock also gave an optimum alloy content for a eutectic aluminium silicon alloy falling under the LM6 specification: 0.012% Sodium, 11.5% Silicon, 0.3% Iron, 0% Magnesium and Manganese, with "as much Ti[tanium] and as little B[oron] as feasible"[2, p250].

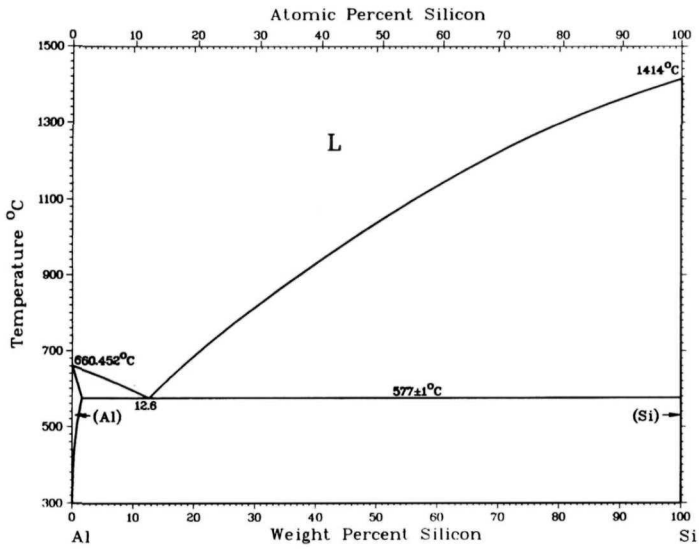

Figure 2.2 Aluminium Silicon phase diagram. From ASM Specialty Handbook: Aluminium and Aluminium Alloys[1].

	Composition Range, wt %	
Element	**413.0**	**LM6**
Silicon	11.0-13.0	10.0-13.0
Iron	2.0 max	0.6 max
Copper	1.0 max	0.1 max
Manganese	0.35 max	0.5 max
Magnesium	0.1 max	0.1 max
Nickel	0.5 max	0.1 max
Zinc	0.5 max	0.1 max
Tin	0.15 max	0.05 max
Titanium	-	0.2 max
Lead	-	0.2 max
Others	0.25 total	0.05 each 0.15 total
Aluminium	remainder	remainder

Table 2.2 413.0 and LM6 eutectic Al-Si casting alloy specifications.

Table 2.3 compares the mechanical properties for the eutectic AA413 and LM6 alloys. The values for the LM6 alloy from BS1490[13] and the values for the EA401 alloy from AS1874[14] are not experimental values, but values that are required to be meet under the respective specifications. Actual strengths should occur above these minimum strengths. One other consideration when it comes to the mechanical properties of eutectic aluminium silicon alloys is that the primary reason for their selection and use in castings is not the mechanical properties, but rather the ease of casting which they confer with their low melting point and high fluidity.

2.1.3.2 Microstructure

The major constituents of the microstructure of aluminium silicon eutectic alloys are:

1. The primary phases, either in the form of aluminium dendrites or silicon crystals;
2. The aluminium silicon eutectic structure;
3. Minor inclusions or particles resulting from reactions between the major and/or minor constituents in the melt.

These constituents, and the form they take, are mostly dependant on the alloying content and the cooling rate during solidification.

Primary Phase. In almost all commercial castings of the eutectic alloy, the major primary phase is aluminium, in the form of dendrites, even at

Eutectic Alloy	Casting Process	Condition	Yield Strength (MPa)	Tensile Strength (MPa)	Elongation %	Source
A413.0	Unknown	as cast	145	295	2.5	[1]
LM6	Sand/Investment	as cast		160 (min)	5	[13]
	Chill Cast	as cast		190 (min)	7	[13]
	Sand Cast	as cast		190 (min)	7	[13]
	Sand Cast	as cast	65	185	8	[8]
	Permanent mould	as cast	90	205	9	[8]
	Pressure Die Cast	as cast	130	250	2.5	[8]
EA401	Sand/Investment	as cast		160 (min)	5	[14]
	Chill Cast	as cast		190 (min)	7	[14]

Table 2.3 Mechanical properties of aluminium silicon eutectic alloys.

slightly hyper-eutectic levels (to 15% silicon content). This is due to a effective eutectic shift arising from both micro-alloying addition (especially modifier addition) and non-equilibrium cooling rates. Primary silicon can form in regions of the bulk casting where the cooling rates are slower or the local alloy content is more favourable towards primary silicon formation. The form of the primary silicon is almost always large faceted blocks. Faceted, primary silicon growth is held to be perpendicular to a (111) plane, with a octahedral morphology. In the presence of defects within the silicon structure, anisotropic growth occurs along the $\langle 211 \rangle$ directions, resulting in hexagonal plate and/or starlike primary silicon.

Eutectic Phase. The greatest microstructural feature of aluminium silicon eutectic alloys is the morphology of the silicon in the eutectic. The modification of the silicon structure in the eutectic represents a major strengthening mechanism of the alloy. The microstructure of the silicon in the eutectic can be generally described as either unmodified (acicular, massive, rod, angular, faceted, flake), partially or fully modified (fibrous, modified angular), or over modified. These descriptions characterize the appearance of the morphology of the eutectic of the alloy in that condition, rather than the crystal structure. This is because modification can be either by cooling rate (quench modification) or chemical addition (chemical/impurity modification) and each method results in a different eutectic silicon crystal growth mechanism, but the gross effect on the appearance of the microstructure and the properties of the alloy is the same.

The unmodified eutectic structure has the appearance of sharp, acicular needles when viewed in cross section, but is actually in the form of interconnected plates or flakes. In the unmodified eutectic, growth is along a [112] direction, with coarse $\{111\}$ twining allowing for limited direction change. In chemical modification, the presence of a suitably sized modifying atom (e.g. sodium, strontium or antimony) the interface propagation at the face of the solidifying silicon is interrupted, resulting in a much finer twinning within up to four $\{111\}$ systems. This "micro-faceted" growth allows branching to occur readily, resulting in a fibrous interconnected silicon structure rather than the plate-like interconnected structure of the unmod-

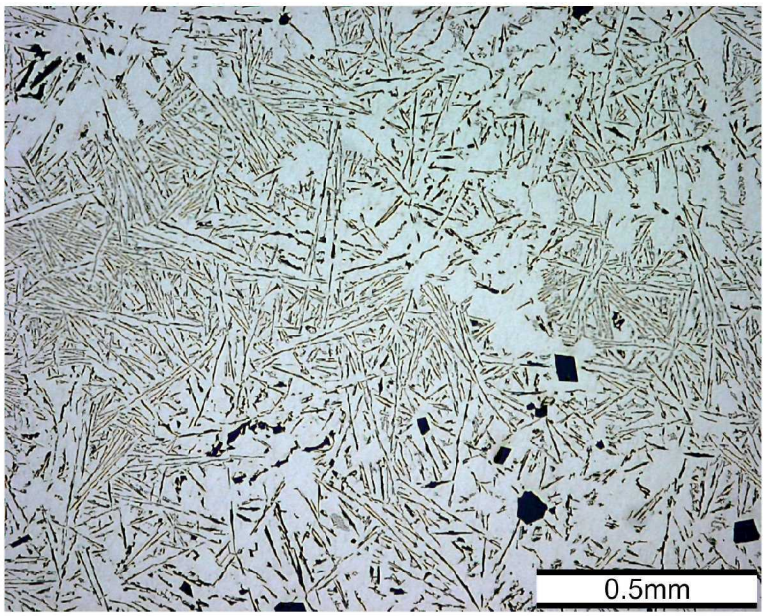

(a) Unmodified aluminium silicon eutectic alloy, with primary aluminium dendrites, primary silicon crystals and coarse, acicular eutectic silicon.

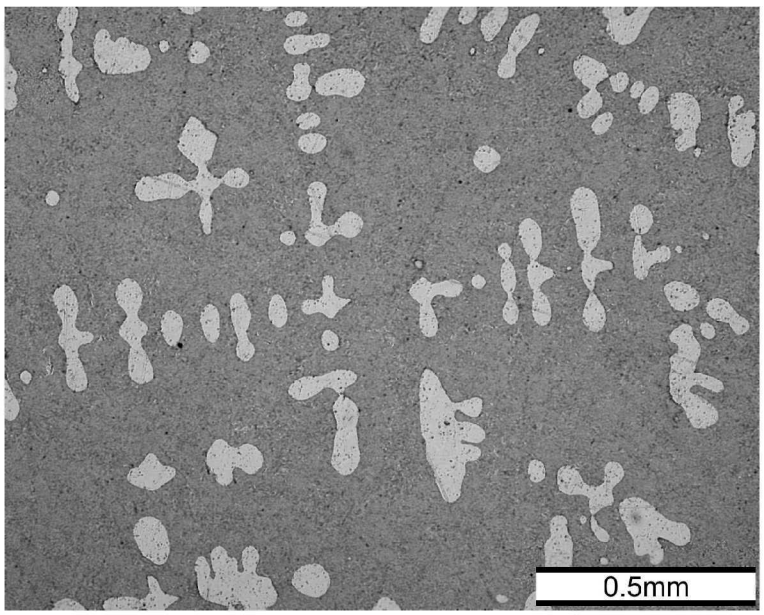

(b) Fully sodium-modified aluminium silicon eutectic alloy. Some retained SiC grinding particles are visible.

Figure 2.3 Common eutectic structures.

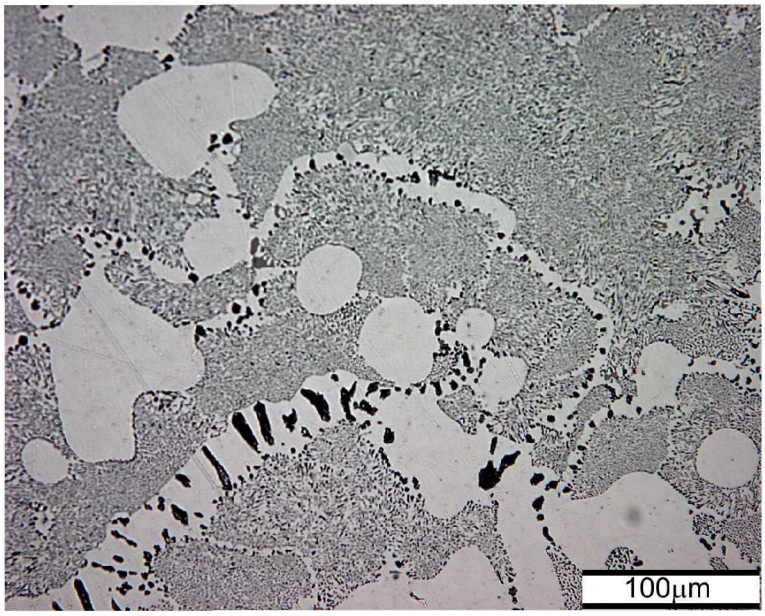

(c) Sodium over-modified structure, with over-modification bands of coarse silicon visible

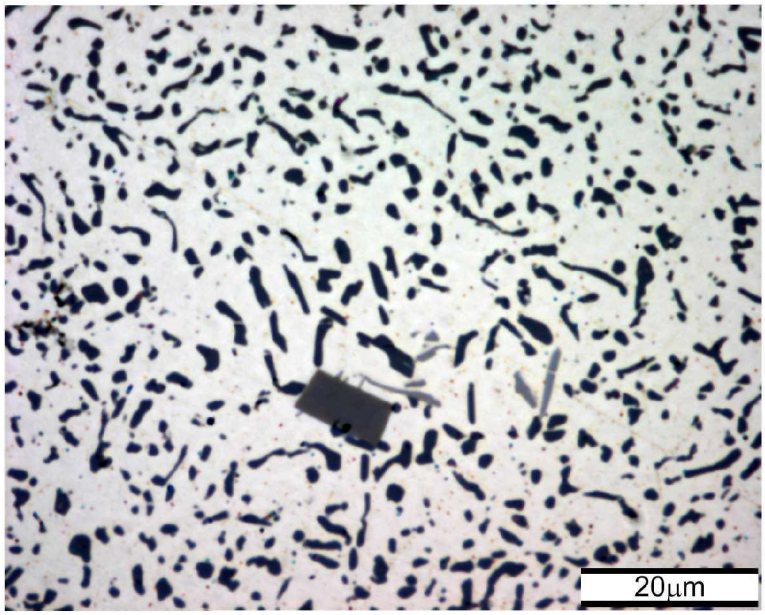

(d) Strontium over-modified structure, showing a single Al_2SrSi_2 intermetallic within the modified eutectic, plus some small βAlFeSi plates.

Figure 2.3 continued.

ified eutectic. Non-equilibrium cooling leads to non-faceted growth via an atomically rough growth surface. The solidifying silicon is not limited to specific growth directions and branches to form a fibrous structure easily. It has been stated that eutectic fibres resulting from quench modification are finer than those of a chemically modified eutectic[1, p535].

The over-modified microstructure is associated with excess sodium modification. During solidification, there is an increase in sodium content ahead of the solidifying eutectic front. This sodium-rich liquid precipitates out AlSiNa compounds which provide nucleation sites for large, un-faceted silicon crystals. This, in turn, reduces the silicon content, leading to large regions of primary aluminium being formed[1, 2, 8]. This can be seen as large silicon crystals in a band of aluminium. Excessive amounts of strontium do not exhibit such overmodification banding. A drop in tensile strength and ductility has been observed[2, p207], along with the presence of blocky Al_2SrSi_2 precipitates when excessive strontium is added[2, 9].

Inclusions The types and form of inclusions in the aluminium silicon eutectic system are a function of the micro-alloying content and the casting process used. Common alloy additions, such as titanium, manganese and magnesium, combine with impurities, such as iron, and the aluminium and silicon present in the alloy. Such inclusions, especially in the form of needles or plates, are usually deleterious to mechanical properties, and so are controlled by chemical addition. A common example is the undesirable βAlFeSi plates which form in commercial Al12Si alloys, especially at the boundaries of the eutectic colonies. Traditionally, manganese has been added to change the morphology from a plate structure to a rounded dendritic structure[4], associated with αAl(Mn,Fe)Si. The cooling rate also has an effect, with a faster cooling rate promoting the more desirable α phase.

[4]The morphology observed in a two dimensional cross section shows the β phase as needles, and the α phase as a fishbone like shape or "Chinese script".

2.2 SQUEEZE CASTING

Squeeze casting is a pressure casting process used to obtain near net shape castings with mechanical properties approaching that of forged components. Also known variously as liquid forging, squeeze forming, extrusion casting and liquid metal stamping, squeeze casting involves the slow, direct application of pressure to a volume of liquid metal before, during and after solidification. The pressure applied during the process increases heat transfer between the casting and the die, reduces or eliminates porosity in the final casting and also ensures complete filling of the die. The net result of these factors is that squeeze casting is the highest integrity casting process currently used[1, p.102].

2.2.1 History of Squeeze Casting.

The origin of squeeze casting is acknowledged to be in Russia/U.S.S.R. The initial concept of applying steam pressure to molten metal was suggested by D. K. Chernov of Russia in 1878. Actual squeeze casting experiments were first carried out in 1931 by G. Welter who was joined by V. M. Plyatskii in 1937. Casting on an industrial scale was underway in the U.S.S.R. in the 1960s, with commercial development in the West being established about the same period[11, 15, 16]. The most notable application of the process was in the production of alloy wheels by Toyota, starting from 1979, using casting machines developed by UBE Industries. The casting process was used to produce a high integrity (low porosity) wheel with the aim of reducing leakage through the porous, cast aluminium. As well as overcoming this obstacle, the squeeze cast wheel was lighter, stronger and more durable than the previous component[15, 17, 18].

In addition to this well publicised example, squeeze casting is now used for a wide range of products, including heavy duty diesel engine pistons, light alloy gears and pulleys, light alloy connecting rods, mortar shell cases and other general engineering components. Squeeze casting is also a major method in the manufacture of metal matrix composites (MMC's), as will be discussed later.

2.2.2 Squeeze Casting Processes

The term squeeze casting covers a variety of different processes with the common factor of the slow feeding velocity of the melt into the die and slow application of high pressure throughout all stages of solidification in the die. Other pressure casting processes, such as low pressure casting and high pressure die casting do not follow this procedure[5].

Low pressure casting uses low pressure on the order of 100kPa to 200kPa to help with die filling, resulting in the minimising of turbulence in the feeding of the molten metal and improving feeding into complex areas of the die pattern.

High pressure die casting involves the high speed injection of molten metal into the die. The high speed helps fill the die, and, if the geometry of the die is such, can form a spray of the liquid metal that coats the surface of the die to give a fine surface finish. Obviously, the high velocities lead to turbulence in the metal, resulting in increased oxide formation in the cast component. Entrapped gases causing porosity are also a result of the high casting velocity. This minimises any further heating allowed (e.g. welding or heat treatment) due to the effect large scale porosity has on the behaviour of the component in a thermally active environment(e.g. blistering of the surface). High pressure die casting can only supply pressure to the entire casting when there is a path for the molten metal to transmit the applied pressure. Once metal in the die has solidified, it can block off the applied pressure, greatly reducing the pressure application into isolated solidifying regions, and minimising the positive effects of the pressure feeding into the die. Shrinkage defects often result from this condition.

By definition, squeeze casting processes are different from the above casting methods, having a higher casting pressure when compared to low pressure casting and a lower feed velocity and complete pressure application compared to high pressure die casting. Table 2.4 compares the relevant pa-

[5]It should be noted at this point that thixotropic or semisolid processes are not considered here, as the casting processes used can be conventional techniques, or those discussed here. The thixotropic/semi-solid processes are a variation on the state of the alloy being cast, not the casting method being used. Some form of positive pressure application, such as that in squeeze casting, can be used on such semi-sold melts to help ensure complete die filling.

rameters for the different pressure casting processes. The casting processes which the term squeeze casting covers, have been grouped by the method of pressure application: i.e. direct pressure, indirect pressure and extrusion casting. All rely on the incompressibility of the liquid metal to generate pressure in the casting.

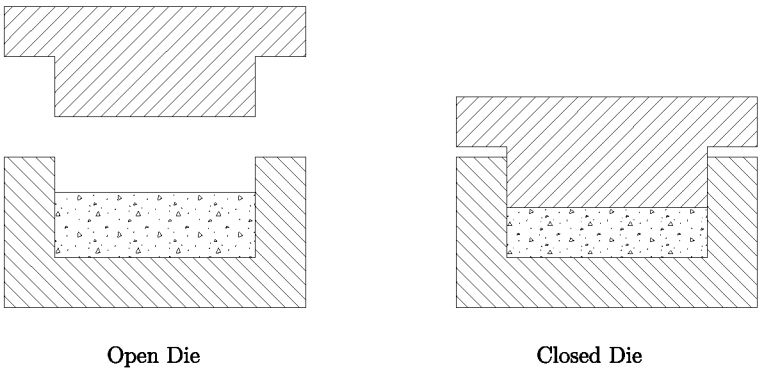

Figure 2.3 Schematic diagram of direct pressure squeeze casting.

Direct pressure processes use a ram or punch to uniformly apply a pressure across the entire free surface of the molten metal, as shown in Figure 2.3, restraining metal movement and hence inducing a pressure in the liquid. Direct pressure squeeze casting is the simplest method of squeeze casting, requiring a simple, axially uniform component.

Indirect pressure processes use a ram or punch to displace a volume of the molten metal inside the die. As the liquid is restrained by the die, the (small) displacement induces a pressure in the liquid metal, see Figure 2.4. This process allows more freedom in the geometry of the cast product and does not require the uniformity of shape needed for a direct pressure squeeze cast component. The complex geometry can lead to a less efficient pressure

	Squeeze Casting	**High Pressure Die Casting**	**Low Pressure Die Casting**
Feed Rate (m/s)	<0.5	10	"Low" [a]
Applied Pressure (MPa)	20-300	2-50	0.1-1
Pressure Application	Direct	Indirect	Indirect

Table 2.4 Quantitative comparisons of pressure casting processes.

[a]Low pressure die casting relies on a smooth filling of the die. This is dependant on the diameter of the feed tube, the temperature of the melt and the applied pressure being used. Typical values would be on the order of 0.1 to 1 m/s

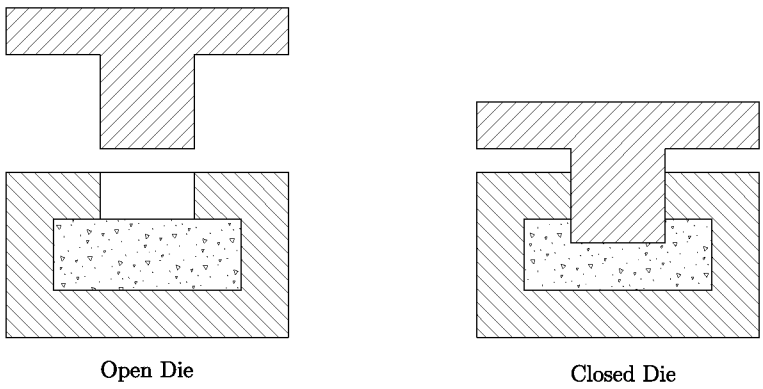

Figure 2.4 Schematic diagram of indirect pressure squeeze casting.

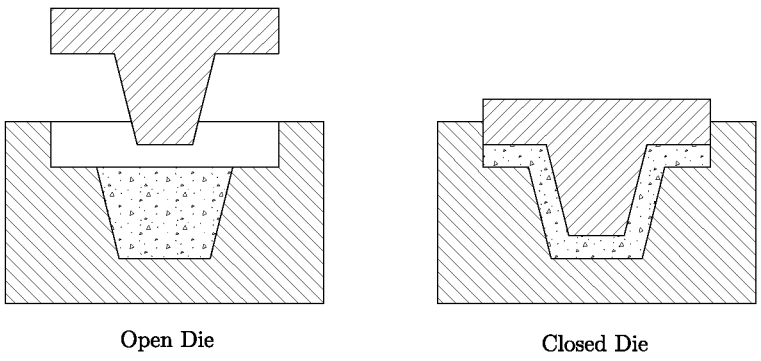

Figure 2.5 Schematic diagram of extrusion casting.

distribution, requiring a higher overall system pressure compared to direct pressure squeeze casting. Indirect pressure application can be used with direct pressure application, after initial solidification has occurred. The solidifying layers do not transmit the applied pressure as the molten metal freezes. The displacing ram can penetrate the solidified layers, ensuring the liquid core is exposed to the required pressure application. In indirect squeeze casting, as in direct squeeze casting, the molten metal remains stationary in the die.

Extrusion casting, also known as backwards extrusion casting, uses the displacement of a descending punch to force the molten metal past the punch until it is restrained by the upper portion of the die, therein applying pressure. This method allows the production of thin walled components. The movement of the metal can lead to increased segregation, cold shuts and increased oxide inclusions, depending on the time and temperature of the casting process. Although this seems similar to direct and indirect casting, it is distinguished by significant movement of the molten metal as well as the movement of the die during the pressure application.

2.2.3 Mechanical and Microstructural Effects of Squeeze Casting on Aluminium Alloys

As stated earlier, the primary reason to perform squeeze casting is to obtain the best possible mechanical properties in the subsequent casting. A summary of available tabulated data that has been reported in the literature, comparing conventional castings directly against squeeze castings, is given in Table 2.5. This does not include data that was only presented graphically and could only be approximated. Such data will be descriptively reviewed below.

Tensile test data almost invariably indicates an increase in yield strength and tensile strength as a function of pressure, tending towards a maximum value at higher pressure. As indicated in Table 2.5, the elongation values are more variable, with results ranging from large increases (e.g. 333%) to appreciable decreases (e.g. -85%). Hardness values are quoted less often, but Chatterjee and Das[5, p120] display graphical data that shows the

Source	Alloy	Casting Process	Yield Strength (MPa)	Tensile Strength (MPa)	Elongation (%)	Change due to squeeze casting,% Yield Strength	Tensile Strength	Elongation
Chadwick and Yue[11]	LM24	Typical chill cast	110	200	2			
		Squeeze cast (as cast)	126	233	2.7	15%	17%	35%
		Squeeze cast (heat treated)	330	368	2	200%	84%	0%
	LM25	Typical chill cast (as cast)	90	180	5			
		Squeeze cast (as cast)	104	214	5.3	16%	19%	6%
		Typical chill cast (heat treated)	240	310	3			
		Squeeze cast (heat treated)	274	331	7	14%	7%	133%
	A357	Typical chill cast (heat treated)	248	313	7			
		Squeeze cast (heat treated)	283	347	9.3	14%	11%	33%
Rajagopal[15]	335-T6	Squeeze casting	-	330	9	-	14%	200%
		Gravity casting	-	290	3	-		
	345-T6	Squeeze casting	-	295	13	-	5%	333%
		Gravity casting	-	280	3	-		
	356-T6	Squeeze casting	265	309	3		66%	-40%
		Permanent mould	186	186	5			
		Squeeze casting	265	309	3		124%	50%
		Sand Casting	138	138	2			
	6061-T6	Squeeze casting	268	292	10	11%	11%	0%
		Squeeze casting	248	341	17	3%	30%	70%
		Forging	241	262	10			
Kaneko et al[18]	356-T6	Squeeze cast	-	289	12.5	-	5%	47%
		Gravity cast	-	275	8.5	-		
Williams and Fisher[12]	7075-T6	Squeeze formed	525	565	6	4%	-1%	-45%
		Die Forgings (longitudinal dirn)	503	572	11			
	2014-T6	Squeeze formed	455	485	2	10%	0%	-85%
		Die Forgings (longitudinal dirn)	414	483	13			
	6061-T6	Squeeze formed	325	335	8	18%	8%	-33%
		Die Forgings (longitudinal dirn)	276	310	12			
	LM5	Squeeze formed (as cast)	142	250	14	58%	9%	40%
		Chill cast (as cast)	90	230	10			
	LM18	Squeeze formed (as cast)	103	187	13	29%	25%	117%
		Chill cast (as cast)	80	150	6			
	LM25	Squeeze formed (as cast)	124	195	15	38%	8%	200%
		Chill cast (as cast)	90	180	5			
		Squeeze formed (heat treated)	250	300	10	4%	-3%	233%
		Chill cast (heat treated)	240	310	3			
Lynch et al[19]	356-T6	Squeeze cast	248	341	17	3%	30%	70%
		Forged	241	262	10			
Dong et al.[20]	LM25	Squeeze cast (as cast)	97	203	8	-25%	4%	321%
		Gravity cast (as cast)	130	196	1.9			
		Squeeze cast (heat treated)	250	337	8	-1%	12%	371%
		Gravity cast (heat treated)	253	300	1.7			

Table 2.5 Selected comparisons of squeeze cast aluminium alloys to conventional processes.

Brinell hardness increasing with pressure, closely following tensile test data.

Chatterjee and Das[5, 6] used a simple, direct squeeze casting process to examine the effect of pressure on LM6 (Al12.7Si) alloy. They concluded that mechanical properties were improved when cast under pressure. This was said to be the result of moving the eutectic composition towards the silicon rich end of the alloy system (as indicated by an increase in primary α phase aluminium), decreasing the dendrite arm spacing and increasing refinement of the eutectic. These conditions all led to a measured increase in mechanical strength and elongation. However, small amounts of porosity were found in castings which had solidified at a pressure below a threshold of approximately 103 MPa. This had no effect on the mechanical properties. Because of this, degassing techniques were said not to be necessary when casting under pressure. Finally, refinement by alloying, in conjunction with casting under pressure, showed further improvement in the mechanical properties, especially ductility.

LM24 (Al8Si3CuFe) and LM25/A357 (Al8SiMg) heat treatable alloys were examined by Chadwick and Yue[11]. They all demonstrated an increase in yield strength and ultimate tensile strength when squeeze castings were compared with more conventional casting. LM24 in a squeeze cast and fully heat treated state had measurably higher mechanical properties than the conventionally superior LM25. This was attributed to a finely dispersed formation of iron aluminide crystals, due to the high cooling rates of squeeze casting, rather than the embrittling massive plate-like forms found in conventional castings. This was also observed in LM25 alloys by Williams and Fisher[12].

The effects of iron and strontium additions on squeeze cast LM25 alloys were examined by Dong et al.[20] Gravity cast specimens were compared against a top poured squeeze casting. An interesting result was that the yield strength of the gravity castings was higher in the as-cast condition than the squeeze castings. This was attributed to increased rate of work hardening due to the high aspect ratio silicon particles (not modified by rapid solidification) in the eutectic of the gravity cast alloy. In the T-6 condition, the yield strengths were equal. The ultimate tensile strength of the squeeze cast alloys in both conditions was superior to the gravity cast

specimens and this was attributed to the lack of porosity, quench modification of the silicon and refinement of AlFeSi particles. For castings that had iron additions up to 1%, squeeze casting improved the ductility from 0.9% to 4.6% in the as-cast condition and from 0.5% to 6.5% in the T-6 heat treated condition. The improvement in ductility was attributed to the change in morphology in the AlFeSi particles, from the needle-like βAl_5FeSi to a "Chinese script" morphology. Addition of a strontium modifier resulted in no change in the eutectic silicon particle size.

For binary aluminium silicon alloys, Chadwick and Yue[11] briefly covered the Al7Si and Al14Si systems. The most obvious effect of the squeeze casting process was reported as a alteration in microstructure, due to the high heat transfer coefficient between the melt and the die, brought about by the high casting pressures. Another effect of the casting pressure was to increase the liquidus and eutectic temperatures of the alloy system. However these were measured and dismissed as of negligible importance when compared with the melt/die heat transfer effects. As mentioned above, a refinement of the morphology of AlFe inclusions was observed due to the high cooling rates.

Suzuki[17] compared squeeze cast A356 alloy wheels against gravity casting, low pressure casting and forging. The squeeze cast wheel had the highest tensile strength and elongation of the cast processes and overlapped the lower half of the range of the forged wheels in both properties. In another study presented by Suzuki[21], it is shown that squeeze cast A356 is stronger in the as-cast (approximately 245 MPa) and T-6 (approximately 304 MPa to 323 MPa) conditions than direct chill casting in the T-6 Condition (approximately 137 MPa). Also, the fracture loads of unspecified products of squeeze cast A390 (approximately 1200kg) and A2011 (approximately 2100kg) were compared against the forged components (approximately 1400kg for the A390 component and approximately 1850kg for the A2011 component).

Evans et al[22] give graphical tensile and fatigue data for squeeze cast AA6061. The squeeze cast alloy had similar yield properties as a permanent mould casting, in the as cast state. However, the squeeze casting had a higher tensile strength and much higher elongation. In a T-6 condition, the

squeeze casting had significantly higher yield and tensile strengths than the as-cast condition, with a small drop in ductility. Micrographs showed a reduction in intermetallic particle size, when compared with permanent mould castings. A five-fold reduction in cell size was observed in the squeeze cast specimen. Severe inter-dentritic porosity present in the permanent mould casting was eliminated by squeeze casting. Segregation at the surface was noted, due to burst feeding of solute enriched liquid through the solidified shell of the casting. The fatigue data compared squeeze cast AA6061 in the T-6 condition at approximately 10^5, 10^6 and 10^7 cycles against a fatigue curve for wrought 6061. The data points for the squeeze casting approximated the curve given for the wrought material. Franklin and Das[16] also reviewed fatigue data at approximately $5x10^7$ cycles, and showed that squeeze cast components failing at stresses 25% to 45% higher than gravity permanent mould castings.

Okada et al[23] studied a wide range of squeeze casting parameters and their effects on the resultant casting. They applied a simple top poured squeeze casting process to a range of aluminium copper (to 10% copper) and aluminium silicon alloys (to 20% silicon). With increasing pressure the density of the aluminium-silicon alloys approached the theoretical maximum at a critical pressure, above which the density did not increase. The higher the silicon content, the higher the critical pressure. For example, at 5% silicon, the critical pressure was approximately 40 MPa and at 20% silicon content, the critical pressure was approximately 78 MPa. A similar result was obtained for defects detected by dye penetrant testing. The geometry of the casting was also considered using an Al8Si alloy, with the critical pressure for a sound casting decreasing asymptotically with increasing casting size. This indicated that the quicker rate of solidification associated with the smaller die size could shut off the pressure application and liquid metal feeding from the molten regions of the casting. Iron and zinc were added to a B295.2 (Al4.5Cu0.8Si) alloy to examine the effects of squeeze casting on impurities. The addition of iron caused a drop in tensile strength and elongation in the squeeze cast alloy and the gravity cast alloy, but the squeeze casting always had an appreciably higher strength or elongation than the gravity casting, independent of iron content. This would permit

an increased impurity content at the same time as retaining similar properties as the gravity casting. Zinc concentration had no noticeable effect on the mechanical properties.

Hong et al.[24, 25, 26] examined the effect of squeeze casting on macrosegregation in Al7Si and Al4.5Cu alloys. In the Al4.5Cu alloys, sound castings were obtained without shrinkage or macrosegregation at a critical pressure region. This pressure region was dependant largely on die temperature, pouring temperature, delay time and humidity. Decreasing the melt temperature to 680°C (from 810°C and 760°C), increasing the die temperature from approximately 100°C to 300°C and decreasing the delay time gave the soundest castings. For the Al7Si castings, it was shown that sound castings, with no macrosegregation or shrinkage defects, can be obtained above a certain casting pressure (approximately 30MPa) and lower pouring temperatures (a maximum of 700°C). Grain refinement also encouraged sound castings.

Nishida and Matsubara[27] examined the effect of pressure on the thermal resistance between a permanent mould die 50 millimetres in diameter and molten pure (99.9%) aluminium. It was shown that with an applied pressure of approximately 150 MPa, the time to complete solidification at the centre of the casting, as indicated by a thermocouple, was 12 seconds. This was about 66% of that predicted by a 1-D heat transfer model. The difference was said to be due to axial heat transfer that was not considered by the heat transfer model. Thermal resistance (the inverse of thermal conductance) was also measured at the mould-casting interface and it was shown that the thermal resistance varied with the pressure by an inverse logarithmic relationship.

Sekahar et al.[28] examined the heat transfer effects of pressure on a casting, but used a eutectic aluminium silicon alloy to "simulate more closely the discrete liquid-solid interface position". A preheated, uninsulated plunger was used to apply pressure to the molten alloy in an insulated 50 millimetre diameter die made from H13 tool steel. Temperature measurements of the plunger and melt during solidification demonstrated a diminishing increase in the heat transfer co-efficient as pressure was increased, with a maximum value of 5.25×10^4 $\mathrm{Wm^{-2}K^{-1}}$ at a pressure of 166 MPa.

The effect of a number of die coatings on the heat transfer co-efficient was also examined, and shown to decrease the heat transfer co-efficient when compared with that obtained with a clean metal die surface. A computational model of thermal behaviour during casting was compared to the experimental results and a "close match" was found.

In summary, the application of high pressures during solidification of aluminium alloys, when compared with casting under atmospheric pressure, has been shown to:

- Increase yield and ultimate tensile strength;
- Increase ductility;
- Increase fatigue endurance;
- Decrease porosity;
- Decrease grain/cell size;
- Decrease dendrite arm spacing;
- Refine deleterious precipitates;
- Modify eutectic silicon;
- Increase metal-to-die heat transfer.

2.2.4 Vertical Die Squeeze Casting

The majority of aluminium squeeze casting research has been done with simple casting dies that use a simple pour of molten aluminium into the top of an open die, with pressure being applied via a piston or ram from the top[5, 6, 18, 27, 22, 19, 23]. This mechanism of die filling has ramifications on the final quality of the casting. The increased surface area of the turbulent flow stream from crucible to die increases the density of oxide stringers in the resultant casting. Non-metallic inclusions such as oxide stringers invariably decrease the tensile, ductility and fatigue properties of cast alloys[1, 4, 29]. The turbulent action of the pour may also entrap gases in the solidifying metal, leading to defects such as blistering and increased gas porosity.

To reduce the amount of turbulence when casting, it has been a common practice to go to a vertical shot feed system[23, 21, 17, 30]. This describes the feeding of a slug of molten metal into the bottom of the die. The primary advantage is the rising metal forces the air trapped in the die out through venting as the metal level rises, reducing trapped air and subsequent porosity. If the feed rate is low enough to avoid turbulence in the rising melt, surface oxidation is also reduced, lowering the density of undesirable inclusions such as oxide stringers. Similar processes are used in high integrity casting processes such as low pressure die casting, which feeds molten metal in to a die with a gas pressure differential, and the Cosworth process casting, where molten metal is pumped electromagnetically into the bottom of a sand mould.

2.2.5 Squeeze Casting and Metal Matrix Composites

Squeeze casting has been utilised in the production of metal matrix composites(MMC's). Metal matrix composites are composite materials where the matrix is a metal, and the reinforcement is either metal, ceramic or carbon. Indeed, traditional metal alloys can be considered to be metal matrix composites if they utilise a dispersed second phase as a form of strengthening. Typically the distribution of the second phase is controlled by the composition of the metal and any subsequent heat treatment. In metal matrix composites, the volume, size, shape and dispersion of the second phase can be precisely introduced into the matrix, allowing specific design of the properties of the final product.

Metal matrix composites, in which the reinforcement phase is discontinuous, and cannot be readily laid up or molded (c.f. carbon fibre), are often fabricated by either powder metallurgy processes or casting processes, with the latter being more prevalent[31, 32]. Most commercial cast metal matrix composites have used an aluminium alloy as the base matrix, due to its light weight, ease of casting and resistance to harsh environments[33]. Every common aluminium casting process has been used to manufacture MMC's, with varying amounts of success depending on the type of MMC being cast and careful design of the feeding and gating to allow for the

change in melt viscosity.

The major considerations when casting MMC's are buoyancy of the reinforcement in the melt, the solidification rate of the melt and the wettability between the reinforcement and the matrix. The first and second considerations affect the distribution of the reinforcement within the casting. Squeeze casting has the advantage of the quick cooling rates and improved feeding of pressure die casting, and the low feed velocities reduce turbulence and allow infiltration of fibreous reinforcement preforms that would otherwise be deformed by the high melt velocity in high pressure die casting.

The last consideration, wetting, affects the ability to transfer loading between the matrix and the reinforcement. The effect of wettability can be modelled by using a worst case scenario of an interface angle of $\theta = 180°$. In this case, there is no wetting occurring between the matrix and the reinforcement. Using various forms of the Kelvin equation:

$$\Delta P_i = \gamma \left(\frac{1}{r_1} + \frac{1}{r_2} \right) \tag{2.1}$$

where γ is the surface tension of the melt and r_1, r_2 are the principal radii of curvature at the infiltration front (nominally half the inter-fibre distance), the pressure required for infiltration and wetting of reinforcements can be found. This required pressure is found to be a function of the diameter of the reinforcement and volume fraction: a lower pressure is required for wetting when using larger diameter reinforcements. For example, Clyne and Whithers[34] state that for fibres with a diameter $d \geq 20\mu$m, infiltrations pressures of approximately 0.1 MPa are required, whereas for fine whiskers ($d \approx 1\mu$m), pressures of 1 to 3 MPa are theoretically required. This was consistent with experimental results. Similar measurements and results are reported by Durrant and Grant[35]. The pressure applied during squeeze casting can easily meet this requirement for wetting of the reinforcement by the solidifying melt.

Chapter 3

EXPERIMENTAL EQUIPMENT

3.1 INTRODUCTION

The design and operation of any casting machine will have consequences on the final cast component. It is evident that the geometry and die material will affect heat transfer rates, and therefore the solidification of the melt. The method of feeding the molten metal into the die, with any associated turbulence and heat loss, will again affect the final structure of the casting. The preparation of the melt, any alloying constituents, and the method of melting will also affect the structure and mechanical properties of the casting. Casting methodology, with such variables as casting temperature, die temperature, time taken to fill the die and the degassing technique (if any) are other variables that affect the final casting. All these parameters must be accounted for and their effects and/or variability minimised if the one parameter of pressure applied to the molten metal during solidification can be fully accounted.

The design, construction and operation of the squeeze casting machine used to produce specimens for analysis represents a significant portion of the work done for this thesis. The isolation of the casting pressure from the other casting parameters required consideration and some control over these other parameters. Previous squeeze casting machines described in other works were examined and used to design a squeeze casting machine that could be used to perform experimental work to satisfy the requirements of the research. This involved researching, designing and constructing a comprehensive casting machine. Melting, filtering, feeding and solidification

under pressure were the requirements of the machine. This chapter reviews the design process of the casting machine and describes the operation of the machine, and its effectiveness in producing squeeze castings.

The basic layout of squeeze casting apparatus, and casting apparatus in general, is well documented[1, 3, 23, 17, 36, 37, 38, 39, 40], but the specific details of the design and operation of such casting machines are not. This chapter will attempt to rectify that, with detailed commentary on the design and operation of the squeeze casting machine undertaken as part of the research.

3.2 EXAMPLES OF SQUEEZE CASTING MACHINES

The simplest form of squeeze casting apparatus is a open die into which molten metal is poured and the pressure is then applied by a mechanically or hydraulic operated ram or punch. An example of such a simple squeeze casting device was developed by Brown[3] in 1995 at the University of Canterbury, shown in Figure 3.1. In this case, the two die halves shown would be bolted together and mounted under a hydraulic press with a plug at the bottom. Molten aluminium would be poured into the die cavity, a plunger inserted into the top of the die and the hydraulic press activated, applying a pressure to the solidifying metal through the top plunger. This pressure applied to the solidifying metal would consequently improve the final mechanical properties. The disadvantage of this process is the turbulent pour of the molten metal into the die. This pouring action would result in oxide inclusions and entrapped gases within the solidifying melt. The effect of such defects reduce the potential maximum property gains from the effect of the applied pressure[21, 30].

Improvements over this basic method have generally involved using a vertical shot feed system. This feeds the molten metal into the bottom of the die, with the metal filling the die from the bottom up. Surface oxidation of the melt is limited during feeding because air within the die is forced out by the upwards motion of the melt and therefore has contact with a smaller surface area of the melt, in comparison to other feed methods. Ube

Industries developed a vertical shot system in 1976 to produce aluminium wheels for Toyota. In this casting system, molten metal was poured into a tilted shot injection unit, which was then drawn upright, docked to the bottom of a horizontally clamped die and then activated to inject the molten aluminium into the die. This only represented a partial improvement in the casting process, as the molten metal was still being poured into the injection cavity, as opposed to being poured into the die. The advantage of this process was the vertical movement of the molten metal upwards, expelling air ahead of it. It was reported that the main reason for using the squeeze casting process to produce wheels was to reduce leakage caused by porosity and to be able to cast heat treatable alloys with minimal segregation[17]. It would appear that oxide inclusion reduction was not considered necessary to obtain the required mechanical properties. Another possible reason for the casting configuration is the short cycle time of 40 to 80 seconds. The size of the casting machine is given at between 300 and 880 tons, dependent on machine configuration.

Okada et al. described a vertical squeeze casting machine, developed in 1982 for Hitachi Mechanical Engineering[23]. The molten metal was fed into the vertical injection sleeve by a "melt push up system". Similar to a low pressure die casting process, a pressurised holding furnace pushed the molten metal up through an immersed stalk into the injection sleeve. The required metal level in the injection stalk was indicated by a signal voltage from a thermocouple. Once the metal level had been reached, the injection ram was automatically operated, giving the initial squeeze to the molten metal. A second, indirect squeeze was applied by a second plunger, after initial solidification of the metal in the periphery of the die enclosure.

The pressure feeding system was presumed to give two major advantages. The first was low turbulence during transfer of the molten metal into the injection sleeve. This would minimise inclusions in the final casting, for reasons given previously. The second claimed advantage of the delivery system was the fact that the molten aluminium was taken from the bottom of the holding furnace, away from the oxide rich (and therefore a source of oxide stringers) surface. As indicated by Wakefield[4], this bottom tapping procedure can increase the mechanical properties and the fatigue properties

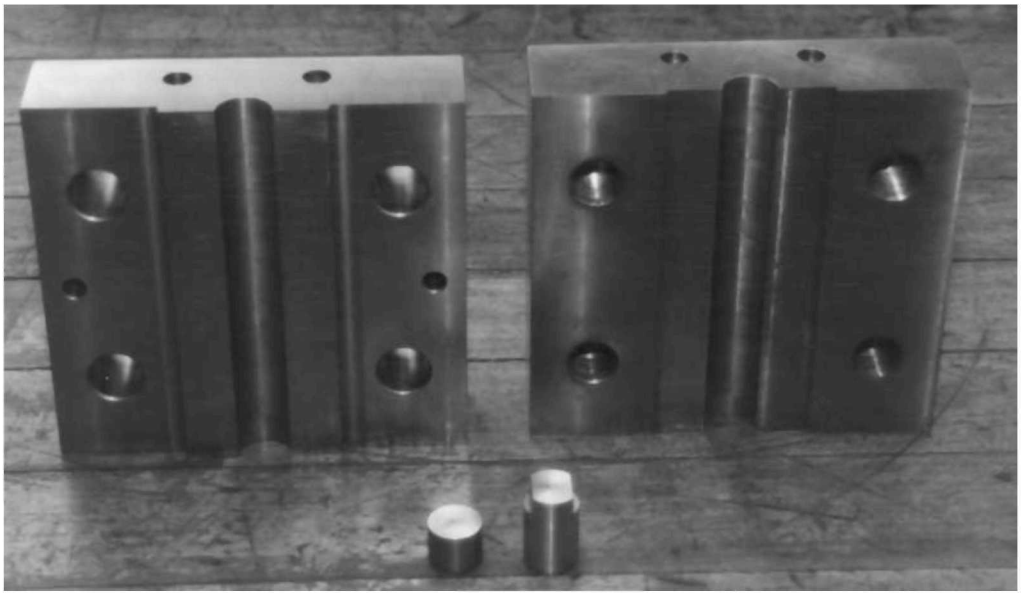

Figure 3.1 Simple squeeze casting apparatus designed by Brown. From [3].

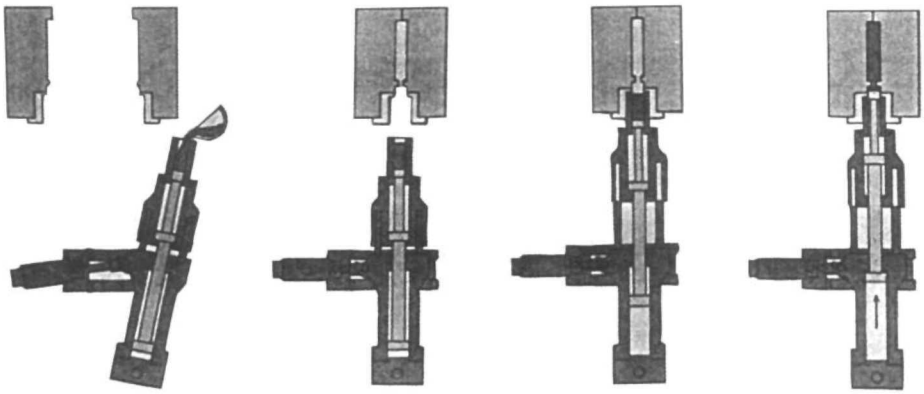

Figure 3.2 Ube Industries vertical shot squeeze casting apparatus. From [17].

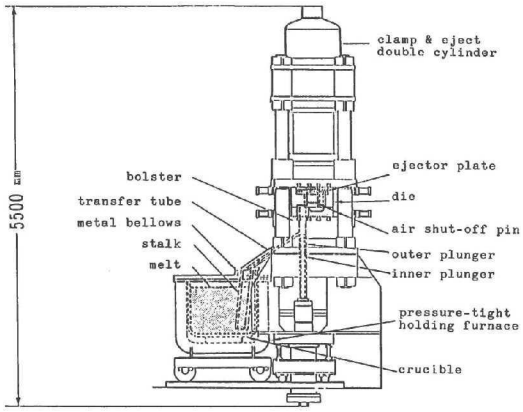

(a) Schematic of the automatic squeeze casting machine developed by Hitachi.

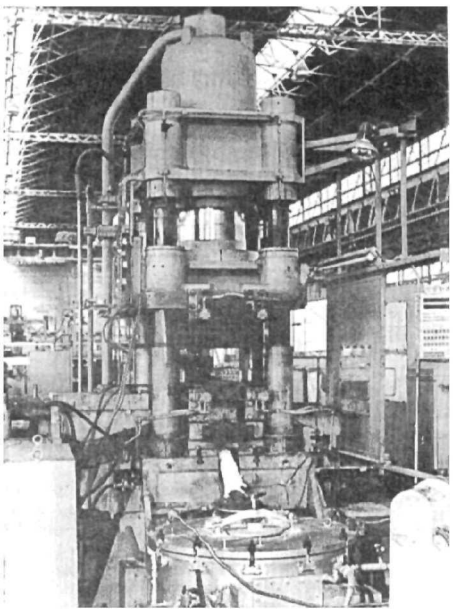

(b) Photograph of squeeze casting machine. Note furnace in foreground.

Figure 3.3 The Hitachi squeeze casting machine. From [23].

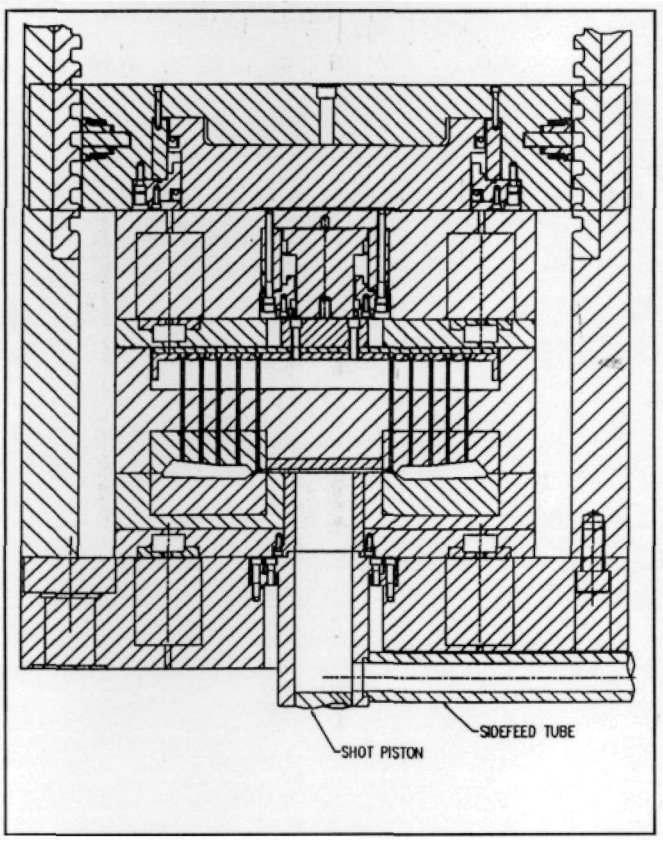

Figure 3.4 Schematic of THT Presses vertical die casting machine. From [30].

of the casting, in conjunction with a high integrity production process, in Wakefield's case, hot isostatic pressing (HIPing) after casting.

A vertical pressure die casting machine as manufactured by THT Presses Inc. was described by Thieman and Thieman[30], in which metal was delivered into a shot sleeve via an insulated horizontal feed tube and then injected vertically into symmetrical multi-cavity die. Short runner and gating length, positive venting of gases in the die and low turbulence feeding are given as advantages. It was mentioned that squeeze casting (probably indirect squeeze casting, given the reported geometry of the casting machine) was possible with the machine, given a die with appropriate gating and runners, and the correct feed rate and casting pressure (less than 250 millimeters per second and 69 MPa, respectively). Another stated advantage of the machine is the reduction in floor space and cycle time compared to horizontal die casting machines.

3.3 DESIGN OF EXPERIMENTAL EQUIPMENT

The design of the experimental equipment followed commonly accepted methodology: statement of aim or need, generation of possible solutions to meet that aim or need, analysis of these possible solutions to select the best path or paths to follow, and then detail design and analysis of the selected design solution or solutions.

The statement of need was to design and build a device that could squeeze cast molten aluminium according to a number of requirements. These requirements, as follows, formed the basis for the resulting design process:

Safe to use. This is generally the prime requisite in design. This particular situation meant retaining molten metal under pressure by ensuring that there are no paths for molten metal to escape and components will not fail under load. Other safety issues were to minimise hot spots on components and design of a safe casting method.

Perform a true squeeze casting action. There should be a direct pressure applied to the melt throughout the solidification process. The casting rig should not rely on melt pressure or velocity to transmit pressure to the whole casting.

Bottom fill mechanism. This is required to minimise turbulence and hence oxide inclusions as shown by previous research. It is presumed that such inclusions could mask the effects on mechanical properties that can occur with squeeze casting.

Must fit into foundry. The design must be able to be located inside the current foundry

Deliver the metal with low turbulence. This is associated with the requirement for a bottom fill die. Low turbulence would also mean minimising sharp corners, utilising an appropriate melt velocity to ensure non turbulent flow, and using a suitable die coating.

Incorporate current uniaxial die. The die designed and built by Brown[3] was to be incorporated into the die casting machine, to give it a simple, direct squeeze casting capacity.

Include a filtration facility. As indicated by the research of Wakefield[4], the addition of filtration of the molten metal in the casting process greatly enhanced the fatigue properties of the casting, once it had undergone a high integrity post-casting process (hot isostatic pressing). Therefore an ability to filter the melt was desirable.

Be as simple as possible. This would reduce the cost and time required to deign, build and operate the casting machine.

Be able to be fabricated in the departmental workshop. This would help to keep the costs down as much as possible.

Be as inexpensive as possible. There was a limited budget available for this project.

3.3.1 Design Sources and Tools

To aid the design process, a number of references, methods and software were used. The main design reference used was Shigely's Mechanical Engineering Design[41]. Specific areas of the design were developed with reference to the publications listed below:

3.3.1.1 Furnace and Die Design References

Brown, *Foseco Foundryman's Handbook*[42]

ASM Handbook Vol. 15, Casting[32]

Upton, *Pressure Diecasting Part 1: Metals - Machines - Furnaces*[37]

Allsop and Kennedy, *Pressure Diecasting Part 2: the Technology of the Casting and the Die*[38]

Street, *The Diecasting Book*[36]

3.3.1.2 Hydraulic and Pneumatic Design

Goodman, *A Primer on Pneumatic Valves and Controls*[43]

Turner, *Engineering Applications of Pneumatics and Hydraulics*[44]

Yeaple, *Hydraulic and Pneumatic Power and Control: Design, Performance, Application*[45]

Barber, *Pneumatic Handbook*[46]

Hehn, *Fluid Power Handbook Volume 1: System Design, Maintenance and Troubleshooting*[47] and *Fluid Power Handbook Volume 2: System Application and Components*[48]

3.3.1.3 Materials Data and Catalogues

Fletcher Steel Limited, *Mild Steel*[49] and *Bright Bar Alloy Steels and Engineering Steels*[50]

Unbrako Pty Limited, *Technical Catalogue 5928*[51]

ASM Handbook Vol. 1, Properties and Selection : Irons, Steels, and High Performance Alloys[52]

3.3.1.4 Design Software

Bentley Systems Inc,
Microstation 95, Microstation Modeler and Microstation SE

MacNeal-Schwendler Corporation and Enterprise Software Products Inc,
MSC/NASTRAN for Windows 2.0

Microsoft Corporation,
Microsoft Excel for Windows

Solidworks Corporation, *Solidworks*

Structural Research and Analysis Corporation
COSMOS/Works 7.0

Demands	Tipping Injection	Cold Chamber Injection	Low Pressure Delivery
Must perform squeeze casting operation	✓	✓	✓
Must fit into foundry	✓	✓	✓
Must deliver required amount of metal	✓	✓	✓
Must bottom fill die	✓	✓	✓
Must be able to be built in dept.	✓	✓	✓

Wishes	Tipping Injection	Cold Chamber Injection	Low Pressure Delivery
Low turbulence filling action	×	∼	✓
Low heat loss	✓	∼	✓
Simple	✓	✓	×
Low cost	∼	∼	×
Easy use	✓	✓	✓
Safe to use	∼	✓	✓
Easy maintenance	∼	∼	×
Ability to include ceramic filtration	∼	∼	∼

Yes ✓ No × Possibly ∼

Table 3.1 Demands and wishes comparison.

3.4 CONCEPTUAL DESIGN SOLUTIONS

When looking for design solutions to meet the described list of requirements, the design of existing squeeze casting equipment was examined to see how others had approached the design problems. The emphasis at this stage of the design was on the melt delivery system, as the configuration of the actual die was a *fait accompli* as this had already been designed and built by Brown[3].

The metal delivery system of the Ube Industries system[21, 17] (tipping injection), the Hitachi design[23] (low pressure delivery), and a system based on cold chamber die casting[30] were compared to see which would provide the best configuration to meet the design requirements.

Comparison charts were developed to help judge which would be the most suitable melt delivery method. These charts are summarised in Tables 3.1 and 3.2. Table 3.1 is a demands and wishes comparison, where the respective preliminary concepts were judged on their ability to meet the demands and wishes of the design requirements.

The final results of the comparisons performed on the three initial concepts gave the indication that the low pressure delivery style would give the best performance in terms of melt quality. The counter to this this was the

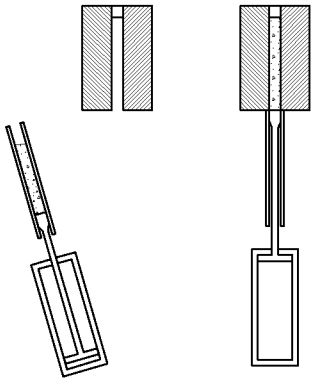

(a) Tipping injection as per Ube Industries

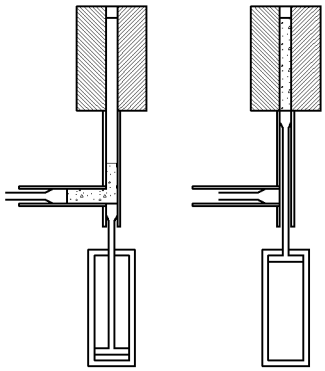

(b) Cold chamber style injection

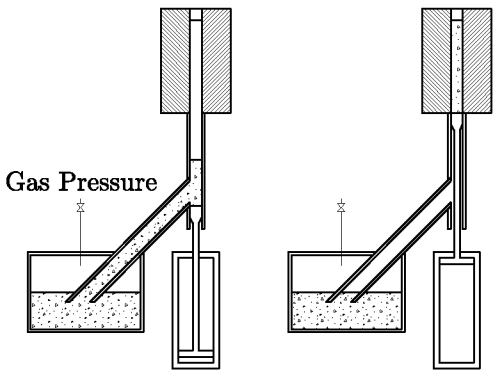

(c) Low pressure melt delivery

Figure 3.5 Schematic of possible melt delivery systems.

Design Proposal		Advantages		Disadvantages
Tipping Injection	1.	Simple melt transfer	1.	Height is constrained by size of die - maximum diameter of the sleeve is limited so length of sleeve needs to be a minimum length.
	2.	Minimal number of metal transfers	2.	Open injection sleeve moves - possible safety hazard.
	3.	Easy access to working parts	3.	2nd ram may be needed
	4.	Simple to design and construct		
Cold Chamber Injection	1.	No external moving parts	1.	Two metal transfers
	2.	Controllable internal metal transfer	2.	Possible added turbulence
	3.	Height can be taken up in length of transfer sleeve	3.	More heat loss through longer metal path
			4.	Possible leakage if internal filtering is required
			5.	Second ram required
Low Pressure Delivery	1.	Filtering may not be needed	1.	Pressure vessel at high temperature
	2.	Control of melt delivery	2.	Large
	3.	Smooth metal transfer	3.	Internal filtering difficult
			4.	Complex

Table 3.2 Advantages and disadvantages comparisons of proposed designs.

obvious increase in complexity over the other two designs. As melt quality was indicated to be an important factor on the effects of squeeze casting, the low pressure delivery from an electrically heated furnace was the chosen configuration.

3.5 FURNACE DESIGN

A bottom tapped melt normally comes from a bottom pour ladle, which was considered unsuitable, as it would preclude the desired bottom feeding of the die: the high quality melt from the bottom of the ladle would still be poured through the top of the die with a bottom pour ladle. A pressure feed method, as used in low pressure die casting machines, and in the Hitachi squeeze casting machine mentioned previously (see Figure 3.3(a)) was proposed as the method of transferring molten metal from the furnace to the die.

The furnace was specified as having a design operating pressure of 0.14 bar, or 14 kPa. This translated to a head of molten aluminium above the level of the melt of approximately 600mm. A transfer stalk, in which the

melt was pushed upwards by the pressure in the furnace, was mounted in the lid of the furnace, sealed by a gland nut arrangement. The stalk was machined from Schedule 80 25NB pipe. The size of the pipe was chosen to match the diameter of the die cavity to avoid turbulent flow due to any change of section. Also, using the same diameter throughout would allow for simple melt volume measurements (100mm height in the stalk would equal 100mm height in the die), and by not decreasing the diameter, further heat loss could be minimised as the surface to unit volume ratio would stay the same.

A facility for ceramic filtration was included by smoothly expanding the stalk out to a diameter of 50mm for a length of 50mm at the top of the upright stalk. This is suitable for ceramic foam filters 50mm in diameter, with an average pore size of 20 pores per inch (ppi). The angled section of stalk join at this point with a flange attachment, to allow easy access to replace or remove the ceramic filter. Once past the filter chamber, the stalk angles towards the injection chamber, where it is mounted against a flat surface machined on the outside of the chamber. A manufacturing drawing of the furnace can be seen in Figure C.3 in Appendix C.

3.5.1 Mechanical Design

The primary concern with the furnace was that it was acting as a pressure vessel, and therefore had to be designed under a suitable pressure vessel code. British Standard 5500 *Unfired Fusion Welded Pressure Vessels*[53] was used as a design guide for the furnace. BS 5500 scope includes vessels subject to electrical heating. However, the standard does not cover vessels which store liquid at pressures below 140 millibar (14 kPa) or "low pressure, above ground storage tanks which have a single vertical axis of revolution designed for the storage of liquids at a pressure not exceeding one bar" and vessels which, when designed to section 3 of BS 5500, do not exceed 10% of the design stress permitted by section 3 of BS 5500.

As initial design calculations did indicate that the furnace would fall outside the scope of BS 5500, first principles were used to design the vessel, with reference to BS 5500 where necessary. This would help keep down

certification and welding costs associated with designing to the standard.

The sizing of the vessel was dependent on the amount of molten aluminium carried in the heated crucible. Ten casts per melt was judged to be a suitable amount. This lead to a crucible diameter of approximately 220mm, if the crucible was to have a minimal surface to volume ratio. This, plus an appropriate allowance for insulation gave rise to the selection of a length of 400API line pipe for the body of the furnace. A 10mm thick plate was welded to one end to form the base, whilst a 15mm thick ring was used at the top of the body as a flange to attach the lid of the furnace.

To facilitate safe lifting of the furnace lid and ancillaries (i.e. avoid handling the hot, heavy lid immediately after a casting), a power screw was attached to the side of the furnace. This lifts the lid, when the screw is turned with a spanner, socket or pneumatic wrench.

3.5.2 Heating Section

3.5.2.1 Initial Design

The heating system initially employed in the furnace was designed as an embedded resistive heating system. Embedded resistor heating elements are simple to manufacture and use, being able to be controlled by a simple temperature controller. However, there is an appreciable lag in the control loop, requiring a period of temperature stabilisation.

Ten metres of 0.8mm diameter ni-chrome wire with single phase AC (240 volts) would give up to 2.4 kW of heating power. This wire was mounted around a bowl-shaped steel liner, which would act as the body of the crucible containing the molten aluminium. Approximately 10mm of a refractory cement was applied around the liner, in which the pre-wound ni-chrome wire was embedded. A further layer of refractory cement was then laid over the top. The ni-chrome was attached to two 2.5mm copper bus bars which connected to the current source on the outside of the furnace body through a sealed duct.

The maximum power output of 2.4 kW was calculated to be sufficient to heat the appropriate mass of aluminium to a suitable temperature (600°C

to 700°C), given that sufficient insulation existed.

After making the embedded resistor crucible, it was found that at temperatures exceeding 400°C a short circuit occurred to the steel liner of the crucible, probably due to thermal expansion of the liner and/or ni-chrome and contact occurring through a thin part of the refractory cement. Testing of the embedded heating element with the steel liner removed confirmed this. A maximum temperature of 550 °C was reached, indicating that further thermal insulation would be required.

3.5.2.2 Final Design

The final heating of the furnace was via a KANTHAL (FeCrAl) resistive heating coil pinned against the furnace insulation in a spiral configuration. With an additional Kaowool layer of insulation to provide both electrical and thermal insulation, a maximum operating temperature of 720 °C was reached. Temperature control was performed by a PID temperature controller and a voltage controller to limit the maximum current flowing through the heating element.

Testing of the furnace with a charge of approximately 6kg showed that it took approximately four to five hours to reach the maximum operating temperature from room temperature. This may impact on the iron content of the final alloy, as holding the melt at temperatures below 720°C can form an iron rich sludge in the bottom of the melt. Therefore careful maintenance of the protective refractory layer is required. With the melt being quiescent, reactions between the melt and the coated crucible were minimised and there was little reaction observed. The main form of damage to the crucible lining was through thermal expansion and contraction causing it to flake from the steel crucible.

3.5.3 Furnace Pressurisation

The furnace was designed to be pressurised by nitrogen, argon or other inert gases. The inert atmosphere inside the furnace would minimise surface oxidation and subsequent presence of oxide inclusions within the melt. The gas was delivered via a pneumatic circuit into the furnace body. The 14 kPa

limit equates to a head of 600mm of molten aluminium. As the metal level sensor, due to its positioning, did not measure the final metal level before injection into the die, a step of approximately 4 kPa (180mm of molten aluminium) is needed after the level sensor has been activated.

It may have been simpler to have the level sensor at the required height of the column of molten aluminium. However, this would have limited the amount of metal deliverable by the furnace to one set amount, varying only through operational irregularities. As the requirement for the amount of melt may change, say for a change in the volume fraction of a cast metal matrix composite, this would be undesirable.

The operational steps for the pressurisation were as follows:

1. Set furnace system pressure, p_{fs}.
2. Increase furnace pressure until metal reference level is reached. Once this has been reached, as indicated by the metal level sensor mounted in the injection sleeve, the flow is stopped by a solenoid valve.
3. Decrease or stop pressurisation.
4. Note furnace pressure, p_f and increase furnace pressure until required metal level is reached, p_f + 4 kPa.
5. Inject metal into die.
6. Exhaust furnace to return the metal level to its depressurised level.

In practise it was found that the injection ram could be activated at a furnace pressure of approximately 14 kPa, as indicated by the pressure gauge. This would result in sufficient melt being delivered into the die.

Where melt volume was not important, castings could be made by simply pressurising the furnace, feeding molten metal until it fills the whole of the die. Activation of the vertical ram would then force metal back down the transfer tube, until the die was sealed by the rising ram. Pressurisation of the melt would then commence. The furnace would be depressurised to drop the melt back into the crucible.

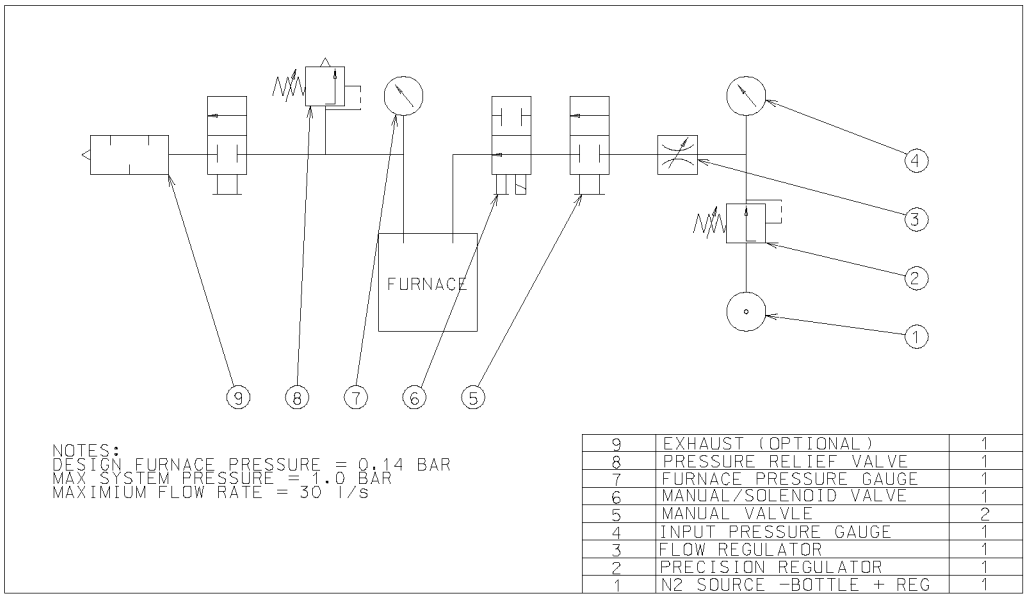

Figure 3.6 Schematic of furnace pressurisation system.

3.6 DIE DESIGN

3.6.1 Uniaxial Die

The uniaxial die as designed by Brown[3], was a simple split die machined out of H13 tool steel and heat treated to 60 HRC. The only change was the addition of a 50mm counterbore to accurately locate the die on the injection block. As there are no nett lateral forces on the uniaxial die, it is held by the locating counterbore and a bracket machined from unequal angle, mounted onto the die bed. Brown designed the die to a maximum design pressure of 200 MPa, and specified a maximum operating pressure of 150 MPa.

3.6.2 Injection Chamber

An injection chamber machined from H13 tool steel was used to connect the major systems of the die: the injection ram, the metal feed from the furnace and the die. Initially, the injection block was to be fabricated from two pieces and welded together, but the cost of machining down a single, large billet was less expensive overall, even with a higher material cost.

The injection chamber was attached to the die bed using a flange, through which four M20 grade 12.9 cap screws were threaded into the bed. A locating boss at the top of the chamber located the chamber into the die bed and provided a location for the uniaxial die. The injection ram was mounted below the injection chamber by four 4140 alloy steel rods, which were threaded into the mounting flange on the injection chamber. The furnace transfer stalk was attached by four M6 cap screws to a flat machined in the body of the injection chamber. A thin copper gasket provided sealing at this interface. Above the intersection of the transfer stalk and the injection chamber is a mount for a 3mm diameter K type thermocouple. This was used to measure the temperature and signal the level of the molten metal in the injection chamber. It was also designed to be rapidly withdrawn to prevent a vacuum lock retaining molten metal in the transfer tube.

Finite element analysis was used to confirm that the stress levels in the injection chamber were suitable. Areas checked were the mounting points of the chamber and injection die and internal pressure from casting.

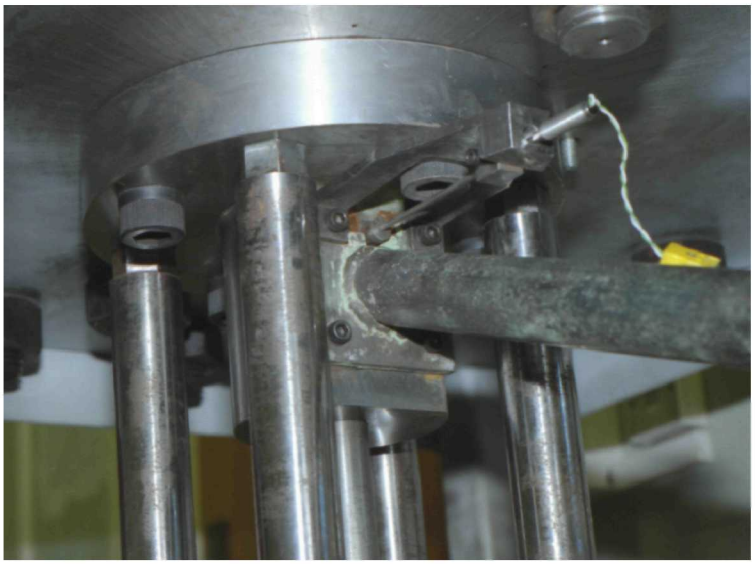

Figure 3.7 Injection block, as situated in operation.

3.6.3 Support Frame

An external frame was used to hold the die bed and attached components. This was fabricated from 50x50x5mm rectangular hollow section, with a 50x50x5mm equal angle to mount the die bed. Assuming a total weight carried of 750 kilograms, each leg of the frame has a factor of safety in compression of 52 and in buckling of 65.

3.7 OPERATION AND TROUBLESHOOTING

This section reviews the performance of the experimental equipment, along with issues arising from the design, manufacture and operation of the experimental equipment other that those already discussed. It is complemented by the user's guide which forms Appendix B.

3.7.1 Furnace

The furnace operated successfully, melting and holding the aluminium at temperatures up to 720°C in an argon atmosphere. Issues involved in the operation of the furnace included:

Easily obtaining a pressure tight seal As manufactured, the lid on the furnace had a bow, due to distortion following welding. The six M6 cap screws used to hold the lid were insufficient to seal the furnace, with another five screws added to allow the lid to fit flush. This made sealing and unsealing the furnace a long process and made the furnace prone to leakage. The large copper o-ring used to seal against the lid needed to be checked for nicks or gaps. They were sealed with a high temperature silicone sealant.

Mounting the heater element spiral The furnace was not designed to support a heating element against the insulation. The R-clips used to pin the element against the insulation are an interim solution. The element has pulled clips out, running the risk of electrical short circuit. The open arrangement of the mounted element also places a safety restriction on the furnace: it cannot be operated while the lid is open.

The element has also burnt out at hot spots, due to a localised increase in electrical resistance. This was generally at the electrical connection to the supply current. Replacement of the connector and/or adjustment of the element was required to reconnect the element. A burn out away from the connection could be fixed by crimping the element wire together or replacement of the element.

Hydroscopic refractory cement To provide the thermal insulation, Fyrecast 1650, a refractory cement, was applied to the inside of the furnace body. Even after baking out, the cement proved to be a source of moisture during the melting process. Having a sealed furnace exacerbated the situation. Discussion with a commercial casting operator[54] revealed that such cements tended to outgas water vapour at "low" temperatures (40 to 400 °C) and again between 700 to 800 °C. This suggests loss of water of hydration at these high temperatures, which is then absorbed back from the atmosphere after cooling. As the furnace temperature was insufficient to completely drive this water from the refractory, the furnace was left unsealed as long as possible, and flushed regularly with argon when the furnace was sealed during the casting process to avoid the water vapour from condensing in the feeding system. This represented the major difficulty in obtaining consistent casting conditions during the commissioning of the experimental equipment.

External temperature During extended operation, the external surface of the furnace body reached a potentially unsafe temperature, high enough to cause burns to unprotected skin. This was also indicative of poor thermal efficiency. A layer of Kaowool insulation was wrapped around the body of the furnace, itself covered in aluminium foil. Another layer of Kaowool was inserted under the body of the furnace to help insulate the furnace from the trolley underneath.

Lid mechanism The power screw used to raise and lower the lid worked well. Operation of the screw would have been faster if it was driven electrically or pneumatically.

Crucible coating The initial crucible coating was Dycote 34 from Foseco. It was found to bubble and crack away from the crucible during heating. It was replaced with a water soluble alumina\chromic oxide paste, ALCOAT-D, used for coating foundry tools. This coating provided a more stable, non-wetting surface that was easy to apply and clean.

3.7.2 Melt Feeding System

As mentioned previously, condensation in the feeding system was the major obstacle in obtaining good quality castings. The condensation resulted from superheated water vapour being released from the furnace refractory cement and travelling up the feed system, whereupon it would cool, condense and pool on top of the injection plunger. If the feeding system was insufficiently pre-heated by the time the melt was feed up into the die, the molten aluminium came into contact with the condensed water, resulting in a small steam reaction. The consequences of such a reaction resulted in anything from extreme porosity in the cast specimen to a blowback of steam and metal into the furnace.

The solution to the condensation problem was to leave the feeding system open to the atmosphere until just before casting commenced. Insulation was added to the feeder tubing to increase the passive heating of the tubing during the melting and holding stages in the casting process. The die heaters were used to preheat the upper part of the feed system to help prevent condensation occurring there.

Control of the volume of metal entering the die was limited. This meant that the actual lengths of the castings ranged from the minimum of 120mm to approximately 180mm. In the smaller specimens, the plunger travelled into the die. In the larger specimens, a section of the casting solidified outside the heated die block. The actual casting volume and the surface against which solidification occurred was therefore variable

Solidification of the melt in the feed tubes was also a limitation of the equipment. Normal casting temperature for a die cast Al12Si alloy would be in the region of 600°C to 680°C. Most melts were heated to 700°C to enable

the metal to have sufficient superheat to avoid premature solidification in the feeder tubes. Solidification did occur, however it was variable, being anything from a thin layer of aluminium to a completely blocked tube. It was observed that blockages were more likely when a high amount of grain refiner was added to the melt. In almost all cases, the entry point into the die cavity became completely blocked after the die had filled, and had to be drilled out. Solidified material in the feeding tubes could be melted out in a separate furnace. When a higher preheat was used (when ceramic filters where incorporated into the feeding system), the solidified material was minimal.

The ceramic filters, when used with the recommended 10 degree extra preheat, had no noticeable detrimental effect to the feeding of the melt into the die cavity.

3.7.3 Uniaxial Die

The operation of the uniaxial die presented no major problems. Minor issues included:

Plunger/bore damage The cast iron plunger had a tendency to pick up hard particles and score out the plunger and bore in which it ran. This was normally insignificant, one large particle required re-machining the bore and replacing the plunger. The tip of the plunger also broke after an operational mishap. The plunger was shortened afterwards with no loss of functionality.

Aluminium buildup Due to the small clearance between the plunger and the bore, small flakes of solidified aluminium would build up in the bore. The easiest way to clean these out was to pour a strong sodium hydroxide solution into the bore and dissolve the aluminium out.

Casting flash The die sealing faces on the die had slightly too much clearance. This resulted in a large amount of flash during most castings, especially at high casting pressures.

3.8 RECOMMENDATIONS FOR FURTHER WORK

The operation of the experimental equipment revealed some shortcomings in the design and operation of the equipment. The equipment worked, in that bottom fed, bottom tapped squeeze cast specimens were produced, but the efficiency of production was low. With the advantages of hindsight, the following recommendations are given:

- Larger capacity die and furnace. This would make the casting less susceptible to premature freezing due to the larger thermal mass in the molten charge. It would also allow larger specimens to be cast, minimising the effects of specimen volume on the final structure. It would require a higher capacity furnace and die.

- Redesign of the feeding system to allow active heating, easier removal of blockages and to reduce the distance the molten metal travels. Easier assembly and replacement would also be an advantage, as quickly replacing blocked tubes would allow multiple casting runs during the same melt cycle.

- Rebuild furnace to utilise Kaowool insulation rather than refractory cement insulation. This would prevent the condensation issues discussed previously. It would also allow a standard mounting of the heating element within the furnace.

- Utilising a quick release system on the furnace lid and the interface with the feeding tubes would decrease the casting cycle time, and be more productive.

- Precise regulation of the hydraulic pressure, especially at low operating pressures (below 50MPa), would enable more research to take place at the casting pressures.

- More precise control of the casting process is required to ensure consistent castings. Ideally, this would involved an automated control system, responding to inputs such as time, temperature and pressure.

Chapter 4

EXPERIMENTAL DESIGN

4.1 APPROACHES TO EXPERIMENTAL DESIGN

The experimental portion of the research was designed to complement Shilvock's previous work on the effects of alloy addition to aluminium silicon eutectic alloys. Instead of alloy content, physical casting parameters were the variables. The initial list of parameters that were considered for examination were:

Pressure. An inherent parameter of squeeze casting, the pressure applied to the melt during solidification will affect the heat transfer rate between the melt and the die, the feeding of the solidifying metal, the phase relationships between the alloying elements, the evolution of gas porosity and the surface finish of the casting. Increasing pressure will increase the heat transfer rate between the melt and die. This will lead to increased cooling rates. This will affect quantifiable parameters such as grain size (increased under-cooling leading to finer grain structure), dendrite arm spacing (higher cooling rate leads to smaller dendrite arm spacing), modification level (increased cooling rate affects eutectic silicon morphology), and a change in the eutectic composition (measurable by α aluminium to eutectic ratios).

Temperature. The initial temperature of the molten alloy will affect both the microstructure and the macrostructure. The variability of temperature could effect the final casting quality: temperatures that are

too low could cause cold shuts, sludge formation and low cooling rates, whereas too high a temperature could increase gas porosity, increase the formation of intermetallics and damage the experimental equipment.

Modifier addition. To meet the strength and ductility requirements of aluminium silicon alloy specifications, the use of modifiers is generally required. Due to the long melting time and lack of access to the melt during casting operations, sodium was unsuitable, as it needs to be introduced to the melt no more than 30 minutes before casting. Therefore either strontium or antimony modifier additions, which do not exhibit such a short fade time, would need to be added to examine modifier action under squeeze casting conditions.

Grain Refiner addition. To improve the mechanical properties, grain refinement by the addition of nucleating agents (normally TiBAl particles) is common practise in aluminium-silicon alloys.

Filtration. To remove large oxide particles and other unwanted inclusions, filters are often used in the runner system when casting. It has been noted that the combination of filtration, to remove inclusions, with hot isostatic pressing, to remove porosity, can enhance the mechanical properties[4]. A similar enhancement should be expected when filtering and then squeeze casting the melt.

Silicon content. It has been shown that the maximum material properties of an aluminium silicon alloy is obtained at a silicon content of 11.3% to 12.5%, or slightly below the eutectic composition[2]. The effect of pressure on the eutectic composition could shift the optimal silicon content. The hypoeutectic microstructure could also be affected by the application of pressure.

Cycle time. The application of pressure on the solidifying metal does not stop once solidification is complete. At temperatures near, but below the solidus, the applied pressure may still greatly exceed the hot strength of the alloy. Whether this has any significant affect on the

alloy is yet to be determined. Removing the pressure application immediately on solidification, or continuing until the pressure is below the plastic flow limit of the alloy could be used to investigate "quasi-HIPing" processing.

When considering the experimental design and the above parameters, it became obvious that an extensive, complete factorial experimental design would not be desirable, given limited time and resources. Therefore a partial fraction experimental design based on a Taguchi orthogonal array (OA) was utilised. A Taguchi OA covers all combinations of parameters in a well designed experiment, but does not isolate single parameters from the influence of others. Taguchi experiments are result-driven. They are widely used in process optimisation and quality control analysis. They are useful in estimating the contributing factors for a process.

The basic methodology of a Taguchi experiment is as follows:

1. Identify the degrees of freedom (DOF) of the process. This includes:
   - the parameters involved in the process, including any interactions between the parameters;
   - the variability, or level, of each parameter.
2. Select an appropriate OA that will accommodate the DOF of the process/experiment, with a minimum of experimental runs.
3. Run the experimental combinations randomly. Statistical certainty can be increased with repetition of each experimental combination.
4. Analyse the results to determine the optimum process parameters, the influence of individual parameters and estimate the performance at the optimum parameters. This last result should be confirmed with a further experimental trial.

4.1.1 Experimental Parameters

The list of process parameters discussed earlier in this chapter was used to select the variables that would be used in the Taguchi OA's. Some of

these parameters were held constant to minimise experimental variation and satisfy process requirements. Another consideration when examining variables was recognition of what could be controlled in normal, commercial, casting processes. Generally, the alloy would be one in common use (e.g. LM6/AA413) with limited alloy additions (modifier, grain refiner or a combination of the two). The processes used during the casting (skimming, degaussing, filtering cycle time) should all be kept constant.

With all these considerations, the Taguchi experimental design was laid out as shown in Table 4.1. The experimental variables chosen were:

- Pressure, at 3 levels, representing low, optimum and high values as indicated by prior research. The lower level was limited by the minimum system pressure in the hydraulic pump. The nominal levels were:
  1. 45 MPa.
  2. 100 MPa.
  3. 150 MPa.
- Filtration, at 2 levels:
  1. No filtration.
  2. Filtration through a 20 pores per inch (ppi) ceramic foam filter.
- Modifier addition, at 3 levels:
  1. Unmodified, 0% strontium.
  2. Optimal modification, 0.02% strontium.
  3. Excess modification, 0.06% strontium[1].
- Grain refiner addition, in the form of TiB, at 3 levels:
  1. No refinement, 0% TiB.
  2. Small amount of refinement, 0.02% TiB.

[1]Strontium is held to not be sensitive to the effects of over-modification, unlike sodium. However, sodium was an impractical modifier addition, due to the nature of the experimental equipment.

Experiment	Pressure (MPa)	Filtering (ppi)	Modifier (% Sr)	Refiner (%Ti)
1	45	0	0%	0%
2	45	0	0.02%	0.05%
3	45	20	0.06%	0.02%
4	100	0	0.02%	0.02%
5	100	0	0.06%	0.006%
6	100	20	0%	0.05%
7	150	0	0.06%	0.05%
8	150	0	0%	0.02%
9	150	20	0.02%	0.002%

Table 4.1 Taguchi orthogonal array for the experimental design.

3. Larger amount of refinement, 0.05% TiB.

The grain refiner levels are described in terms of percentage weight of titanium. The actual refiner would be in the form of TiB particles plus some $TiAl_3$ particles. Boron is present at a ratio of 1:5 to the titanium. The actual levels of grain refiner were also affected by the addition of any modifier, as the modifying alloy also contained 1% of titanium/boron grain refiner at the same 5:1 ratio of titanium to boron. Therefore, when only modifier was added, a small amount of refiner was also added. The amount of refiner added took account of the refiner present in any modifier addition. Silicon was added at a ratio of 12.7% by mass to the aluminium content of any modifier and refiner addition. This prevented any major movement from the eutectic aluminium silicon composition.

4.1.2 Experimental Measurements

The quantitative experimental measurements to examine the effects of the parameters were to be as follows:

- Material Properties.
  - Tensile strength.
  - Ductility.
  - Micro-hardness.

- Metallographic Properties.
  - Grain size.
  - Modification level.
  - Dendrite arm spacing.
  - Porosity.
  - Phase proportions/effective eutectic shift.

Examination of the microstructure would also enable qualitative descriptions of inclusions, including oxide stringers and intermetallic constituents.

During the initial microstructural examination it became obvious that there was extensive differences in the macrostructure of the squeeze cast specimens due to variable castings conditions. The large scale macrostructure differences were of the order of the diameter of the proposed tensile test specimens. Such structural variability within the test samples would mask any effect from the experimental variables. Therefore tensile testing was not carried out.

4.1.3 Metallographic Specimen Preparation

Sections were taken from the cast specimens as shown in Figure 4.5 and in Figure 4.6. The sections were machined or cut from the the cast bar on a lathe. The sections, approximately 25mm in diameter, were then prepared with a five stage semi-automatic polishing process, using a Leco AP automatic polisher, as described by Vander Voort[55]. 280 grit paper was used to grind the specimens until plane. Successive polishes using 9, 3 and 1μm diamond paste was followed by a final polish using a 0.025μm colloidal silica suspension. Fine scratches were mostly unavoidable in the softer aluminium, but did not obscure significant details.

Etching was performed only when required. For general microstructural examinations, Poulton's reagent was used to highlight the eutectic structure. However, this did not reveal any more information than the as-polished condition. For revealing grain/eutectic structure, either a 10% solution

of $FeCl_3$ or $CuCl_2$ was used. Shilvock[2] used $FeCl_3$, as $CuCl_2$ requires subsequent removal of copper deposits with nitric acid. $CuCl_2$ was used when etching with $FeCl_3$ was insufficient or inconclusive as it tended to reveal primary dendrites within grains or colonies rather than grains and colony boundaries in some specimens.

Specimens were examined on a Lecia DM IRM inverted optical microscope, under brightfield, polarised light and differential interference contrast illumination. Digital images were acquired with a Zeiss Axiocam digital camera at a resolution of 1280x1024 pixels for examination using Adobe Photoshop and Corel Photopaint image editing software.

4.1.4 Micro-hardness Testing

The bulk hardness of the cast specimens was measured using a Leco M-400-H Hardness Testing Machine equipped with a Vickers indenter. Micro-hardness tests were taken at three points in the bulk of the casting. Three indentations were taken in areas of the finest eutectic, and three further indentations were taken in the nearest suitable region of primary aluminium to the eutectic indentations. Micrographs were taken of the eutectic hardness indentations, for further image analysis. With non-equilibrium cooling, any apparent shift of the eutectic to a silicon rich composition is expected to increase in the amount of silicon in the eutectic and therefore an increase in the hardness of any particular eutectic colony [5].

4.1.5 Grain Size Measurement

After the specimens were prepared for examination using an appropriate etch ($FeCl_3$ or $CuCl_2$) , they were placed under four halogen cold light spotlights with red, green, yellow and blue filters attached. The combination of the coloured light revealed individual grains. A digital image of the area of interested was obtained. A MATLAB script was used to facilitate analysis. The Heyn intercept method provided the basis of the MATLAB routine. Concentric circles were overlaid on the image and boundary intercepts and triple points counted to obtain the ASTM grain number. Shilvock's definition of a grain was followed, i.e. either a region occupied by primary

aluminium of a single orientation (unlikely in the eutectic alloy) or the region occupied by a single eutectic colony. This grain equivalent is supported by The ASM Handbook Volume 9[56, p620], which defines a eutectic grain as

> "...the portion that nucleated at a certain site and/or in which the phase particles have definite crystallographic and metallographic relationships to one another".

Grains of different orientation were well revealed in the sand cast specimens, with some ambiguity with the boundary of the individual colonies. Unfortunately, the squeeze cast specimen's grain size was too fine to be revealed adequately by the etchants used. The orientation of the colonies were revealed, but the darkened boundaries between the colonies dominated the visible structure, rendering grain size measurements useless. This would appear to be due to harsh nature of the etchant.

4.1.6 Porosity Measurement

Areal analysis was used to quantify the amount of porosity in the sand cast specimens. Although this is time consuming to do manually, analysis software was written in MATLAB to automate this process. The specimens were examined in an as-polished condition. The best method of obtaining a digital image of the cross section was to scan the polished surface of the specimen using a flatbed scanner. This revealed porosity as bright reflected light within the dark grey bulk of the material. Corel Photoshop image processing software was used to filter noise from the image and convert to a one bit (black and white) image. Using a MATLAB script, each pixel within a certain distance (slightly less than the radius of the cross section) of the centre of the image was examined and the ratio of black pixels (aluminium) and white pixels (porosity) was calculated, to obtain a percentage value.

The quantitative results obtained from the analysis was compared to calibrated images to validate the results.

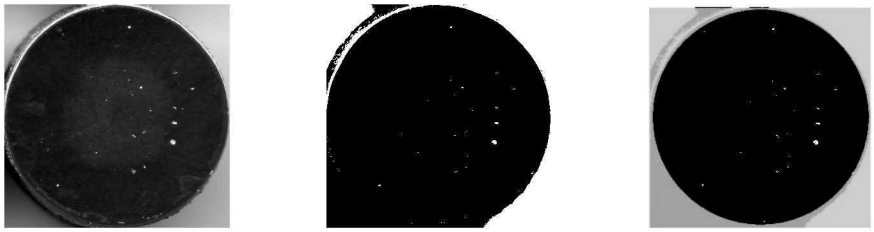

(a) As-scanned image of specimen showing highlighted porosity

(b) 1-bit black and white filtered image of porosity in specimen

(c) Representative area of specimen analysed by MATLAB script to obtain percentage porosity

Figure 4.1 Example of porosity images of sand cast specimens. The section shown was calculated to have a porosity of 0.31%.

4.1.7 Phase Proportions

The proportions of phases (e.g. primary dendrites to eutectic, eutectic silicon to eutectic aluminium) was again analysed by areal analysis. Because the differentiation between phases was not so obvious as for porosity, a more complex curve fitting comparison was performed, as well as a standard point count.

4.1.7.1 Point Counting

A standard point count method as described by Vander Voort[57] was used as the basis for a MATLAB routine. The image under examination was displayed on screen, with a grid of points randomly laid over it, and a mouse was used to input the appropriate count for each point, i.e. points within (a value of 1.0) or bordering the region of interest (a value of 0.5). The sum of the points counted over the total number of points give an approximate percentage of the phase of interest. This allowed for quick analysis of the phase proportions, especially when multiple grids were used for statistical confidence.

4.1.7.2 Threshold Analysis

It is common for digital image editing software to have a histogram function, wherein the discrete levels of individual pixels are displayed as a histogram. If there are two or more areas of distinct colour or shade in an image, this is shown on the histogram as two or more separate peaks. Given sufficient disparity in the colour or shading, it is simple to find a threshold value above or below which represents the proportions of each shade. This is an approximate reading, accurate, depending on noise values, to within 0.5%. A more accurate analysis of the image histogram is given below.

4.1.7.3 Bimodal Curve Fitting Analysis

An eight bit greyscale digital image was obtained of the section of interest. An example examining the proportion of primary phase aluminium to eutectic is shown in Figure 4.2(a). The greyscale value of each pixel can be recorded. This is shown in Figure 4.2(b). A theoretical bimodal normal distribution, as given in Equation 4.1, was fitted to the recorded data using a non-linear optimisation algorithm.

$$PDF = \frac{p}{\sigma_1\sqrt{2\pi}} \exp\left(-\frac{1}{2}\left(\frac{x-\mu_1}{\sigma_1}\right)^2\right) + \frac{1-p}{\sigma_2\sqrt{2\pi}} \exp\left(-\frac{1}{2}\left(\frac{x-\mu_2}{\sigma_2}\right)^2\right) \tag{4.1}$$

Where p is the proportion of the normal distribution with mean μ_1 and standard deviation σ_1. The other normal distribution has the mean μ_2 and standard deviation σ_2, with the proportion being $1-p$. Fitting this equation to the measured data gave a theoretical proportion of one phase to another. The minimum between the two means in the combined distribution could be used as threshold for a simple count of pixel intensities above and below the threshold.

Using the raw image data was problematical, in that there were embedded inclusions from the polishing process, showing up as black pixels. Also, where the eutectic was coarse some of the aluminium in the eutectic would be measured as primary aluminium, rather than part of eutectic. To avoid these problems, the image was processed with a median filter to remove such

spurious data. This is shown in Figure 4.3(a). The distribution of the pixel intensities is shown in Figure 4.3(b). It can be seen that there was very little overlap between the primary aluminium and the eutectic greyscale values once filtering had been performed on the data.

To confirm the fully automatic curve fitting, a point count program was created. This used the accepted relation $P_p = V_v$, or that the point count percentage of the phase of interest is equal to the volumetric percentage of the phase of interest. This method does require operator input and can be prone to subjective interpretation of whether or not a point lies in the phase of interest, at the boundary of the two phases or outside the phase of interest. Even though it is accepted as the most efficient method of measuring proportions[57], it still requires significant time to analyse each cross section, especially if a high (10 to 20) number of counts is required to give statistical certainty. Because the curve fitting method samples the whole image, rather than a few points, only one analysis is required to provide a reliable figure. Table 4.2 summarises the results for the theoretical curve fit, threshold count and point count for both the original and filtered image as given in Figures 4.2(a) and 4.3(a).

4.1.7.4 Multi-modal Curve Fitting Analysis

For analysis of sections with more than two phases present, an adapted MATLAB script was used. Figure 4.4 shows a highly magnified image of an aluminium silicon eutectic, with a third phase present along non-obvious grain boundaries (probable β Al-Fe-Si).

Image	Distribution proportion, p	Curve Fit Threshold Count	Data Threshold Count	Point Count[a]
Original	12.1%	13.8%	13.2%	15.1±1.4%
Filtered	15.5%	15.5%	14.8%	15.1±1.4%

Table 4.2 Primary aluminium phase proportions by different methods.

[a]20 random 64 point grids laid over section of interest.

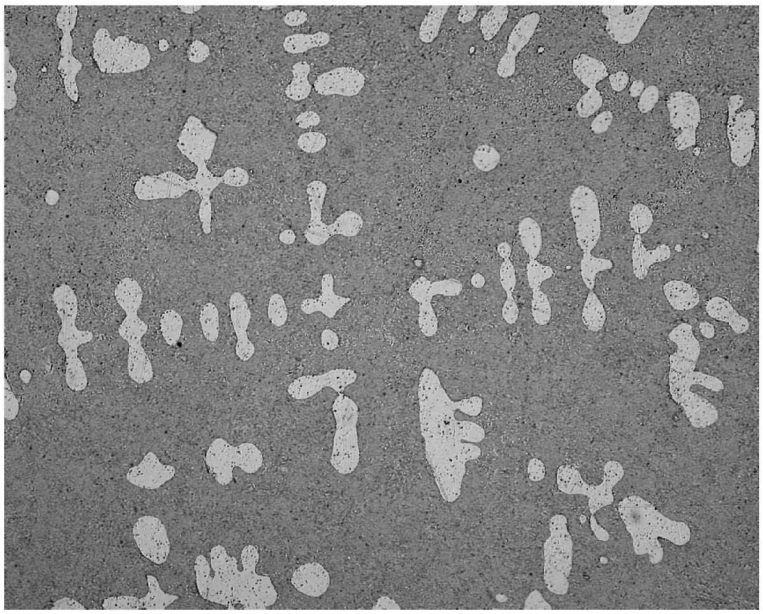

(a) Greyscale image of two phase section showing primary aluminium dendrites plus the surrounding AlSi eutectic.

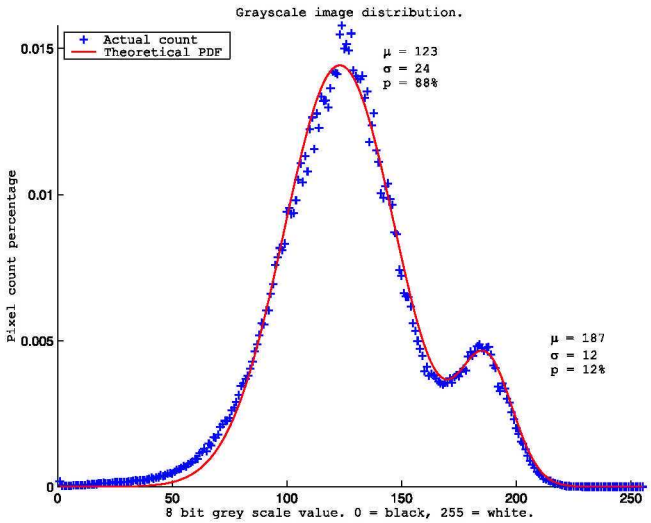

(b) Original image distributions, showing the mean (μ), standard deviation (σ) and proportions (p) of each distribution.

Figure 4.2 Cross section of sand cast specimen with associated intensity distribution.

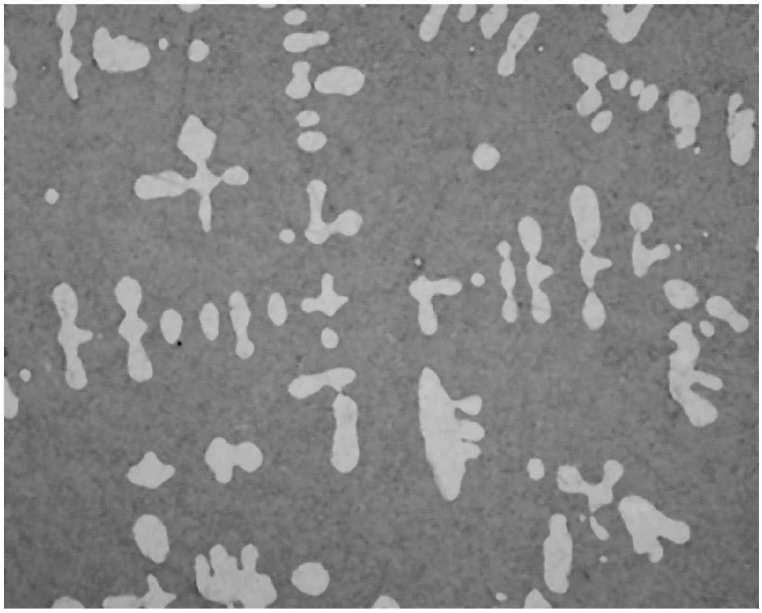

(a) Filtered image of aluminium dendrites surrounded by aluminium silicon eutectic.

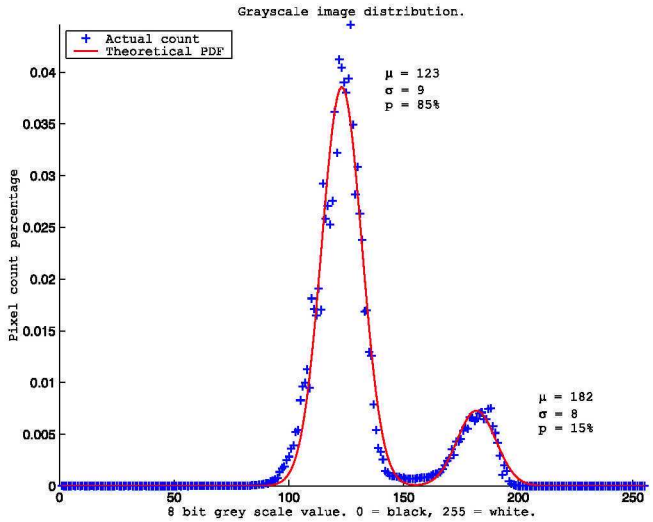

(b) Filtered image distributions, showing the mean (μ), standard deviation (σ) and proportions (p) of each distribution.

Figure 4.3 Filtered cross section of sand cast specimen with associated intensity distribution.

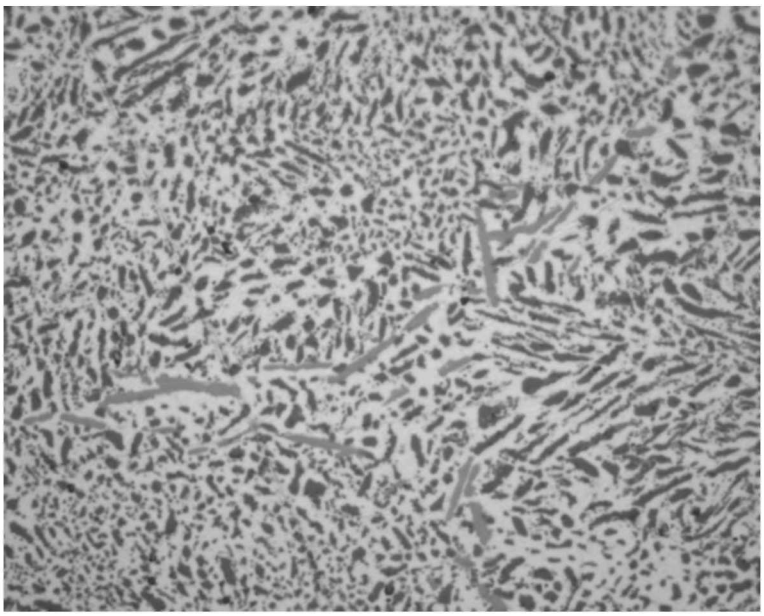

(a) Micrograph of eutectic, 1000x

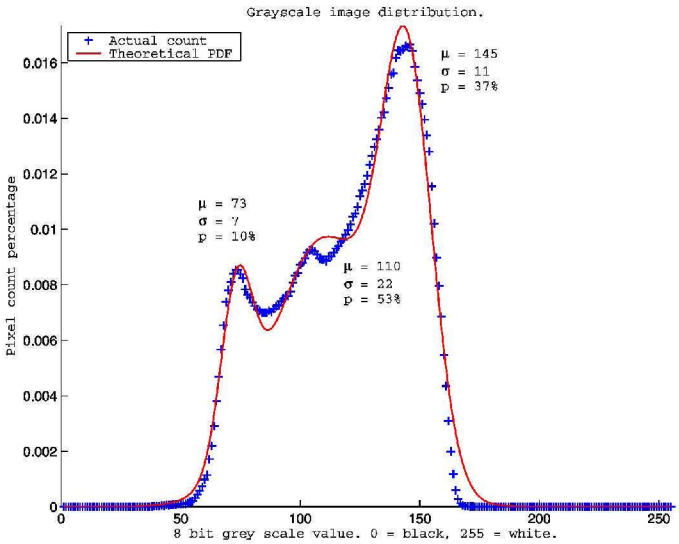

(b) Original image distributions, showing the mean (μ), standard deviation (σ) and proportions (p) of each distribution. Note that the mid peak (the grey intermetallic) has been given a proportion of 37%, due to the curve fitting algorithm being swamped by noise

Figure 4.4 Greyscale image of Al-Si eutectic with a third intermetallic phase (probably β-AlFeSi).

A more general case of Equation 4.1, with any number of normal distributions present is:

$$PDF = \sum_{i=1}^{n} \frac{1}{\sqrt{2\pi}} \left(\frac{A_i}{\sigma_i} \exp\left(-\frac{1}{2} \frac{(x-\mu_i)^2}{\sigma_i^2} \right) \right) \tag{4.2}$$

where A_i is the area of the ith distribution of mean μ_i and standard deviation σ_i. Note that the proportion of each mode is given by:

$$p_i = \frac{A_i}{\sum_{i=1}^{n} A_i} \tag{4.3}$$

It was found to be difficult to automatically identify the number of distributions present and their means. Therefore the software required user input to identify the peaks in the sampled distribution from the image. This was fed into an more advanced solver algorithm, supplied by Lintott[58]. Care had to be taken to achieve a high signal to noise ratio, i.e. increasing the contrast between the phases. At high magnifications, with very small particles, this contrast was low. As the algorithm minimises the residual error between the theoretical distribution and the measured distribution, this low contrast would cause the solver to seek a global minimum in the residual error, away from the desired solution, which would be represented by a local minimum in the residual error. This could be avoided by limiting the solver to values near the selected initial values. As there was little need for multi-phase analysis in this research, this was not pursued, but could easily adapted to the MATLAB non-linear minimisation routine.

4.1.8 Electron Microscopy

For examination of the specimens by electron microscopy, a JEOL JSM-6100 scanning electron microscope (SEM) was used to obtain secondary electron and back-scatter electron images. Semi-quantitative composition analysis was performed with a Link Systems exL EDS (electron dispersive spectroscopy) system attached to the SEM. Crystallographic data, in the form of backscattered electron diffraction (EBSD) patterns was obtained

from specimens tilted at 70 degrees with a HKL Technology Nordlys detector and analysed with HKL Technology Channel 5 software.

4.2 CASTING METHODOLOGY

4.2.1 Experimental Conventional Castings

After the initial castings performed during the testing of the squeeze casting machine, it became obvious that only one casting per melt could be produced. The excess melt was ladled into small ingot molds for reuse. When the experimental casting runs were carried out, the first ladle of the excess melt was poured into a bonded sand mould. This would allow for some comparison of the squeeze casting against the more conventional sand casting, cast after melting and holding at the same temperature and composition. The size, shape and location of experimental specimens is shown in Figure 4.5

One casting was carried out using the uniaxial squeeze casting die as a conventional permanent mould die. A feeder head was added to the top of the die halves to conventionally feed molten alloy during solidification. The die was heated to 300°C and molten eutectic alloy at 700°C was poured in and allowed to cool. This was used to confirm the initial die temperatures and operation, and the cast specimen was used as a prototype in the development of the analytical techniques.

4.2.2 Squeeze Casting Methodology

Initial castings were carried out to test the operation of the squeeze casting machine. These were used to develop the following casting parameters:

- Die Temperature at 350°C
- Melt Temperature at 700°C
- Maximum furnace pressure at 15kPa.

The casting methodology was as follows:

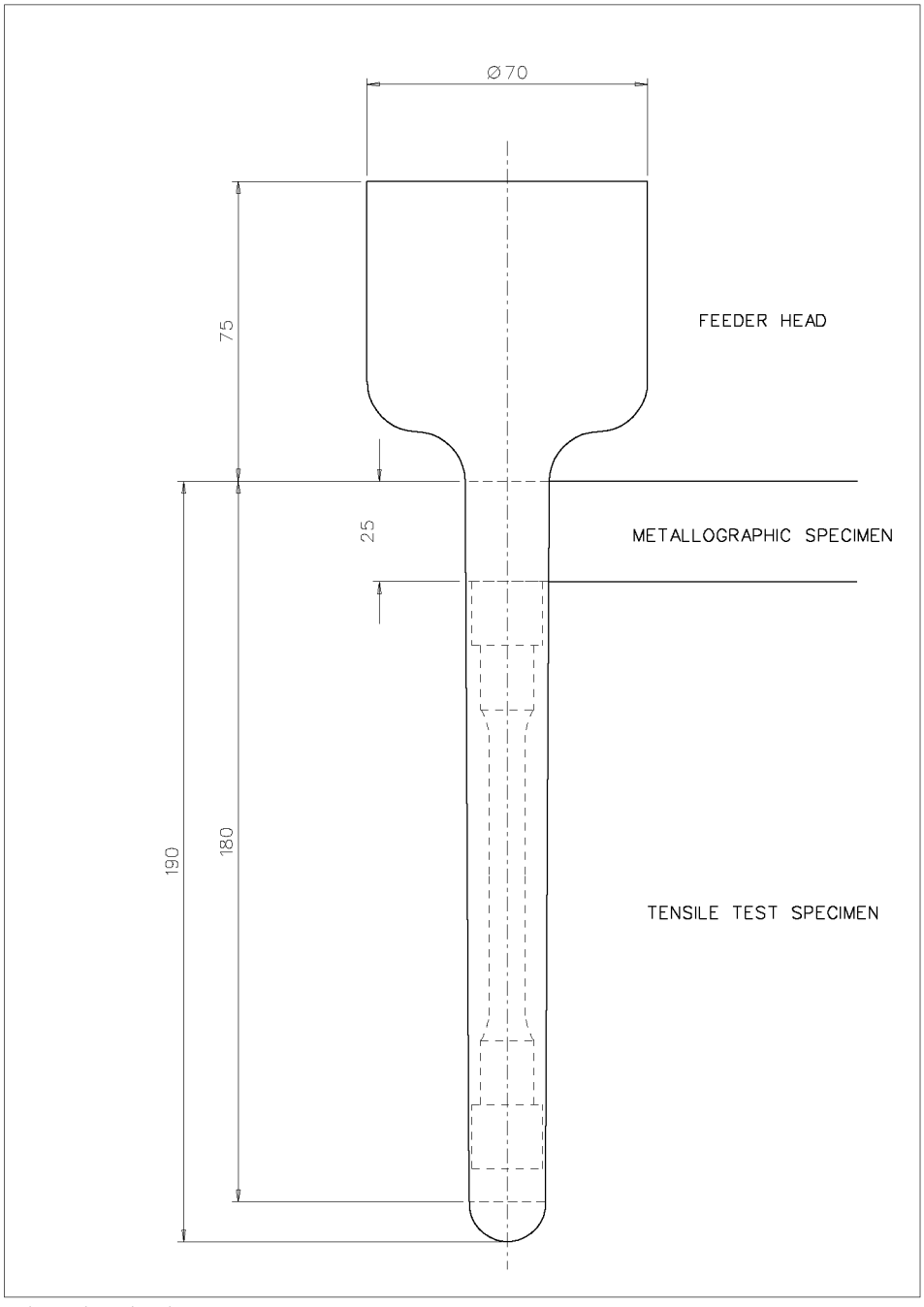

Figure 4.5 Sand cast specimen. After Shilvock[2].

1. 5.5 kg of EA401 (equivalent to AA413.2/LM6) ingot, and appropriate alloy additions were placed into the furnace and preheated for two hours, with the furnace unsealed, at 400°C, to drive off moisture.

2. The die heaters were turned on, and ingot was melted with the furnace sealed and flushed regularly with argon.

3. Once liquid, the metal was heated to 700°C, and held at that temperature for one hour.

4. With the die at a steady state temperature of 350°C, the feed tubes were attached to the die.

5. The pressure in the furnace was increased until it had reached 15kPa, and at this point the injection ram was activated.

6. The appropriate pressure was applied for 3 minutes, after which it was released, the die opened and the casting removed.

7. The furnace was opened and one sand cast specimen was poured into a test mold. The rest of the molten metal was poured into ingot molds for later re-cycling.

8. The die and furnace were cleaned and coated for the next casting run.

A more detailed methodology and guide to the use of the casting equipment is given in Appendix B. The layout of the squeeze cast specimen is shown in Figure 4.6. Due to the varying length of the squeeze castings, the location of the metallographic specimens changed. The surface used for metallographic examination was held to be 25mm from the bottom of the casting, or from the bottom of the die, which ever suited the length of the specimen.

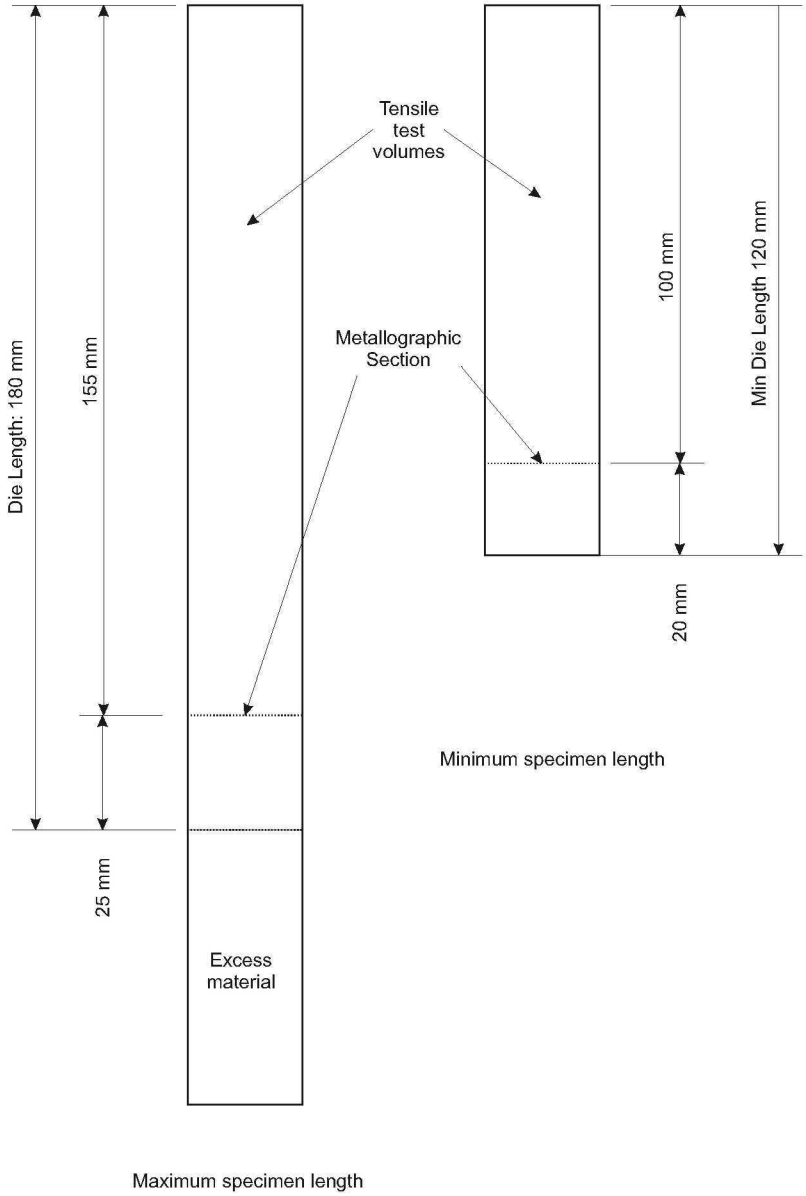

Figure 4.6 Squeeze cast specimen.

Chapter 5

EXPERIMENTAL RESULTS AND DISCUSSION

The following chapter summarises the experimental results obtained from the casting schedule carried out using the experimental equipment. The results are presented as both tabulated and graphical data, and illustrated with representative micrographs. For clarity, the results will be discussed as they are presented.

The low number of castings, and the large scale variability between the castings produced, reduced the amount of meaningful quantitative data available for analysis. Where possible, significant data points were obtained independent of the variable macrostructure. These readings are supplemented with qualitative observations from assessment of both the macro and micro structures present. Trend lines have been included on the graphical data to help indicate observations. These trend lines are not a mathematical representation of expected behaviour, merely an indication of observed behaviour. The statistical variation at each data point precludes a simple R^2 comparison, instead the average values of measured results at each data point is compared in the Taguchi analyses, and these should be used to interpret overall trends.

5.1 CASTING OBSERVATIONS

5.1.1 Squeeze Castings

The initial judgement on whether or not a casting run was successful relied on the appearance of the surface of the cast specimen as it was removed from the die. If the specimen had good surface finish, no surface defects, such as porosity or lapping, and no noticeable extreme porosity, it was considered to be a successful casting and used for microstructural examination. The approach to the casting process from a commercial point of view (standard casting alloy, commercial alloy additions) would require a nominally fully sound component to be utilised in the research. The initial castings were unalloyed, being plain eutectic aluminium silicon (LM6/EA401). This alloy was cast at a variety of melt and die temperatures until a suitable as-cast appearance resulted. It was observed that at high die temperatures (approximately 430°C to 480°C), surface finish was excellent, but considerable surface shrinkage was visible. At low die temperatures (250°C to 300°C) there was an increase in visible cold laps and shuts on the surface. An acceptable appearance of the surface of the casting was obtained at 350°C, and this die temperature was used for the remainder of the study.

The initial casting temperature was chosen to be 700°C, as this represented an upper limit for acceptable castings as shown by Hong[25] in an Al7Si casting alloy. The upper limit was chosen as the maximum superheat was desired to minimise any problems with premature solidification in the feeding system. As was discussed in Section 3.7.2 this turned out to be unavoidable. When a melt temperature of 710°C was used (to allow for the effects of a ceramic filter in the feed system) the premature solidification, although still present, was minimal.

The gross effects of the alloy additions on the melt and the immediate appearance of the castings was noticeable. When strontium was added to the melt, the surface of the melt was covered in a heavy oxide layer. In one (unsuccessful) casting, it was noticed that a large remnant of the strontium master alloy rod had not melted, but had floated on top of this oxide skin. Removal of dross from the feeding system was observed to be easy after a

strontium modified casting run. Conversely, the addition of titanium only, in the form of Tibor rods, resulted in a very clean melt surface, with only a thin oxide layer present. However, the increased nucleation promoted by the titanium resulted in larger blockages. The addition of either micro-alloying component also tended to result in less, or almost no, casting flash on the specimen.

The castings used in the study had a range of lengths. This was due to the inability to obtain fine control over the volume of melt injected into the die. Therefore the lengths of castings in an acceptable as-cast condition varied from a minimum of 120mm to approximately 180mm. This introduced another (unwanted) variable to consider. As will be discussed later, the smaller castings were associated with a noticeable change in the macrostructure of the castings.

5.1.2 Sand Castings

There was very little variation in the casting of the sand cast specimens, other than the comments already made about the fluidity and cleanliness of the melt.

5.2 MACROSTRUCTURE

The macrostructure, considered independently of porosity, observed in the sand castings was as expected: a chill zone was present at the outer extremities of the casting, with an equiaxed structure within the bulk of the casting. This was basically identical in all sand castings, as would be expected.

The macrostructure of the squeeze castings was more variable, appearing to be partially dependant on the volume (or aspect ratio) of the castings. The macrostructure, notwithstanding porosity, ranged from essentially featureless (as shown in Figures 5.1(a),5.1(c),5.1(d),5.1(j)) to small areas of segregation (Figures 5.1(g),5.1(i)), through to extremely segregated cross sections with the appearance of coring (Figures 5.1(b),5.1(e),5.1(f),5.1(h)). It was thought that this was independent of the location of the metallographic specimen, and was checked by taking sections at points below the

level of the section of interest. This was not applicable for the specimens with small casting volumes. However, even if the section is not representative of the entire specimen, it is still representative of a possible structure within that specimen.

The coring macrosegregation observed in castings 2, 4, 5 and 7, but not casting 6, had the appearance of a homogenised structure in the bulk of the casting, with a less altered, more conventional cast structure in the centre of the casting. The appearance suggests plastic deformation has occurred in the bulk of the casting at some stage in the casting process. This was then followed by liquid feeding into the centre of the casting to fill shrinkage. In casting 6, the reverse was true. The bulk of the specimen was of a conventional cast structure, with a small, circular region of deformed material at the centre of the casting. Micrographs of the circular region, along with the interface with the rest of the cast structure, are shown in Figures 5.23(e) and 5.23(f).

Casting 8 had an unusual form of macrosegregation, as shown in Figure 5.1(i). Moderately thick (two or three millimetres) curved regions of a slightly altered cast structure were present in the bulk of the casting. These were obviously remnants of a chill zone which had been broken off the die wall by the movement of the injection ram, and had floated into the bulk of the casting and were trapped there when the rest of the metal solidified. Micrographs of these chill regions are shown in Figures 5.25(e) and 5.25(f).

(a) Macro-photograph of squeeze casting 1. No obvious macrosegregation visible.

(b) Macro-photograph of squeeze casting 2. Coring segregation visible.

(c) Macro-photograph of squeeze casting 2A. No obvious macrosegregation visible.

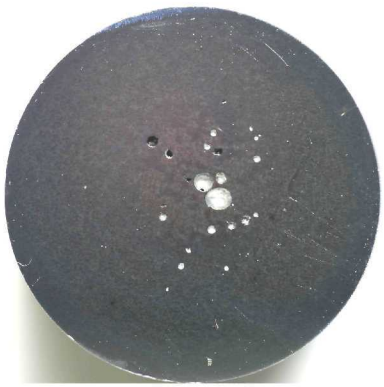

(d) Macro-photograph of squeeze casting 3. Excessive central porosity visible.

Figure 5.1 Macrographs of squeeze cast specimens. As polished, 2x magnification

(e) Macro-photograph of squeeze casting 4. Coring segregation visible.

(f) Macro-photograph of squeeze casting 5. Some coring segregation visible, along with thick chill zone and central macrosegregation.

(g) Macro-photograph of squeeze casting 6. Small region of central macrosegregation visible.

(h) Macro-photograph of squeeze casting 7. Coring macrosegregation visible.

Figure 5.1 continued.

(i) Macro-photograph of squeeze casting 8. Entrapped chill zone fragments are visible.

(j) Macro-photograph of squeeze casting 9. No macrosegregation visible

(k) Macro-photograph of sand casting 9. Typical appearance of sand castings.

Figure 5.1 continued.

5.2.1 Solidification Modelling

A finite element analysis (FEA) model of the solidifying melt in the squeeze casting die was developed to identify the likely solidification behaviour at the specified casting pressures and in a range of possible melt superheats. Although the exact behaviour of the casting would not be simulated, such modelling gave an indication of local solidification times and an indication of the solidification front as it travelled through the casting. This would provide some insight into the structure of the castings.

ABAQUS 6.5-1[59] was used to generate a static 2-D axisymmetric model of the die and melt immediately after injection of the molten metal into the die. Movement of liquid alloy was not considered in this model, only the transfer of heat through the melt and into the die during the cooling of the liquid, solidification of the eutectic alloy and the cooling of the subsequent solid material. The following assumptions were made:

- The heat transfer co-efficient was held to be constant during the solidification process.
- There was no relative movement of the die and the plunger. In reality, some movement is likely to occur due to shrinkage of the melt when cooling.
- The thermal conduction between the die, plunger and top plug was ideal. In practise, there would be thermal resistance due to any gap present.

Thermal and physical properties for the die, plunger and melt were obtained from the literature[1, 28, 52] and are listed in Table 5.1. The heat transfer coefficients used between the die and melt were obtained from Sekhar et al[28] and used in the finite element model to define a gap conductance function for unit area of the form:

$$q = k(\theta_A - \theta_B) \tag{5.1}$$

	Die/Plug/Plunger	**Melt**
Thermal Conductivity, Wm-1K-1	33.5	162
Density, kg m^{-3}	7800	2660
Latent Heat, J kg^{-1}	-	389000
Liquidus Temperature, °C	-	581
Solidus Temperature, °C	-	580
Specific Heat J kg^{-1}	684.6	963

Table 5.1 Thermal and physical properties used in the FEA solidification modelling.

where q is the heat flux per unit area crossing the interface from point A to point B , θ_A and θ_B are the temperature at each point and k is the heat transfer co-efficient.

Quadratic 2-D hexahedral elements were used in the FEA model. Initial models used different material properties for the plunger, plug and die. However initial results suggested that the relatively minor differences in specific heat and conductivity between H13 steel and grey cast iron were insignificant, so for computational simplicity the same material properties were used for all components in contact with the aluminium alloy.

The model was run with two variables. The first was to vary the heat transfer co-efficient to the levels associated with applied pressures of 50 MPa, 100 MPa and 150 MPa, as applied to the casting experiments. The initial temperature of the melt was also varied, to outliers of the possible temperatures before application of pressure, 700 °C (the temperature in the die) or 600 °C (e.g. after cooling in the runner system). By examining the output of these two models it was possible to obtain an estimate of the casting structure and solidification times. Figure 5.2 shows the geometry and the initial temperatures used in the analyses.

It can be seen in Figure 5.3 that the heat transfer between the die walls and the melt dominates any other heat transfer. The solidification away from the ends is essentially axisymmetric, with the centre being last to solidify. Therefore the centre should be the preferred location for any segregation and porosity observed. The centre should also have the most conventional cast appearance, notwithstanding any segregation effects.

Two sets of results for thermal behavior of the nodes highlighted in Figure 5.3 are shown in Figure 5.4(a) and Figure 5.4(b). They represent

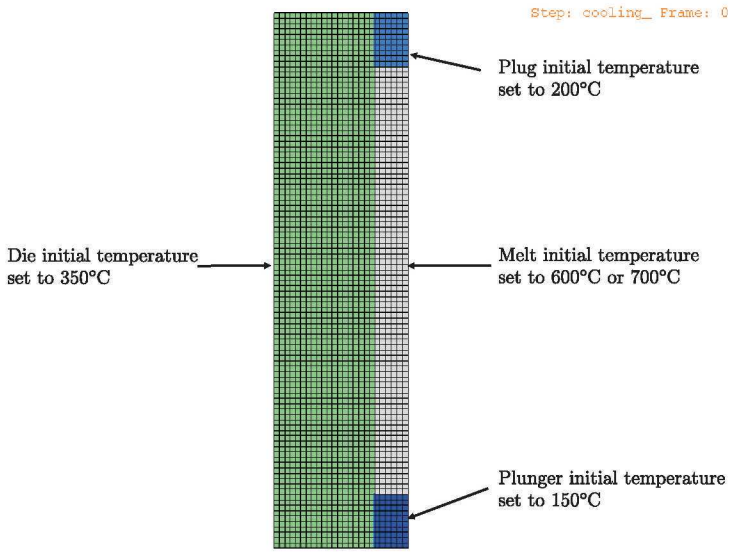

Figure 5.2 Geometry and initial conditions for the FEA solidification model. Model is symmetric through the centre of the melt.

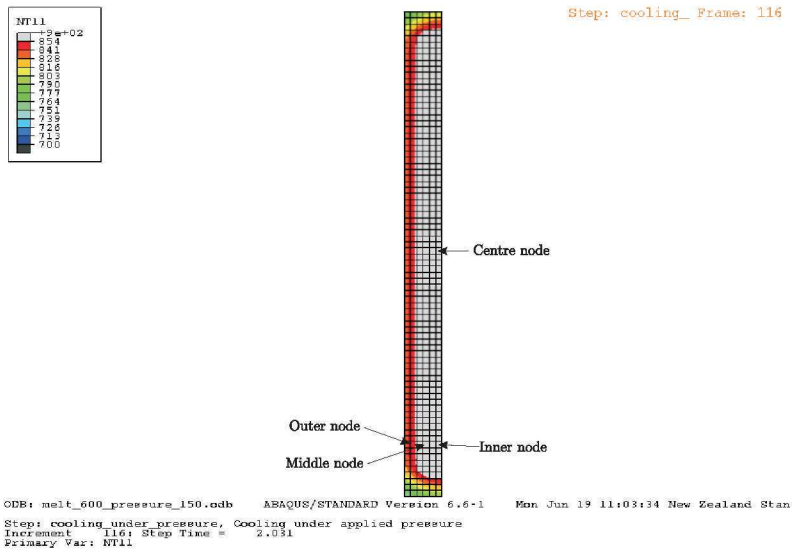

(a) Temperature contours two seconds after pressure application.

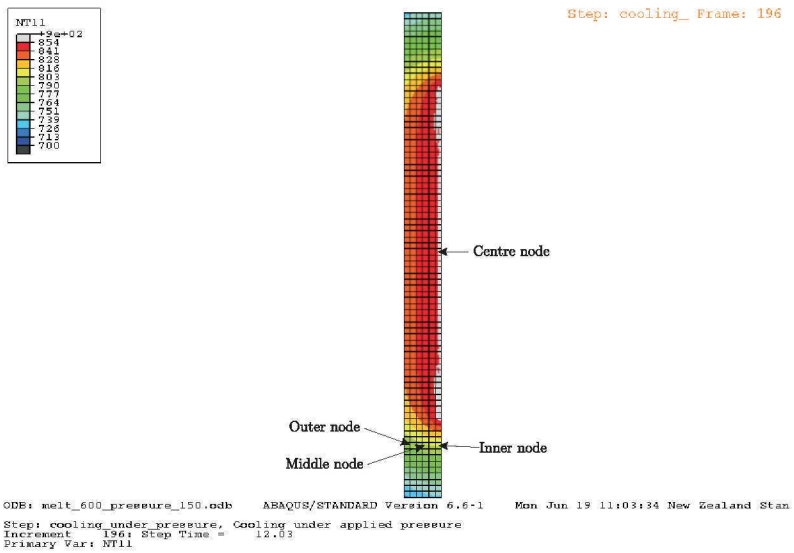

(b) Temperature contours twelve seconds after pressure application.

Figure 5.3 Temperature contours of FEA solidification model two seconds after pressure application. Pressure set at 50 MPa, casting temperature set at 700 °C. Grey contour represents molten metal. Temperatures given in Kelvin.

the two limits of the solidification times modelled. Maximum heat transfer, and hence cooling and subsequent solidification, was obtained at the highest casting pressure (150 MPa) and lowest melt temperature (600 °C). Conversely, the lowest casting pressure and highest melt temperature gave the longest solidification times.

5.3 POROSITY

All sand castings had extensive amounts of porosity. The shape and homogenous distribution, shown in Figure 5.1(k) suggested that it was mostly gas porosity. As the melt from which the specimens were cast was not actively degassed, and the furnace tended to have a humid atmosphere, the large amount of porosity was not surprising. The effect of alloy content on the porosity of the sand cast specimens can be seen in Figures 5.5, 5.6 and 5.7. As shown in Figure 5.5, the addition of strontium tended to slightly increase the measured porosity. Figure 5.6 shows a similar trend for titanium. When the total alloy addition is examined, the trend was repeated, as shown in Figure 5.7.

The average effect of the alloy additions is shown in Figure 5.8. This is a "Factor Effect" Taguchi diagram, and is used to identify the most beneficial factor, based on the average results for that factor. In this case it shows that for sand casting, the average effect of alloy addition was to increase the porosity.

For the squeeze cast specimens, in all but one specimen there was little gross porosity observable, and this reflected in the quantitative data. As shown in Figures 5.5, 5.6 and 5.7, there was no appreciable change in porosity with alloy additions in the squeeze cast specimens. The effect that pressure had on porosity is shown in Figure 5.9. A small decrease in porosity is shown with increasing pressure. It should be noted that the actual values (save for one, as discussed below) are quite small, but the variation in porosity was almost eliminated at the maximum casting pressure used.

The one squeeze cast specimen with noticeable porosity represented a dilemma in the Taguchi analysis for the squeeze cast specimens. The specimen, casting 3, had large, rounded pores grouped in the central region

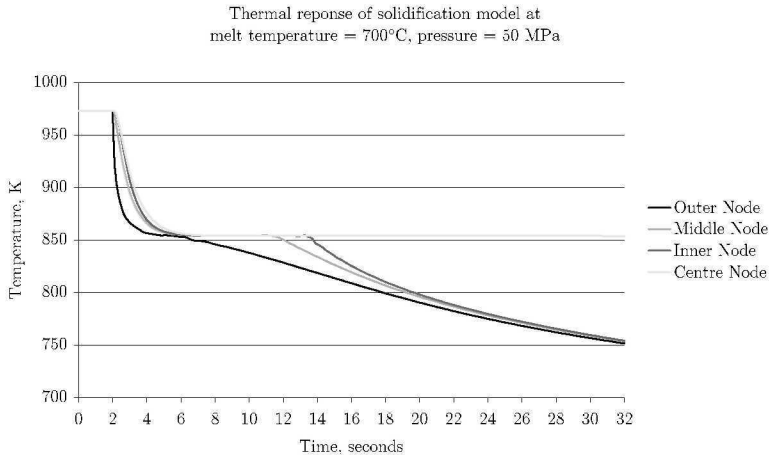

(a) Applied pressure of 50 MPa and a initial melt temperature of 700 °C.

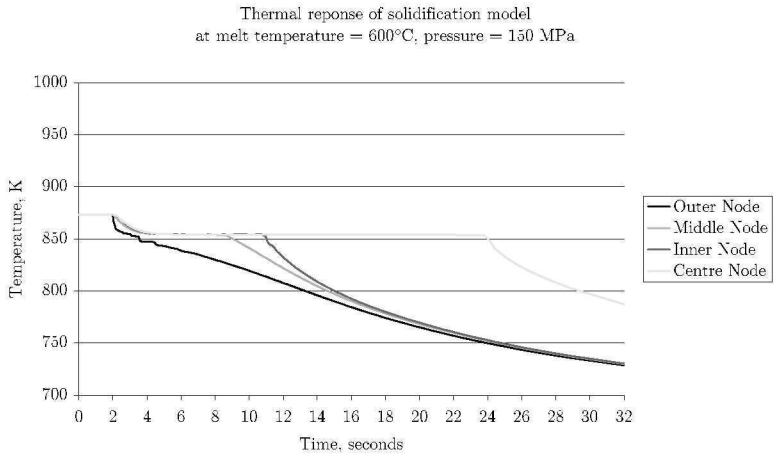

(b) Applied pressure of 150 MPa and a initial melt temperature of 600 °C.

Figure 5.4 Thermal behaviour of selected nodes in solidification model.

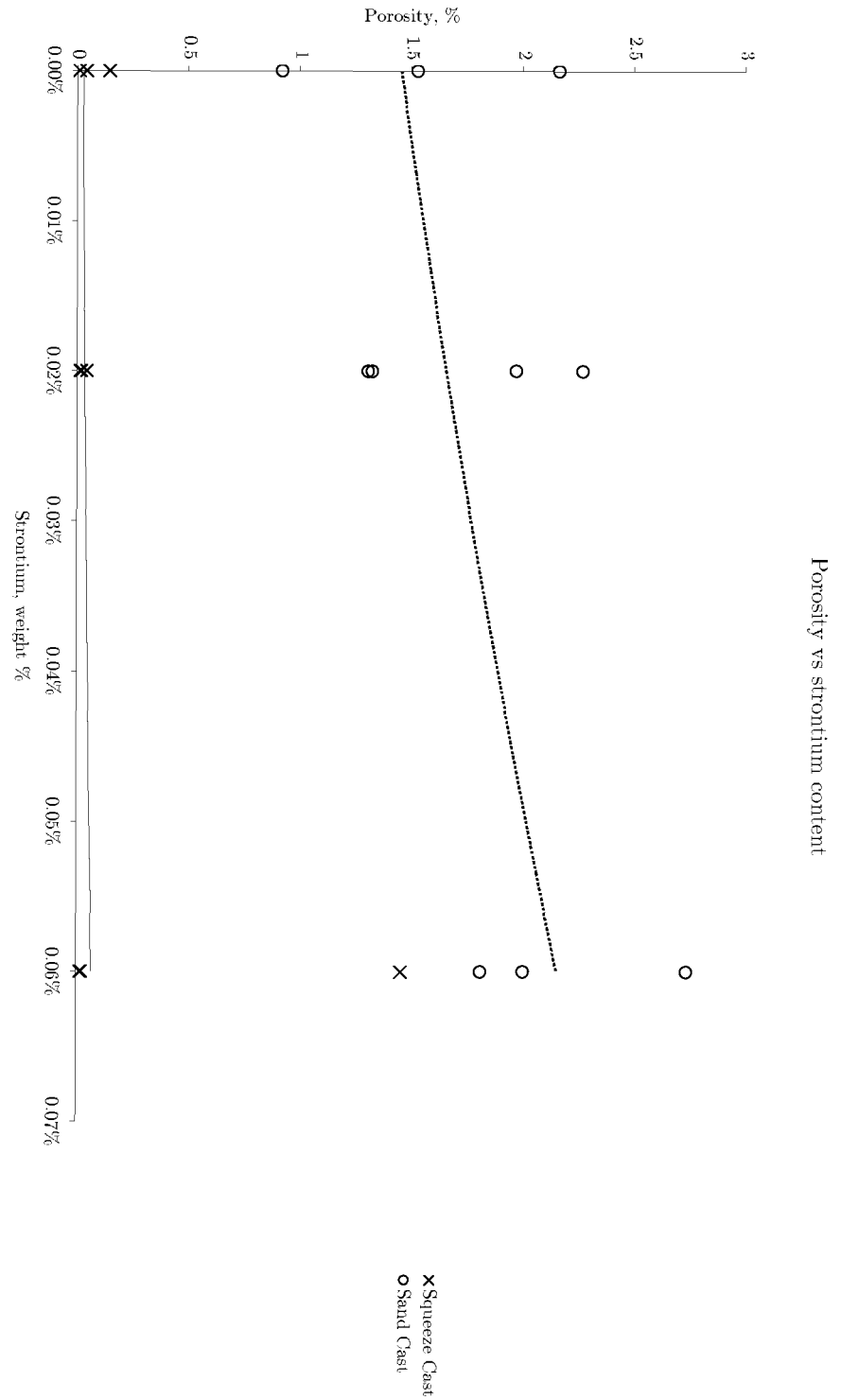

Figure 5.5 Measured gross porosity as a function of strontium content.

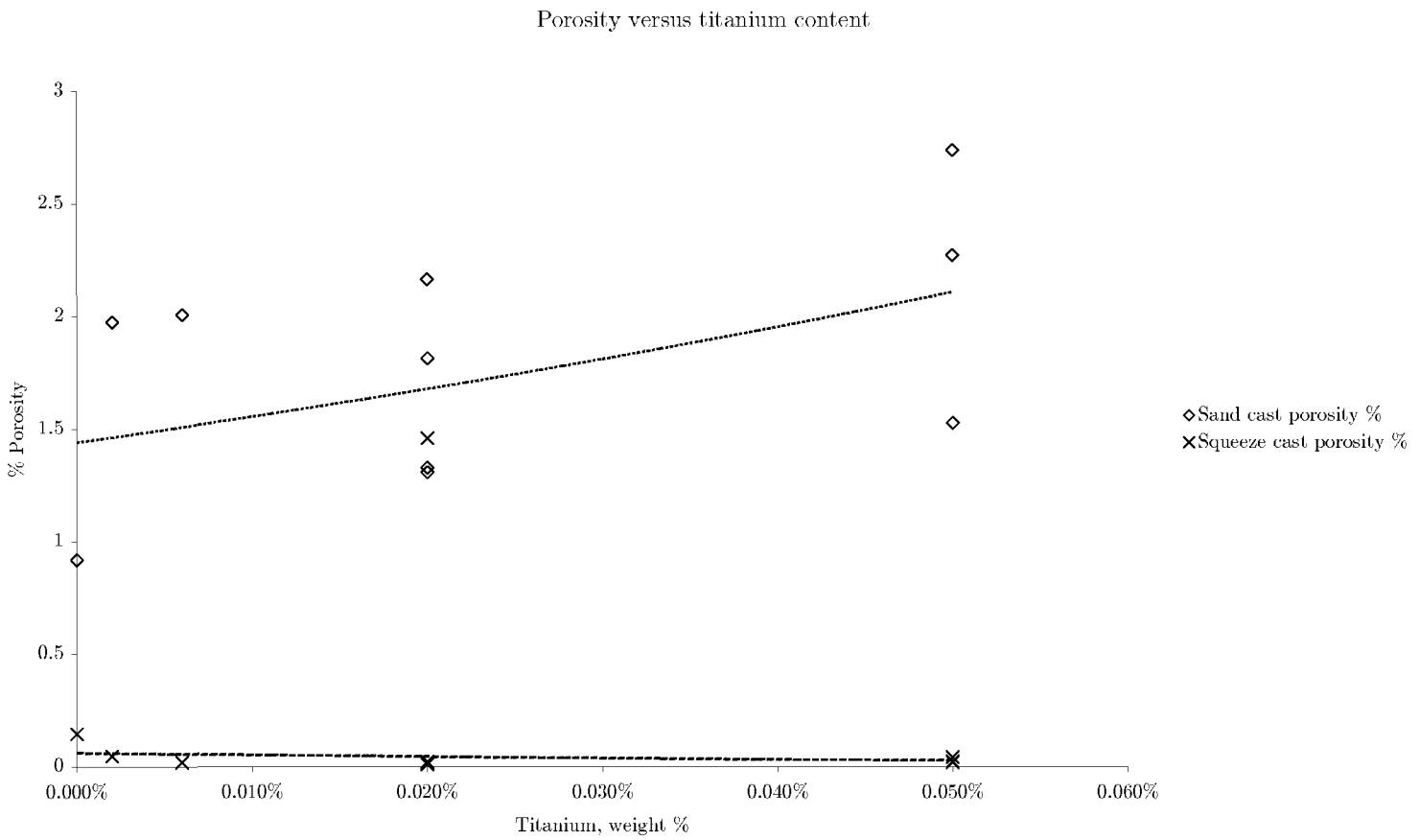

Figure 5.6 Measured gross porosity as a function of titanium content.

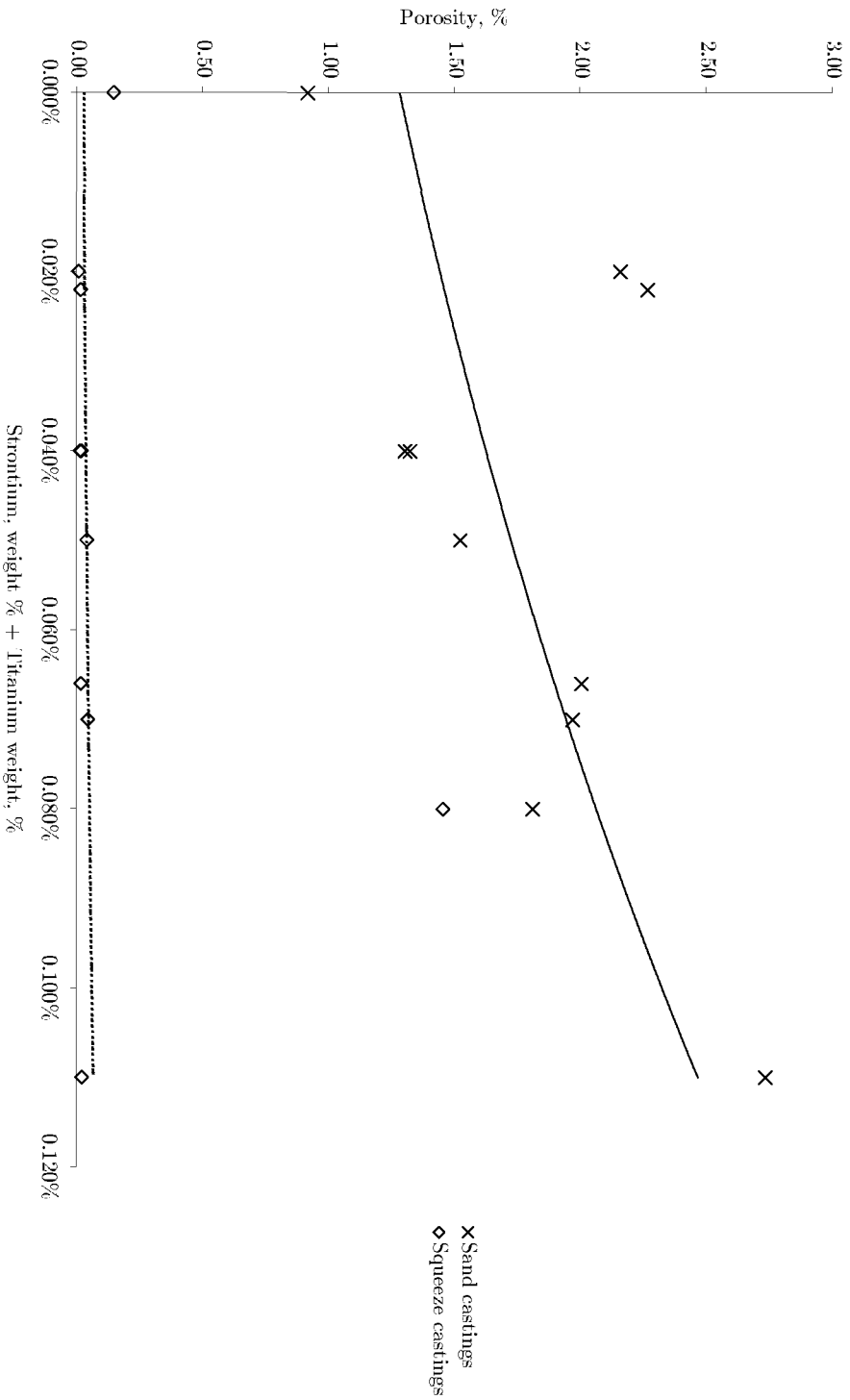

Figure 5.7 Measured gross porosity as a function of total alloy content.

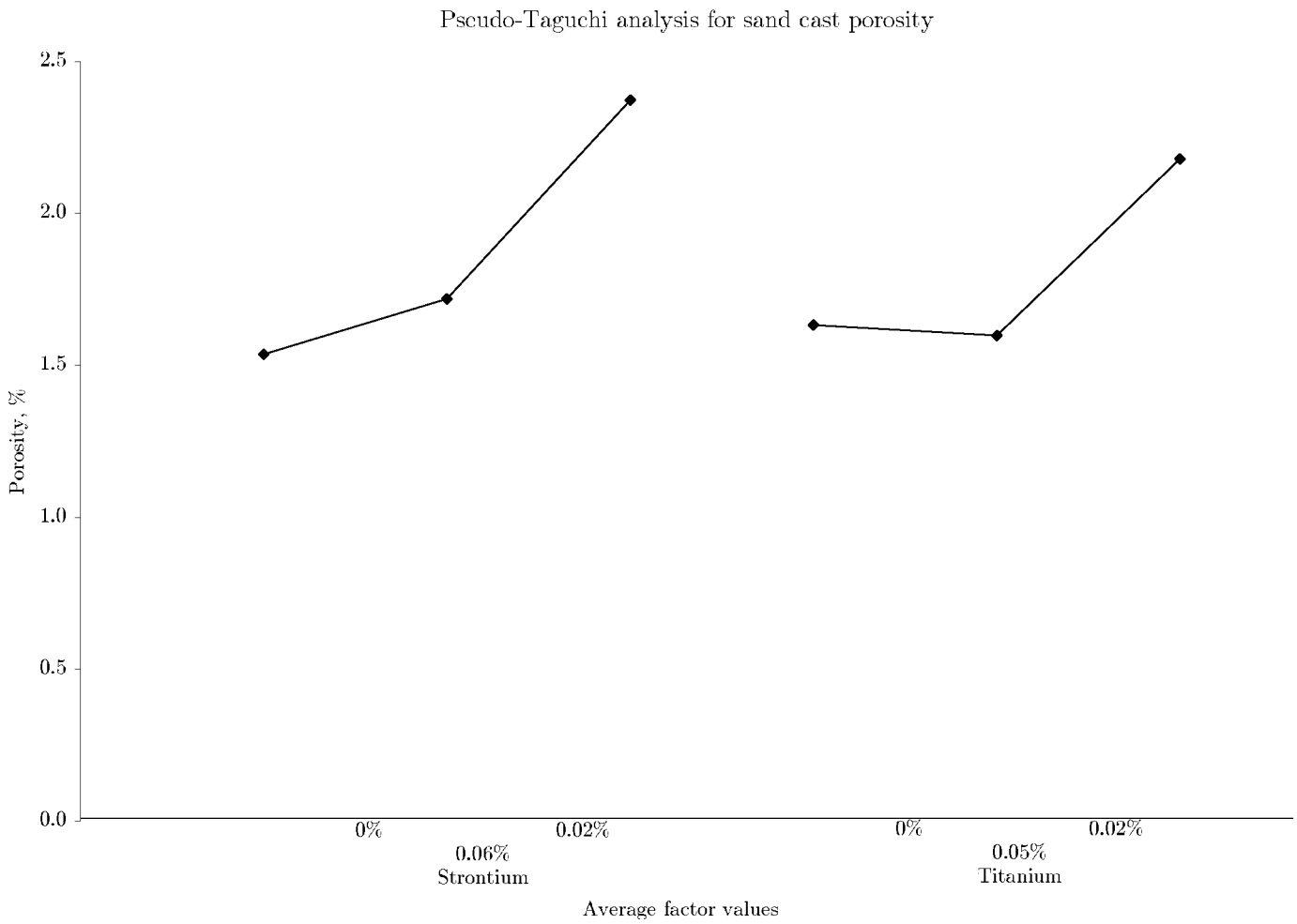

Figure 5.8 Average effect of alloy additions on measured sand cast porosity.

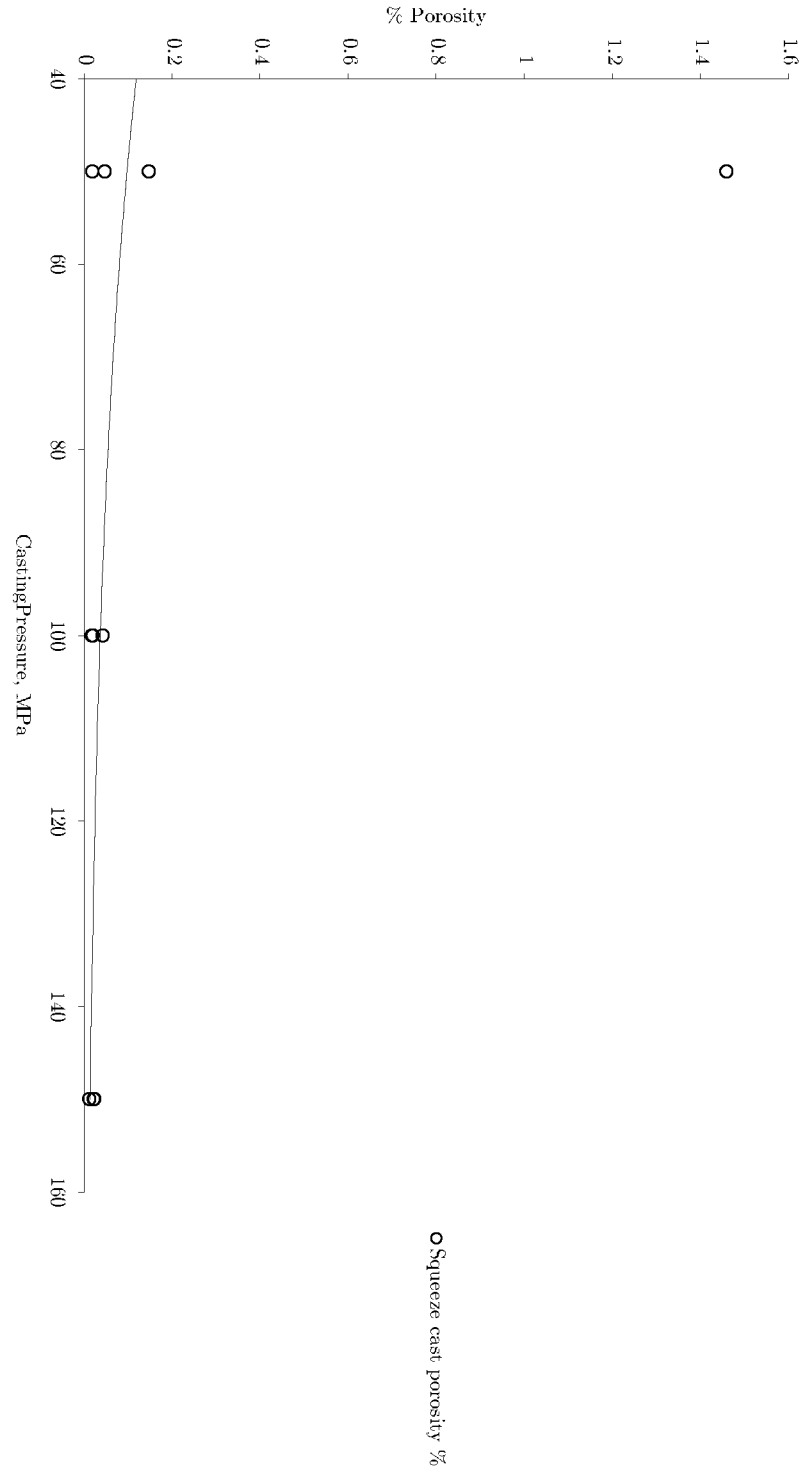

Figure 5.9 Measured gross porosity as a function of applied squeeze casting pressure.

of the casting. There is no porosity in the outer region of the casting, and it resembled a squeeze cast structure. This suggests that the porosity formed after the outer region solidified, under pressure, and started to accommodate the force being applied to the solidifying structure. This would possibly affect the pressure distribution into the remainder of the still solidifying metal. If the porosity was gas porosity, as is likely due to the morphology of the pores, then it is possible the remaining liquid metal in the centre of the casting was enriched with the gas and the decrease in applied pressure allowed it to rapidly come out of solution.

Because the difference in porosity was so extreme when compared to all the other squeeze cast specimens, the average values were distorted from the representative values. All other quantitative data obtained from the specimen was in accordance with the other squeeze cast specimens. Therefore, for the Taguchi analysis only, this particular specimen was not considered for the porosity analysis. This only affected the strontium and filtering factors, as there were excess data points available to incorporate into the average values for the titanium and pressure variables. The data point is shown on all other porosity related charts.

Therefore, examination of the Taguchi factor effect chart, as shown in Figure 5.10 reveals that minimal porosity is found with the maximum casting pressure used (150MPa), the maximum amount of strontium used (0.06% by weight), 0.02% by weight titanium addition and no filtration. However, the actual values are very small, and with the small number of samples, the variation seen near the minimal values of porosity is probably not significant.

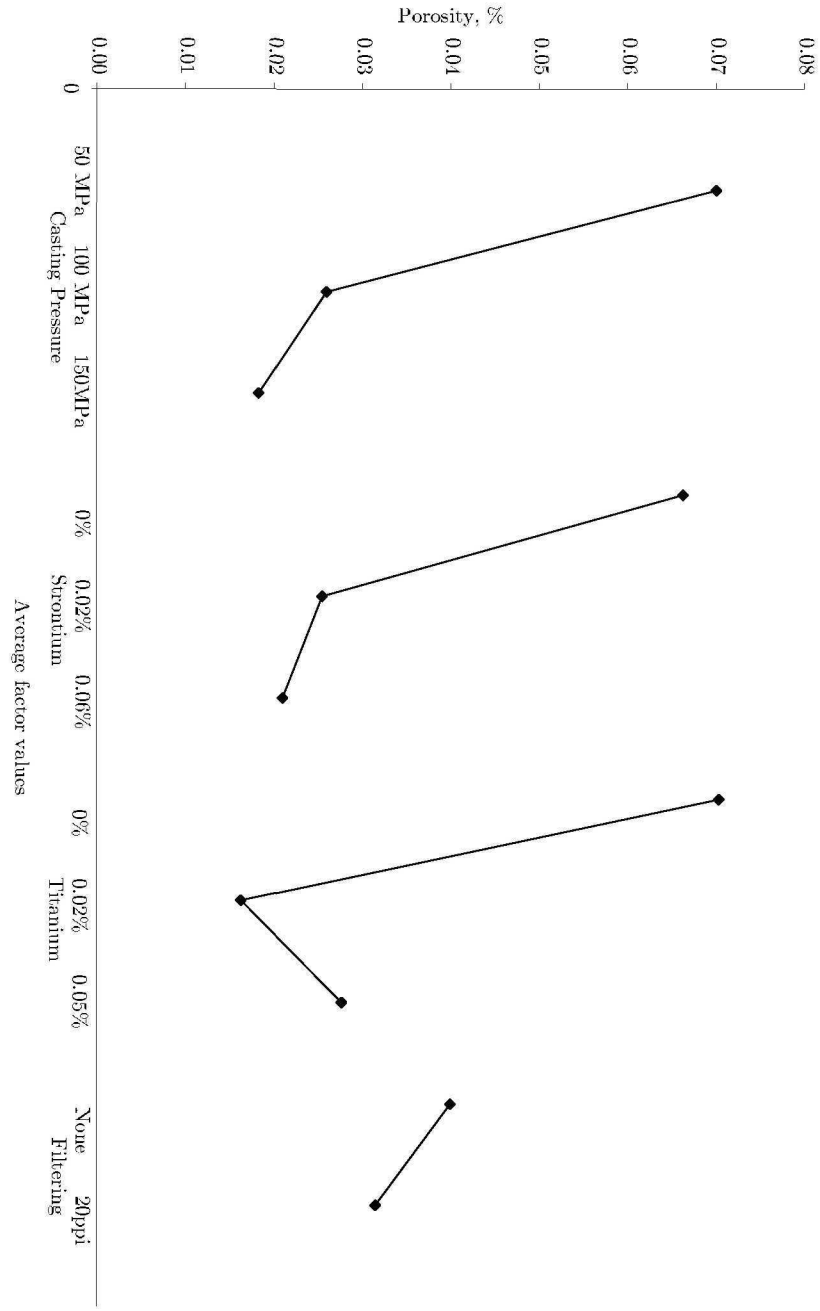

Figure 5.10 Average effect of experimental parameters on measured porosity.

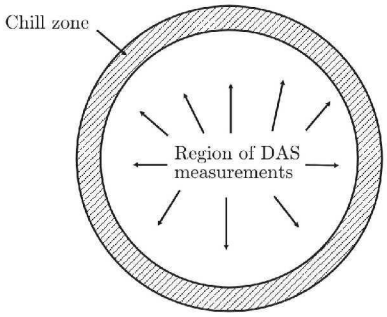

Figure 5.11 Schematic of casting cross section, show areas where dendrite arm spacing measurements were taken.

5.4 DENDRITE ARM SPACING

Dendrite arm spacing was measured in both sand cast and squeeze cast specimens. Since the solidification in the region adjacent to the wall was dominated by the heat transfer at the melt/mould interface, resulting in a localised chill zone, all measurements were taken in the bulk of the specimen away from this zone, as shown in Figure 5.11. In some sand castings, the actual composition of the alloy was, generally, slightly hypereutectic, with limited regions of primary aluminium. Suitable measurements were difficult to obtain in such specimens, and therefore the sample size was low. In squeeze castings, the dendrite arms tended to be shorter, and the spacing and width of the secondary arms was variable. In the squeeze specimens that had the deformed, core-like segregation, the dendrites themselves were distorted. Measurements were taken off the least distorted dendrites, and preferably tangential to the deformation lines. Unless no other suitable dendrites were obvious, no dendrites were measured at the centre of the castings.

It is mentioned by Vander Vort[57] that for alloys with a high eutectic content, dendrite cell size is a preferable measurement over the secondary dendrite arm spacing. However, no exact method or definition of the cell size was given. Assuming it is represented by the diameter of the secondary dendrite arm, measurements were taken such that both the dendrite arm spacing and dendrite arm diameter were the same, i.e. the width of the dendrite arms was the same distance as the inter-arm spacing. This allowed comparison to existing data (i.e. [1]) for both secondary dendrite

arm spacing and dendrite cell size.

It would appear from Figure 5.12, that the addition of strontium decreases the dendrite arm spacing, in both the sand castings and the squeeze castings. The trend is slight, especially in the squeeze cast specimens, but allowing for the obvious outlier, the effect is noticeable, and more pronounced in the sand cast specimens. Also noticeable is the overall reduction in dendrite arm spacing between the sand cast and squeeze cast specimens.

Figure 5.13 shows that, with the addition of the Tibor grain refiner, there is a small but noticeable increase in the dendrite arm spacing for the sand castings. This is an unexpected result, as it is generally held that dendrite arm spacing is analogous to the grain size. However Hu and Li[60] report a similar effect for a permanent mold cast Al8Si3Cu alloy, where the dendrite arm spacing decreased upon the addition of Ti, and then gradually increased with further Ti additions. It should be noted that the eutectic colony size is the actual equivalent of a grain size in this alloy, not the secondary dendrite arm spacing of the primary aluminium dendrite. The squeeze cast specimens showed essentially no change in dendrite arm spacing with increasing titanium content.

The average effects on the squeeze castings are shown in Figure 5.14, and Figure 5.15 shows the effect on the sand cast specimens. For the squeeze cast specimens, the most noticeable effect is that of strontium, clearly showing a decrease in the average secondary dendrite arm spacing with an increase in strontium addition. The addition of titanium also reduces the average dendrite arm spacing, although to a lesser extent. There is no significant change in dendrite arm spacing arising from increasing casting pressure or filtration. That casting pressure had no effect was unexpected. It has been shown that an increase in pressure increases the heat transfer rate, and therefore the rates of cooling and solidification[27]. Dendrite arm spacing has also been widely shown[1, pp537-538] to be strongly dependant on cooling rate.

Although the cooling or solidification rate was not directly measured, the studies mentioned above[1, pp537-538] and modelling of the solidification (see Section 5.2.1) can be used to obtain an estimate of these factors. Graphical data shows a logarithmic relationship between dendrite arm spac-

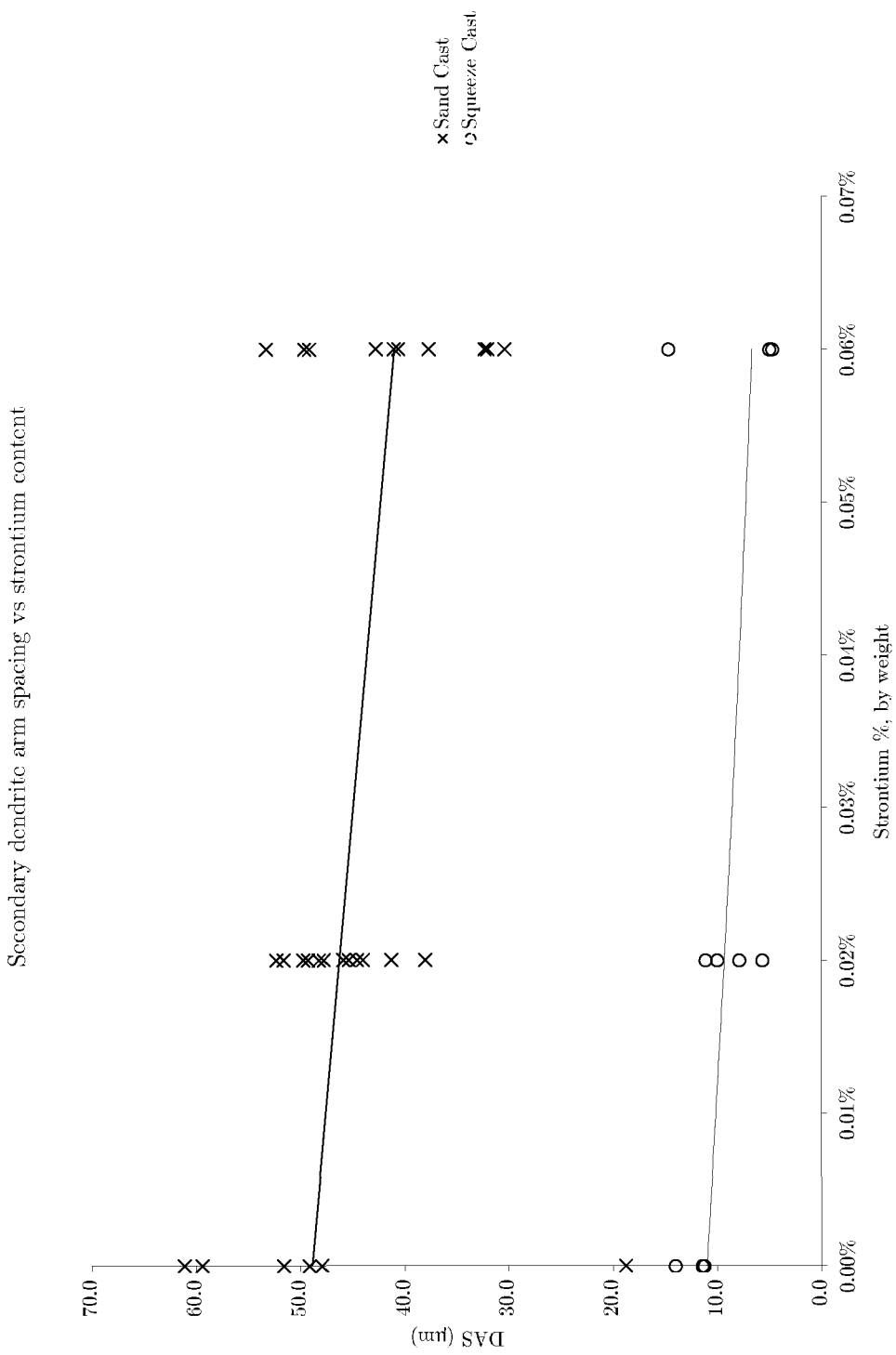

Figure 5.12 Measured dendrite arm spacings as a function of strontium content.

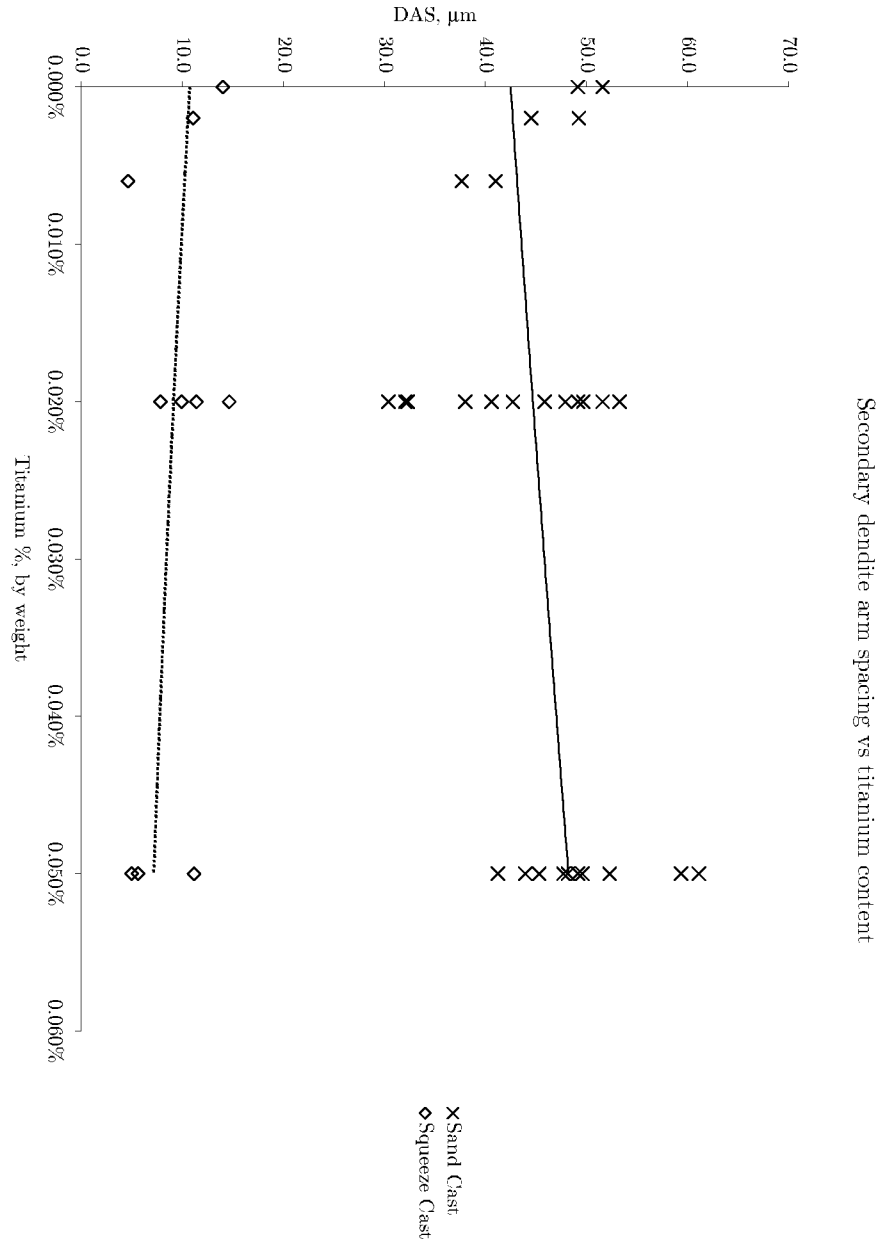

Figure 5.13 Measured dendrite arm spacings as a function of titanium content.

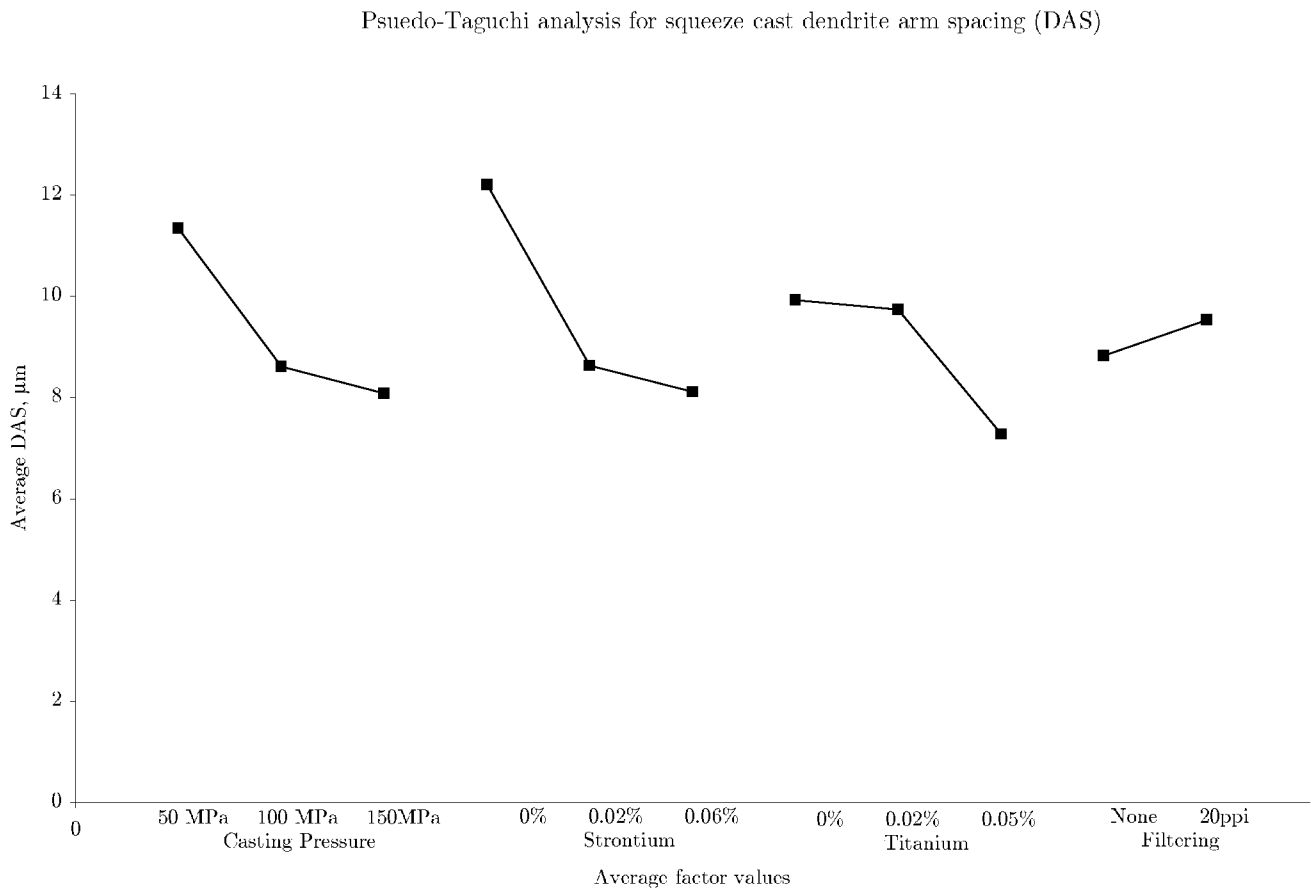

Figure 5.14 Average effect of experimental parameters on measured dendrite arm spacings of squeeze castings.

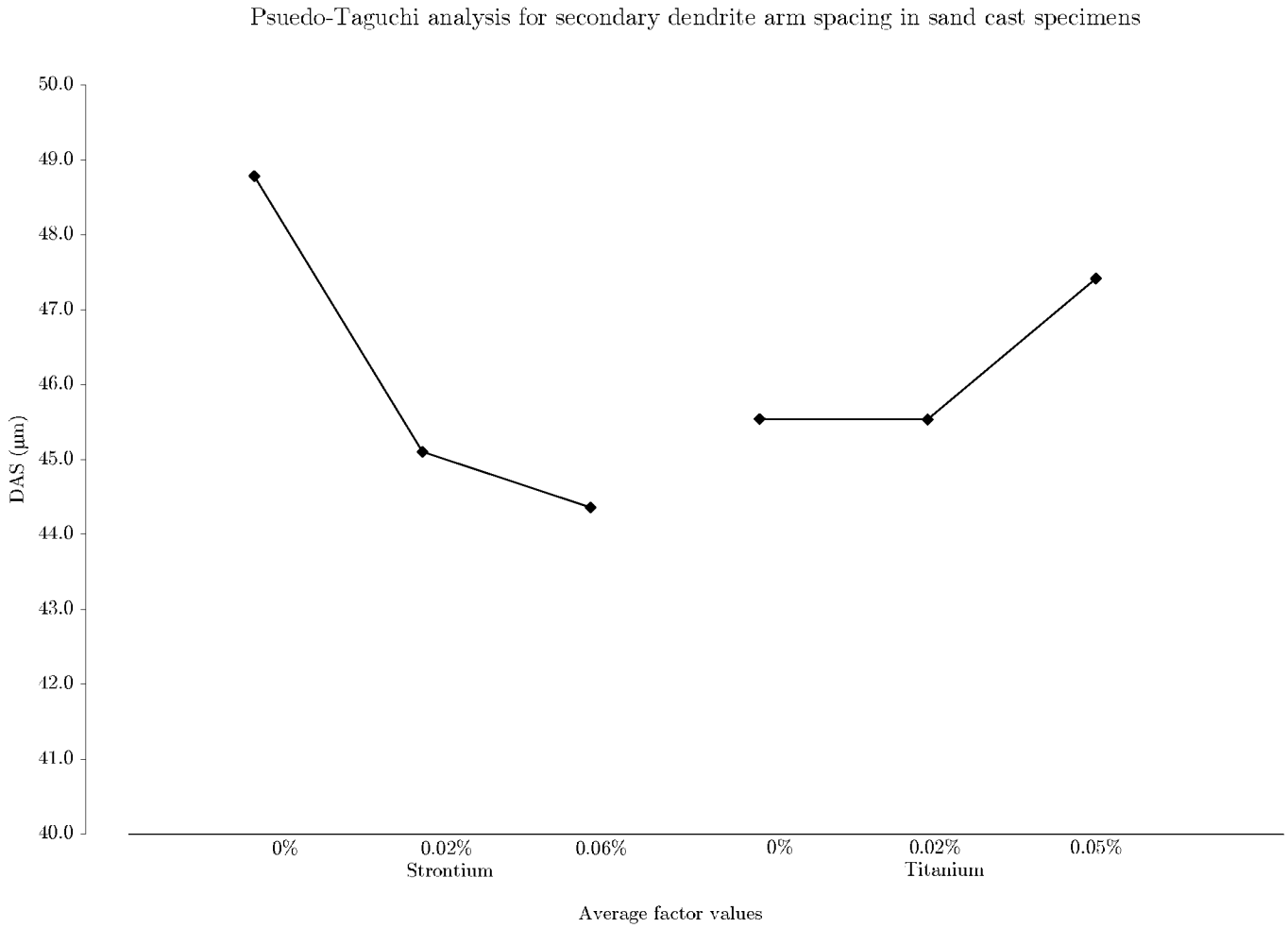

Figure 5.15 Average effect of experimental parameters on measured dendrite arm spacings of sand castings.

ing and local solidification time for a variety of aluminium silicon alloys. The data suggests that dendrite arm spacings of between 40 and 60 micrometres, as observed in the sand cast specimens, are associated with local solidification times of between 40 to 100 seconds. This matches well with observations made during the casting of the sand castings. The dendrite arm spacings measured in the squeeze cast specimens (between 12 and 8 micrometres) are below the minimum values given in the chart. The smallest dendrite arm spacing given, 20 micrometres, is associated with a local solidification time of approximately 4 seconds. Squeeze castings of larger diameters have measured solidification times, from the onset of nucleation to a drop from the eutectic temperature, of 8 to 12 seconds, depending on pressure, and location in the casting[27, p275]. It appears reasonable that solidification for these smaller specimens occurs in less time, as also indicated by the FEA modelling results discussed in Section 5.2.1.

Similar data exists for cooling rates as a function of dendrite cell size. Notwithstanding the confusion over the actual definition of dendritic cell size versus secondary dendrite arm spacing (ASM Handbook, Volume 9: Metallography and Microstructures[56] appears to use the two interchangeably), the measured values for the sand castings are associated with cooling rates of 0.5°C to 1°C. Whereas the measured arm spacings/cell sizes for the squeeze castings are associated with cooling rates of 10°C to 20°C.

5.5 OPTICAL MICROSCOPY

Extensive micrographs were taken, to obtain both quantitative data, and to illustrate qualitative comments on the appearance of the microstructure. The general microstructure of each squeeze casting was taken, along with high magnification images of areas of interest, such as the eutectic structure and intermetallics. The micrographs are shown in Figures 5.17(a) through 5.26(d).

Most of the images were taken with brightfield illumination, in the as-polished condition. Contrast between the phases was readily visible, and was enhanced with the digital camera capture software. This was suitable for identification of all the major constituents. Grain/eutectic colony

boundaries were not visible at all when the sample was viewed with a conventional microscope. Other illumination methods used included cross polarised light and differential interference contrast. Some intermetallic particles were highlighted in cross polarised light, allowing them to be separated from eutectic silicon via a colour difference. Differential interference contrast highlighted the polishing relief between the soft aluminium, the slightly harder eutectic and the much harder primary silicon crystals.

5.5.1 Primary Phases

The microstructure of the sand cast specimens was typical of that for a eutectic aluminium silicon alloy. At low magnifications, the structure consisted of widespread primary aluminium dendrites, the aluminium silicon eutectic and some non-eutectic silicon crystals. The amount of primary aluminium dendrites ranged from approximately 18% (by histogram analysis) with no, or sparsely distributed, non-eutectic silicon visible e.g. Figure 5.20(a), to almost no aluminium dendrite structure visible, and approximately 4% non-eutectic silicon visible, e.g. Figure 5.25(a). In the last structure (Figure 5.25(a)) there are regions of aluminium distinguishable from the eutectic, but the coarseness of the eutectic is such that there no way to be sure of the exact amount. In other structures, e.g. Figures 5.17(a),5.21(a),5.23(a), both primary aluminium and non-eutectic silicon have formed, due to local solidification conditions. Primary silicon was not visible, or sparsely distributed in the castings which were highly modified, and more common in the castings which were unmodified and had the higher levels of grain refiner added.

The squeeze cast structures that had conventional as-cast microstructures were different to the sand cast structures - any primary phase was noticeably smaller. This was quantified for the primary aluminium dendrites secondary arm spacing, in Section 5.4. The length of the primary dendrite arms also appeared to be shorter. Histogram analysis of the cross sections shows dendrite amounts ranging from 20% to 34%, indicative of a significant eutectic shift. Any non-eutectic silicon crystals were visibly smaller and there was a change in the common morphology of some the

non-eutectic silicon crystals. Along with the large, equiaxed silicon crystals in the section of interest, there were needles (possibly plates in three dimensions) of non-eutectic silicon. Both forms are visible in Figures 5.18(a), 5.19(a), 5.23(b), 5.25(b) and 5.26(b). The total amount of non-eutectic silicon formed did not significantly change as the area on the micrographs of the silicon crystals remained around 1%. The non-eutectic silicon changed to a more numerous distribution due to the increased number of smaller crystals. As can be seen, in any one region, both primary aluminium and non-eutectic silicon have formed during solidification. This, plus the apparent eutectic shift, indicates non-equilibrium solidification.

5.5.2 Eutectic Structure

The eutectic structure in the sand castings varied from a unmodified structure (e.g. Figures 5.17(a), 5.23(a), 5.25(a) to a fully modified structure e.g. Figures 5.20(a), 5.22(a), 5.24(a), as a function of any strontium added. From the appearance of the eutectic in the sand cast specimens, it would appear that the chosen addition for peak modification, 0.02% strontium by weight, was insufficient for peak modification. In the alloys with the 0.02% addition, the eutectic was generally modified in discrete regions and tended towards full modification at the centre of the casting, due to solute enrichment of the strontium via a segregation mechanism during solidification. Examples are shown in Figure 5.19(a), where there is a large area of modified eutectic, towards the centre of the casting, and in Figure 5.21(a), where smaller patches of partial or fully modified eutectic are distributed evenly through the micrograph.

The appearance of the sand cast eutectic structure at high magnifications correlates with the expected behaviour. Unmodified eutectics had coarse, acicular silicon, present in large, irregular networks, as seen in Figure 5.23(c). Modified eutectics had the eutectic silicon in the form of a regular, fibrous structure (rounded particles in a 2-D section), as shown in Figures 5.20(c),5.22(c). The size of the silicon particles, or plates, was dependant on the location in the casting - the finest structure tended to be at the centre of the casting, presumably where solute concentration of the modifier (or

any other impurity) was highest.

In almost every case, the appearance of the eutectic structure in the squeeze castings was finer than that of the sand castings. In squeeze castings with no modifier addition, the morphology was similar in appearance to the sand castings, but at a smaller scale. This can be seen by comparing Figures 5.17(c) and 5.17(d). This was unexpected, as at the rapid solidification rates assumed to have occurred, the eutectic silicon has been described in the ASM Aluminium Alloys Handbook as having a fibrous morphology[1, p535]. This source states that the transition from flake silicon to fibrous silicon occurs at growth velocities of between 400 to 800 micrometres per second. The average growth velocity, as indicated by the measured secondary dendrite arm spacing was no less than 1000 micrometres per second (see Section 5.4).

When strontium was added to the melt, the appearance of the eutectic in the squeeze castings changed from the flake silicon to a mixture of fibrous and angular silicon. With low strontium modification, this occurred in patches in the microstructure. For the high strontium castings, all but one had an altered microstructure, but in areas which were recognisably "conventional", e.g. the centre of casting 5 (Figure 5.22(h)) and the bulk of casting 3, the modification was essentially complete. Casting 3 had many variations of the modified structure, all displaying the angular eutectic silicon associated with quench modification, as shown in Figures 5.20(d) and 5.20(e). A very fine eutectic, with no angular eutectic silicon, was present at the centre of casting 3, as shown in Figure 5.20(f).

The altered microstructures present in castings 2, 4, 5 and 7 were presumed to be from deformation of the solidifying structure during and/or immediately after solidification, and appeared to be a function of casting volume. The primary aluminium dendrites, if they were discernable, were distorted with a skewed appearance, typically shown in Figures 5.19(e), 5.22(g) and 5.24(b). There were also large bands of silicon free aluminium which where presumably highly distorted remnants of primary aluminium dendrites.

The appearance of the eutectic silicon did not resemble that of a typical cast structure. In two dimensions, the silicon particles appeared to be bro-

ken up and "homogenised", supporting the possibility of plastic deformation having occurred. Non-eutectic silicon, in the form of polyhedral crystals, did not seem to be affected as in Figure 5.24(g). Towards the centre of the casting 5, the structure was less deformed, and some typical eutectic structure was observed, as shown in Figure 5.22(h). Castings 2, 4 and 7 did not, and tended to have a mixed structure of the homogenised eutectic separated by irregular layers of aluminium. This is shown in Figures 5.19(b) and 5.24(f).

5.5.3 Modification Level Assessment

The modification of the aluminium silicon eutectic, as stated previously, has the greatest effect on the physical properties of the alloy. Quantification of the modification would be of use in the analysis of these casting methods used. An approach that can be used is a comparison against standard images. This is easy, but it is not fully quantitative. The American Foundrymen's Society modification scales are an example. Micro-sections are rated against six micro-structures, from 1 (unmodified) to 6 (fully modified). Shilvock[2] proposed a modification to this scheme to allow for extremely coarse unmodified eutectic (given a rating of 0) and to allow for partially and fully over-modified structures (ratings of 7 and 8).

Quantative image analysis can be performed, but there are limitations. Over-modification and gross inhomogeneity of the modification level of the eutectic is difficult to automatically recognise with automated image analysis. Automated image analysis would be limited to measurement of particle size and shape within an area of homogenous modification. One method to quantify modification would be to use a point count grid on a representative structure, and assign a modification rating to each point which falls within a eutectic region. The mean and deviation of such a count would give a good indication of the modification level and variation within the casting.

Another obstacle in the quantification of modification, especially for the squeeze castings, is that at different magnifications, the appearance of the eutectic is different. This was observed for squeeze cast specimens with low modifier additions. At low magnifications, the eutectic structure appears to

be fully modified, but at higher magnifications, retains the flake structure of unmodified eutectic silicon.

5.5.4 Intermetallics

The intermetallics observed optically in the sand castings could be grouped into four morphologies:

Grey needles These were present in all sand castings. The morphology and distribution suggested an initial identification as βAlFeSi. In unmodified or partially modified castings, these were often seen in conjunction with small areas of modified eutectic silicon. This suggests some solute segregation occurring during the solidification of the eutectic colonies. The last regions to solidify have the highest concentration of impurities, which either affect the growth of the eutectic silicon or form intermetallic particles. Such regions can be seen in Figures 5.18(e), 5.19(c) and 5.19(d). In highly modified structures, there was a definite distribution of the needles along the boundaries of eutectic colonies and at the interface between eutectic colonies and aluminium dendrites. Examples are shown in Figures 5.22(d) and 5.24(a). In these highly modified structures, the needle-like intermetallics were the dominant intermetallic visible. The approximate sizes ranged from 10-200 micrometres in length and 1-5 micrometres thick.

Grey scripts In unmodified or partially modified castings, the most commonly observed intermetallic took the form of a grey complex dendrite or script. This was consistent with αAlFeSi. The sizes were irregular, ranging from small, simple script structures 5 micrometres or smaller, to complex script structures 30 to 50 micrometres in diameter. The locations of the intermetallics were widely distributed, being commonly associated with aluminium dendrites, small patches of modified eutectic and coarse eutectic. Small intermetallics with this morphology were also associated with coarse eutectic silicon. These script intermetallics were rare in the highly modified castings. Examples are shown in Figures 5.17(c), 5.18(c), 5.19(d) and 5.21(c).

Irregular grey blocks More apparent in highly modified sand castings, it was thought these fairly rare intermetallics were another form of αAlFeSi or βAlFeSi, or possibly $AlFe_3$[1, p490]. As they tended to be associated with βAlFeSi, is was thought likely to be βAlFeSi plates orientated at a smaller angle to the section plane.

Small blue-grey blocks These intermetallics were only noticed in highly modified sand cast structures, and were initially thought to be embedded silicon carbide particles from the grinding process, as they were hard to distinguish from chunky eutectic silicon. However, they did resemble Al_2SrSi_2 as mentioned in McIntyre et al.[9]. As they were only seen in castings with high levels of strontium additions, this was a feasible identification. The intermetallics were approximately 5 to 10 micrometres in size, and were distributed either along the eutectic colony boundaries or in the bulk of a eutectic colony. Once such intermetallic is shown in Figure 5.16.

In contrast to the wide range of types and sizes of intermetallics in the sand castings there were only two intermetallic morphologies discernable in the bulk of all squeeze castings. A small grey script, similar in morphology to the smaller αAlFeSi in the sand castings, was randomly distributed in and around the eutectic cells. An example of such intermetallics is shown in Figure 5.17(d). In squeeze castings with the high strontium additions, needle-like precipitates at the boundaries of eutectic colonies were obvious towards the centre of the castings. This was only observed if the central region of the casting had a conventional cast structure (i.e. no deformed or segregated appearance). Figures 5.20(f) and 5.22(h) are examples of this.

Further examination and identification of the intermetallics present in the castings was carried out using electron microscope techniques, as discussed in Section 5.7.

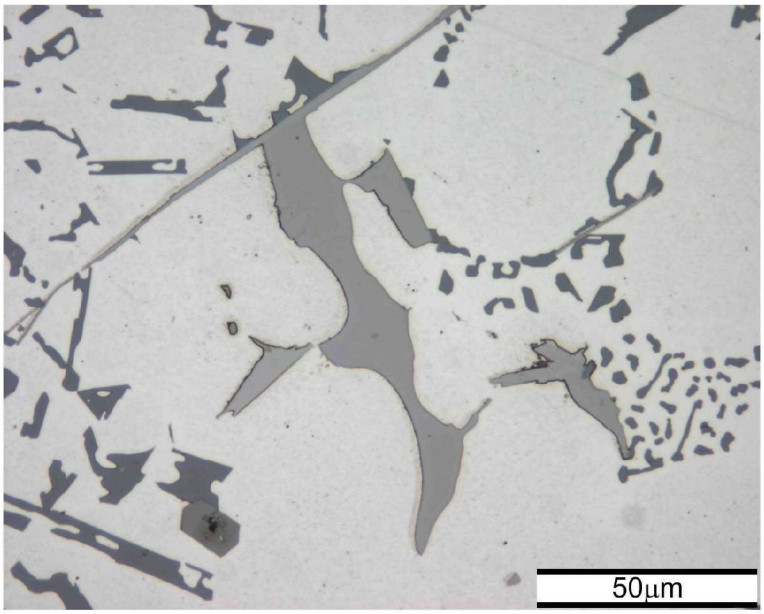

(a) Optical image of sand cast precipitate field, 500x. Strontium precipitate at lower left

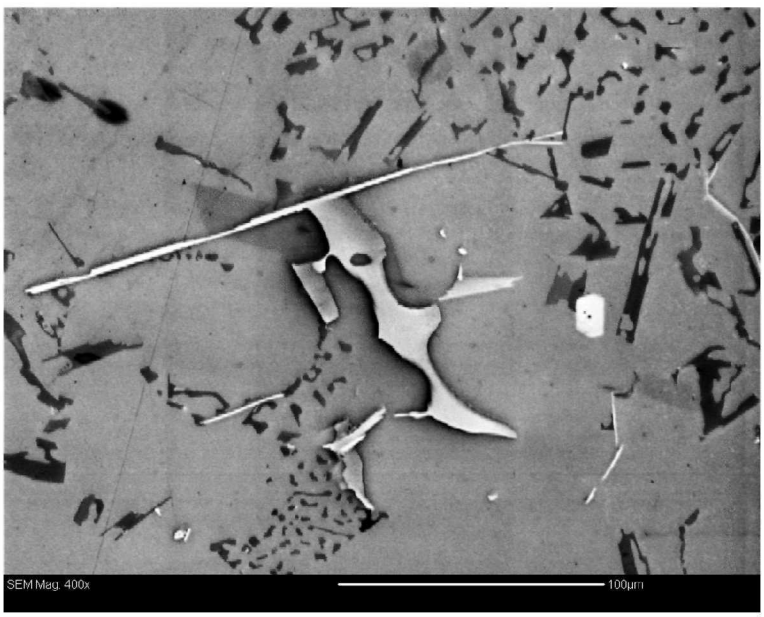

(b) Back-scatter electron image of sand cast precipitate field. Bright strontium precipitate at centre right

Figure 5.16 Precipitate field in sand casting 7, showing large precipitates containing iron (α or β AlFeSi) and one small blocky precipitate containing strontium (Al_2SrSi_2).

5.5.5 Representative Micrographs

This section contains optical images taken of all the cast specimens, to illustrate the points covered in this discussion. Sand casting micrographs are compared with squeeze cast micrographs of the castings with the exact composition and casting temperature, with the only nominal difference being the different die material and applied pressure.

The images are generally at two magnifications: 50x to show the large scale microstructure, e.g. coarse eutectics and intermetallics, and 1000x magnification to show details of the microstructure. Most figures will display a sand cast structure above an equivalent squeeze cast structure at the same magnification. This allows a direct visual comparison between the microstructures.

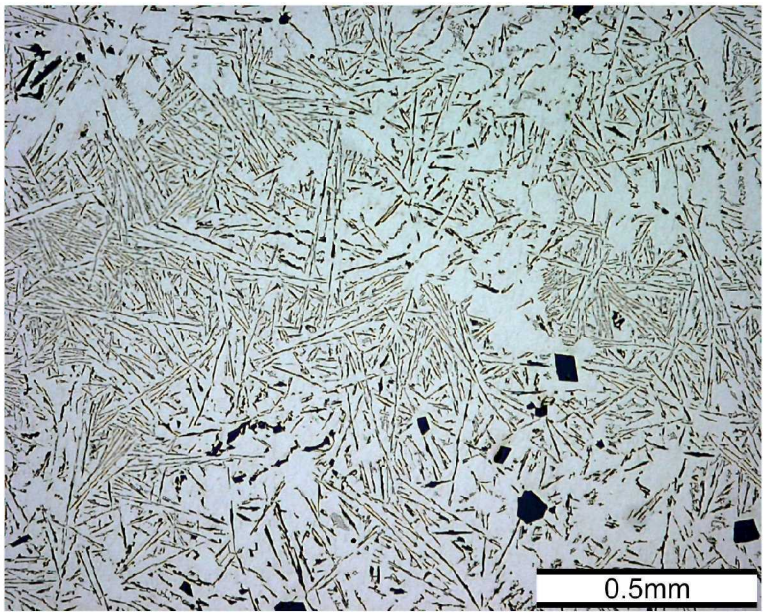

(a) Sand cast unmodified and unrefined Al12Si eutectic alloy. As polished, 50x magnification.

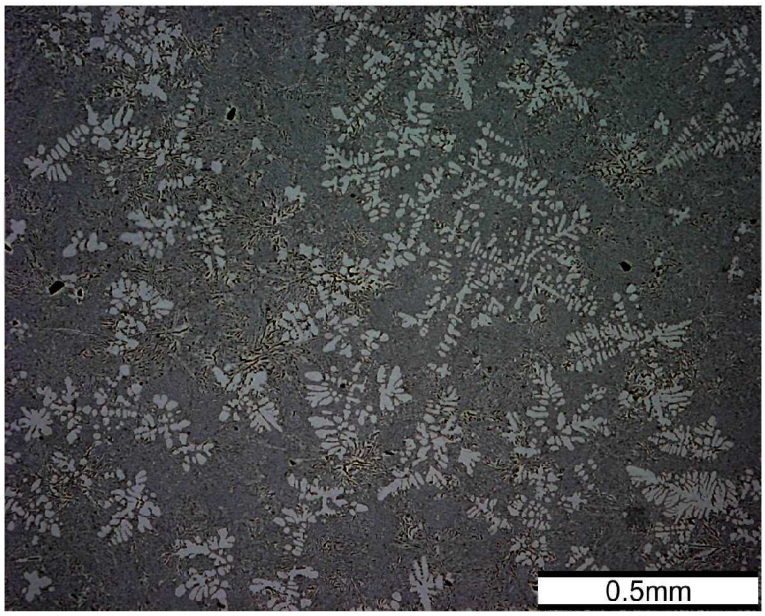

(b) Squeeze cast unmodified and unrefined Al12Si eutectic alloy. As polished, 50x magnification.

Figure 5.17 Experiment 1 - an unmodified eutectic alloy, sand cast and squeeze cast at 50 MPa.

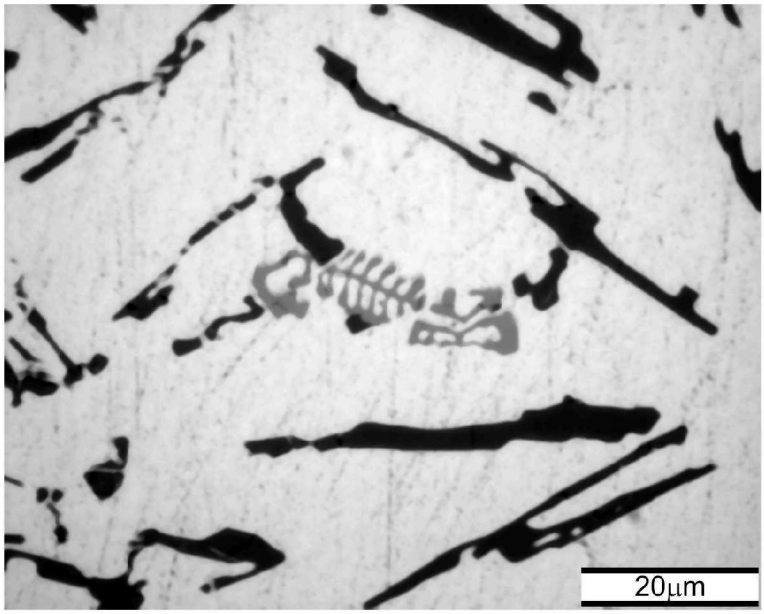

(c) Sand cast unmodified and unrefined Al12Si eutectic alloy. As polished, 1000x magnification. Note the large $Al_{19}(Fe,Mn)_5Si_2$ script.

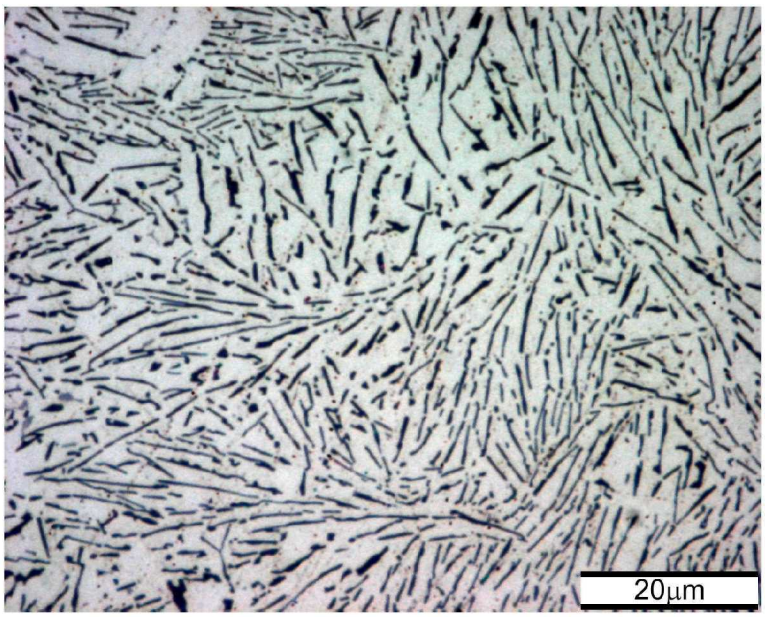

(d) Squeeze cast unmodified and unrefined Al12Si eutectic alloy. As polished, 1000x magnification.

Figure 5.17 continued.

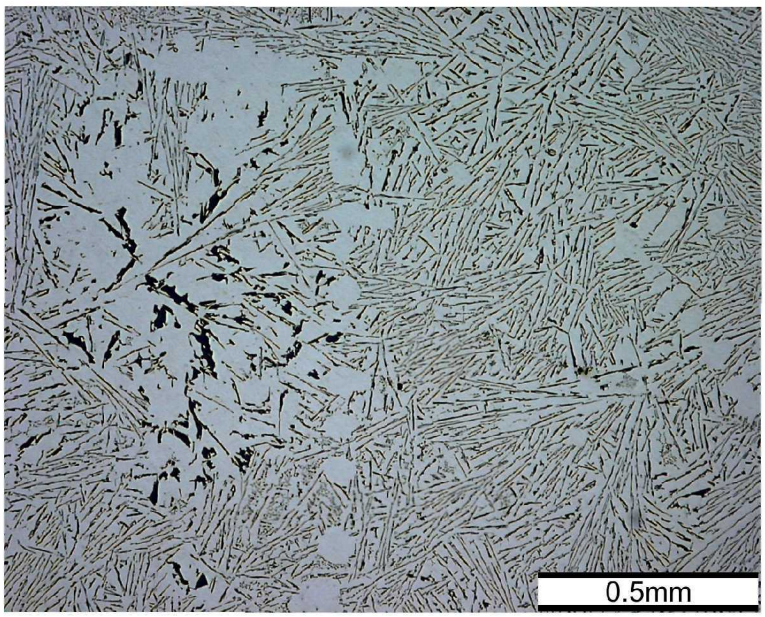

(a) Sand cast 0.02% Sr modified Al12Si eutectic alloy. As polished, 50x magnification.

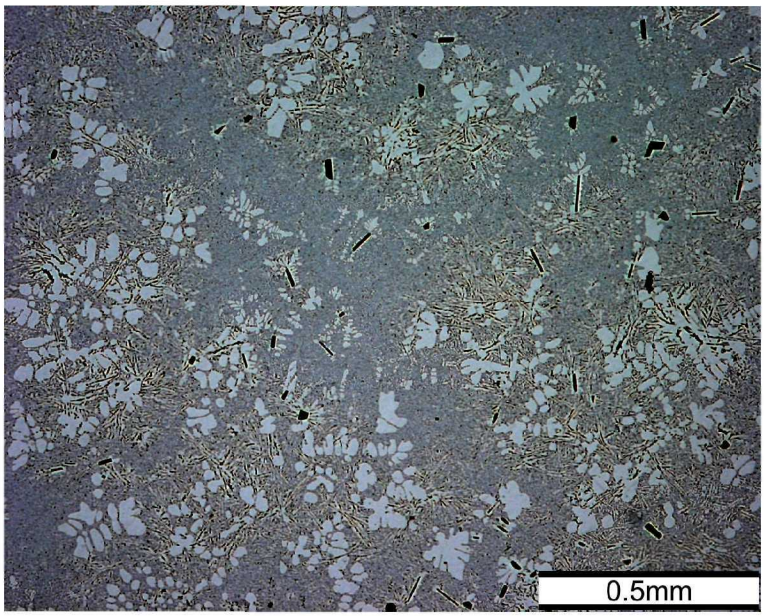

(b) Squeeze cast 0.02% Sr modified Al12Si eutectic alloy. As polished, 50x magnification.

Figure 5.18 Experiment 2A - addition of 0.02% strontium modifier, sand cast and squeeze cast at 50 MPa.

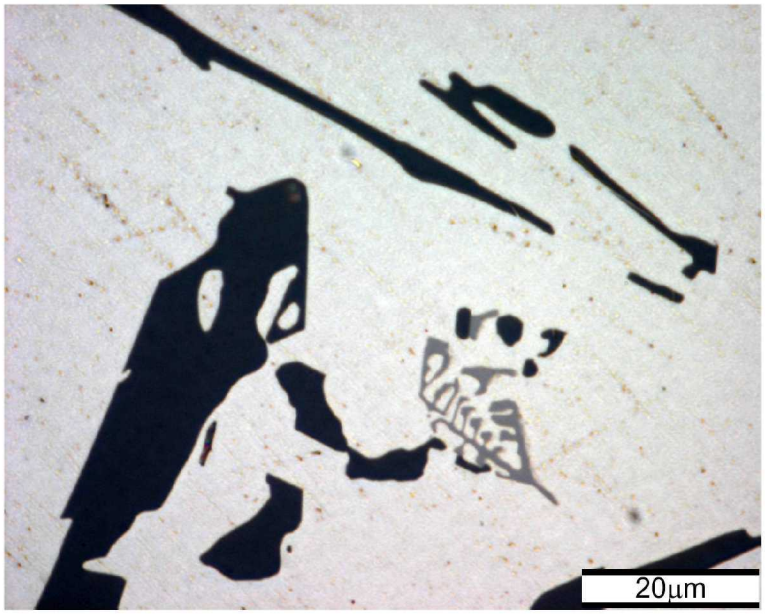

(c) Sand cast 0.02% Sr modified Al12Si eutectic alloy. As polished, 1000x magnification. Coarse, unmodified eutectic, with probable αAlFeSi inclusion.

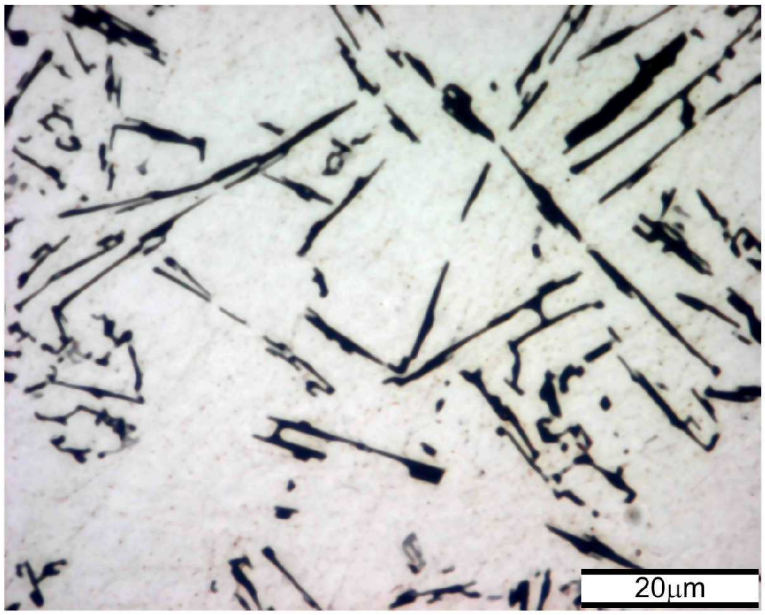

(d) Squeeze cast 0.02% Sr modified Al12Si eutectic alloy. As polished, 1000x magnification. Unmodified eutectic present in bulk of casting. Note small, grey intermetallics, probably αAlFeSi.

Figure 5.18 continued.

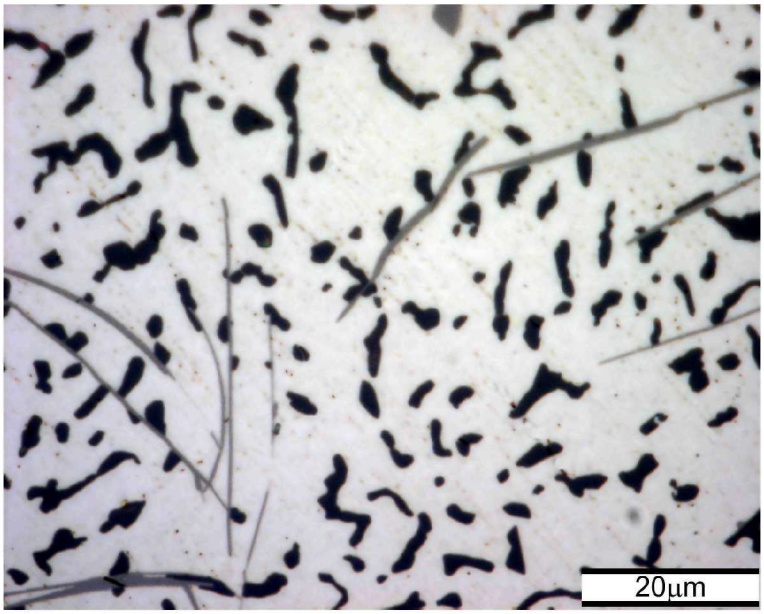

(e) Sand cast 0.02% Sr modified Al12Si eutectic alloy. As polished, 1000x magnification. Fine, modified eutectic present in the centre of the casting. Note βAlFeSi intermetallics.

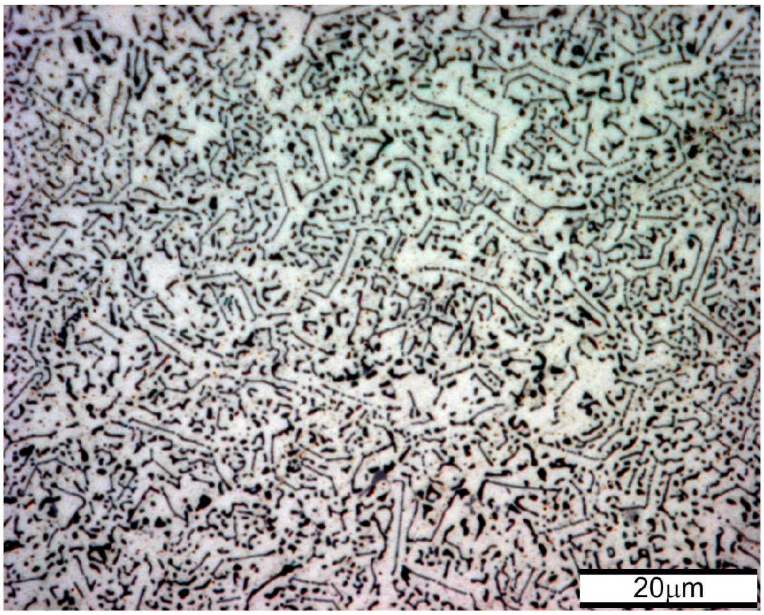

(f) Squeeze cast 0.02% Sr modified Al12Si eutectic alloy. As polished, 1000x magnification. Fine eutectic structure occurring in a minority of the casting, showing the angular structure associated with quench modification.

Figure 5.18 continued.

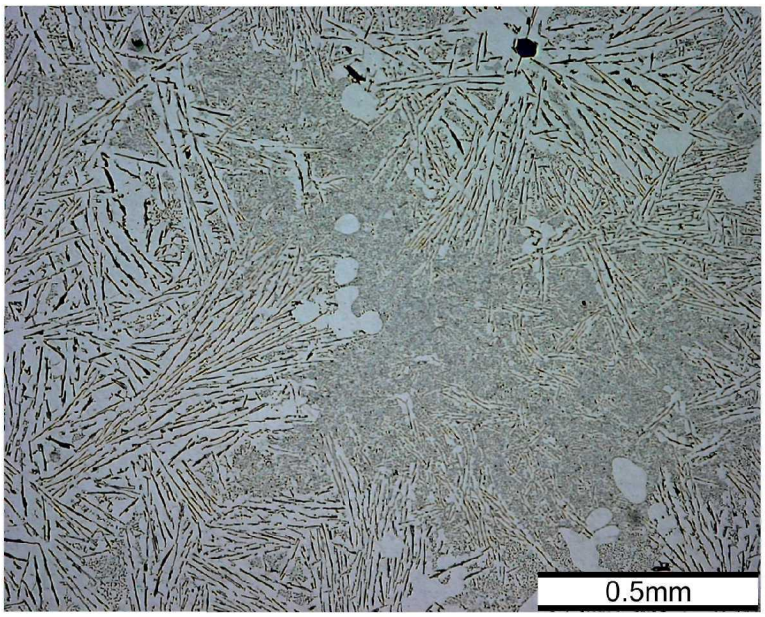

(a) Sand cast 0.02% Sr modified, 0.05% TiB refined Al12Si eutectic alloy. As polished, 50x magnification.

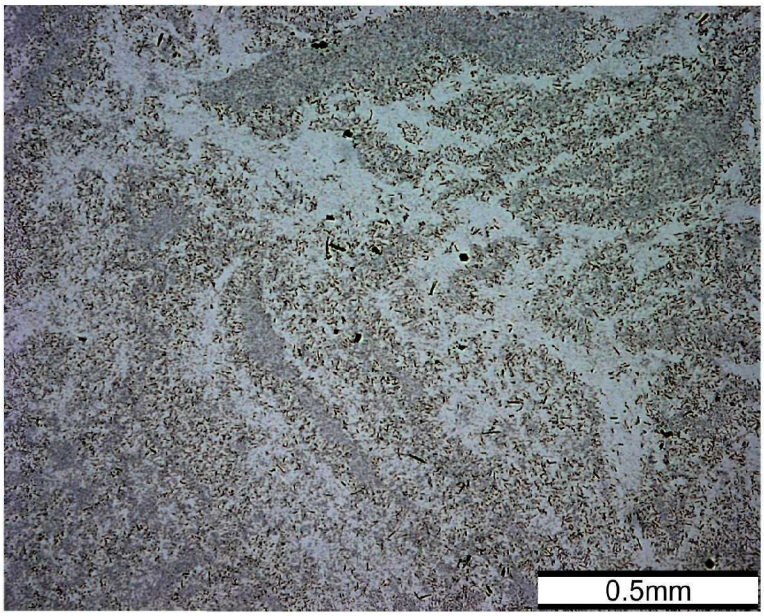

(b) Squeeze cast 0.02% Sr modified, 0.05% TiB refined Al12Si eutectic alloy. Central region of casting. As polished, 50x magnification.

Figure 5.19 Experiment 2 - addition of 0.02% strontium modifier, plus 0.05% TiB refiner, sand cast and squeeze cast at 50 MPa.

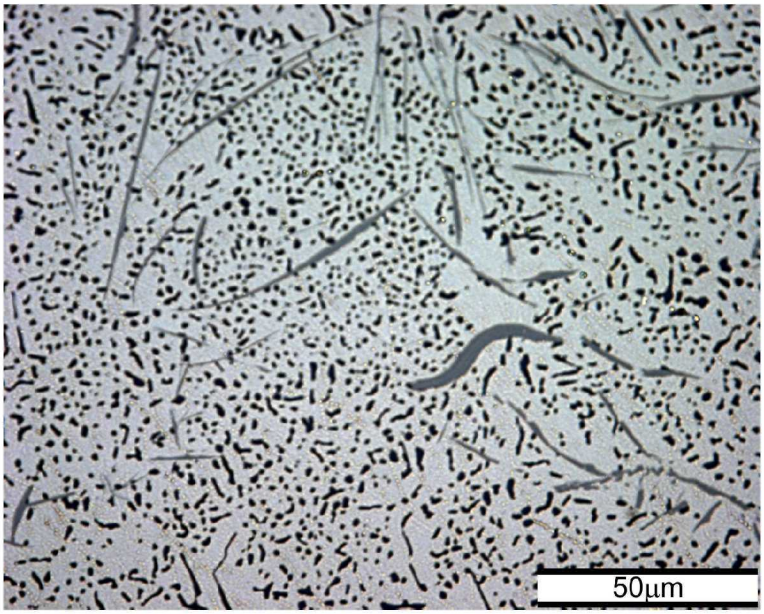

(c) Sand cast 0.02% Sr modified, 0.05% TiB refined Al12Si eutectic alloy. As polished, 500x magnification. Finely modified structure with network of probable βAlFeSi plates.

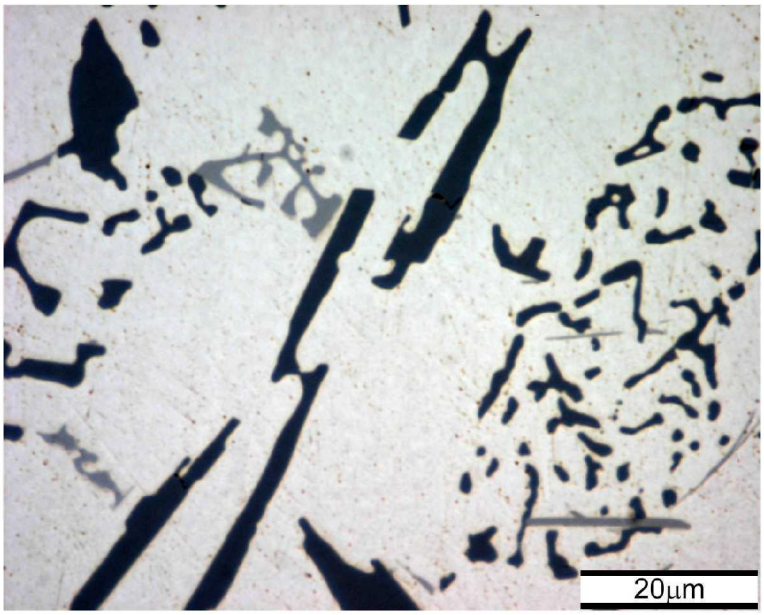

(d) Sand cast 0.02% Sr modified, 0.05% TiB refined Al12Si eutectic alloy. As polished, 1000x magnification. Both unmodified and modified eutectic silicon is visible, along with probable αAlFeSi and βAlFeSi

Figure 5.19 continued.

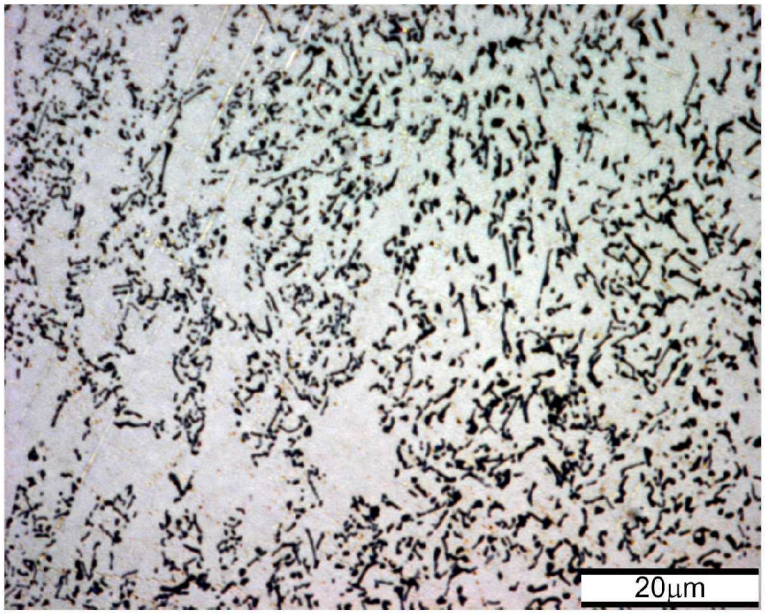

(e) Squeeze cast 0.02% Sr modified, 0.05% TiB refined Al12Si eutectic alloy. As polished, 1000x magnification. A distorted primary dendrite is near the left edge of the micrograph. This homogenised eutectic structure is typical of this specimen.

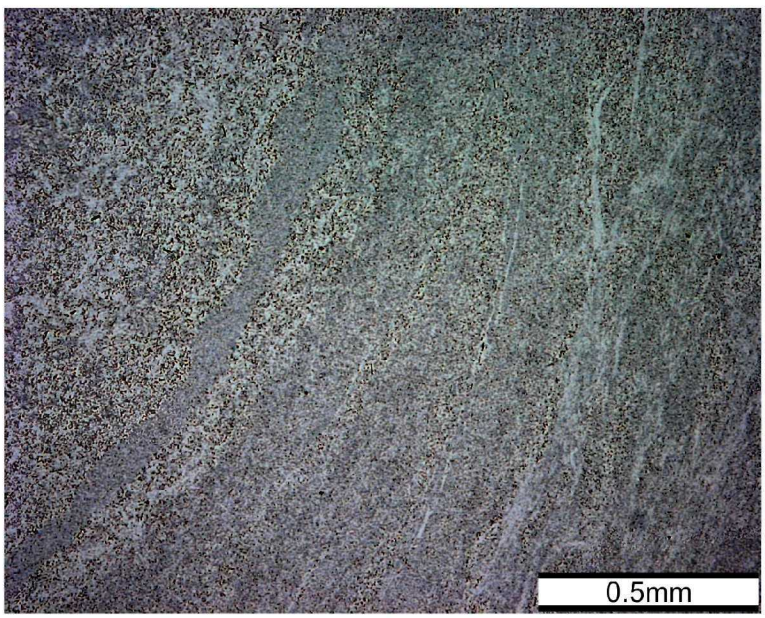

(f) Squeeze cast 0.02% Sr modified, 0.05% TiB refined Al12Si eutectic alloy. As polished, 50x magnification. Highly homogenised eutectic structure with some radial segregation (centre towards upper left), possibly due to plastic deformation immediately after solidification.

Figure 5.19 continued.

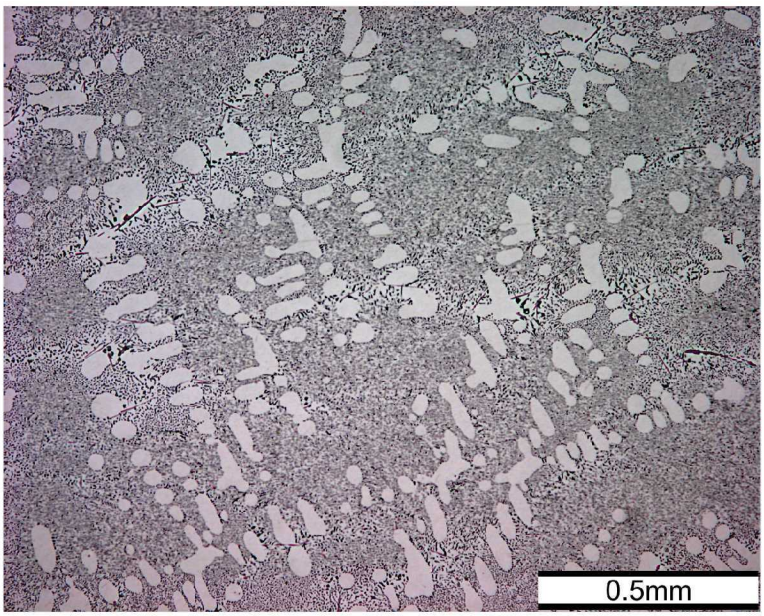

(a) Sand cast 0.06% Sr modified, 0.05% TiB refined Al12Si eutectic alloy. As polished, 50x magnification.

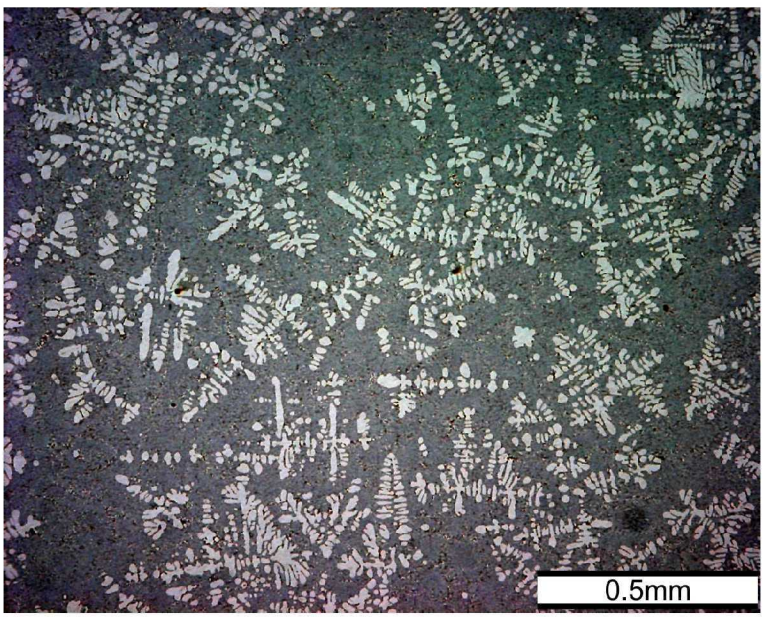

(b) Squeeze cast 0.06% Sr modified, 0.05% TiB refined Al12Si eutectic alloy. As polished, 50x magnification.

Figure 5.20 Experiment 3 - addition of 0.06% strontium and 0.02% titanium, sand cast and squeeze cast at 50 MPa.

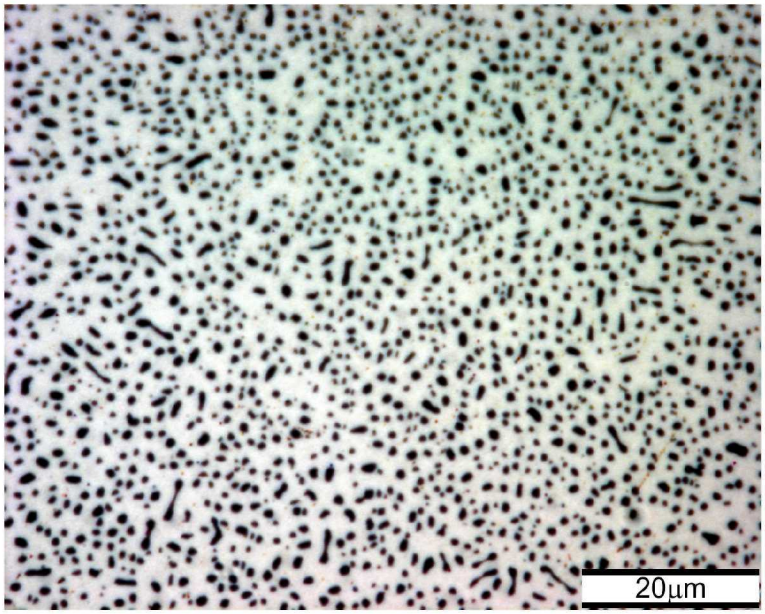

(c) Sand cast 0.06% Sr modified, 0.05% TiB refined Al12Si eutectic alloy. As polished, 1000x magnification. Fine eutectic structure towards the centre of the casting

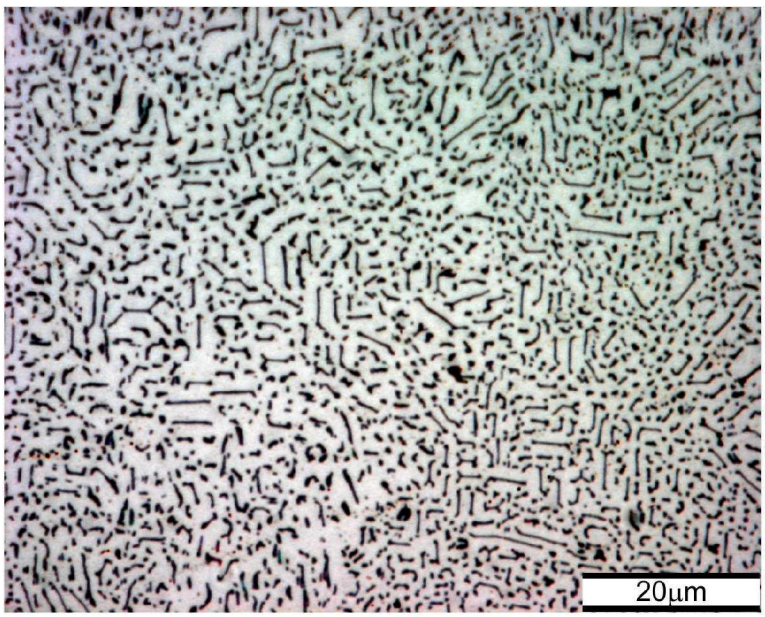

(d) Squeeze cast 0.06% Sr modified, 0.05% TiB refined Al12Si eutectic alloy. As polished, 1000x magnification. Fine, representative eutectic structure towards the centre of the structure. Note slightly angular appearance of eutectic silicon.

Figure 5.20 continued.

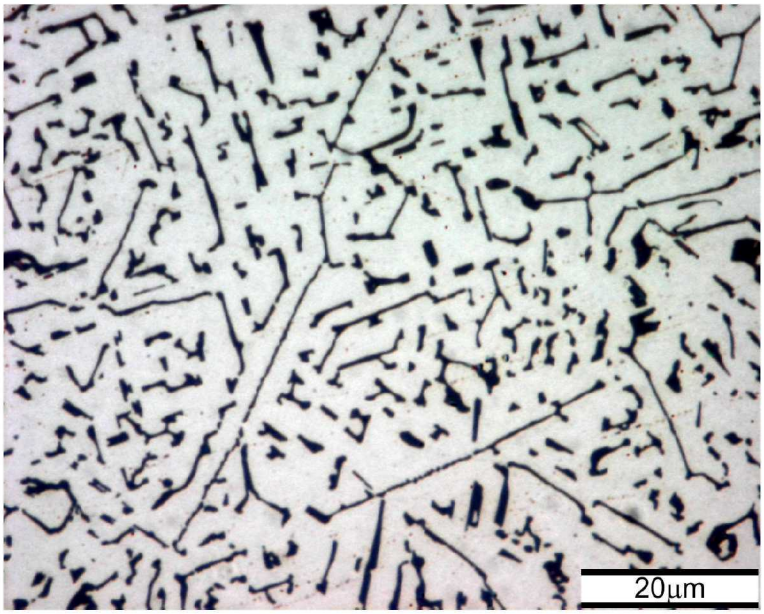

(e) Squeeze cast 0.06% Sr modified, 0.05% TiB refined Al12Si eutectic alloy. As polished, 1000x magnification. Coarsest eutectic structure in casting. Note the angular growth of eutectic silicon

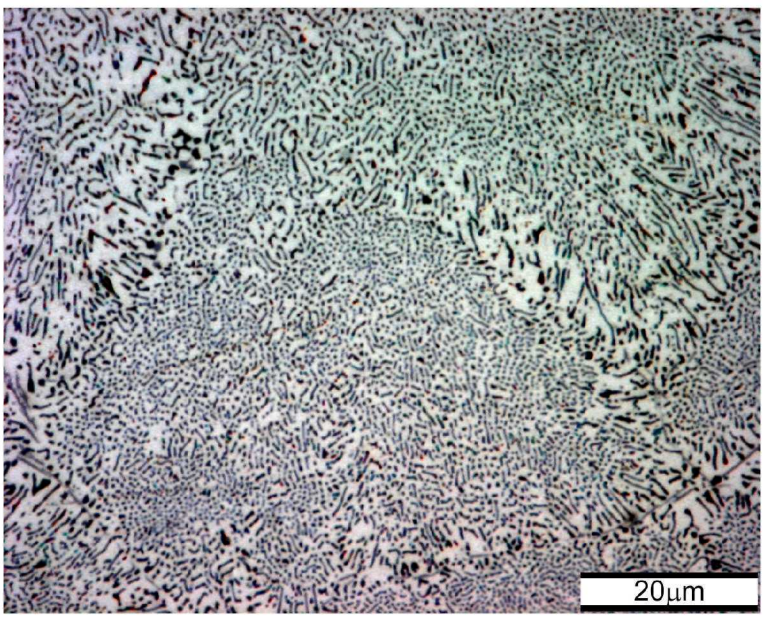

(f) Squeeze cast 0.06% Sr modified, 0.05% TiB refined Al12Si eutectic alloy. As polished, 1000x magnification. Ultra-fine eutectic structure at centre of casting. Note the coarser structure at the eutectic colony boundary, with fine network of probable βAlFeSi intermetallics.

Figure 5.20 continued.

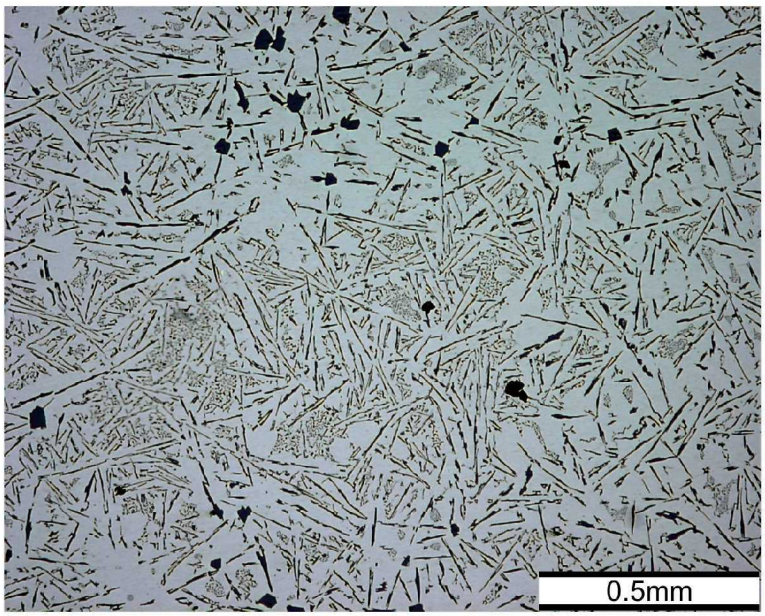

(a) Sand cast 0.02% Sr modified 0.02% Ti refined Al12Si eutectic alloy. As polished, 50x magnification.

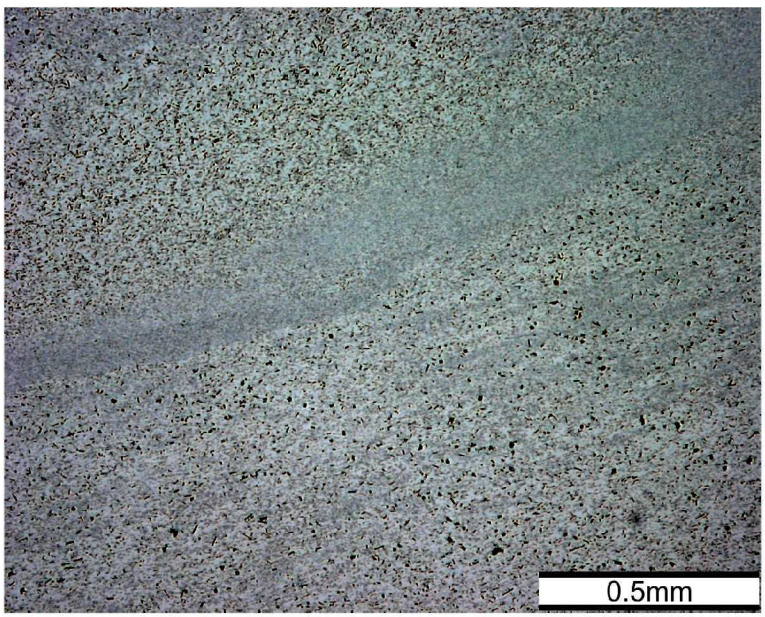

(b) Squeeze cast 0.02% Sr modified Al12Si eutectic alloy. As polished, 50x magnification.

Figure 5.21 Experiment 4 - addition of 0.02% strontium modifier and 0.02% titanium refiner, sand cast and squeeze cast at 100 MPa.

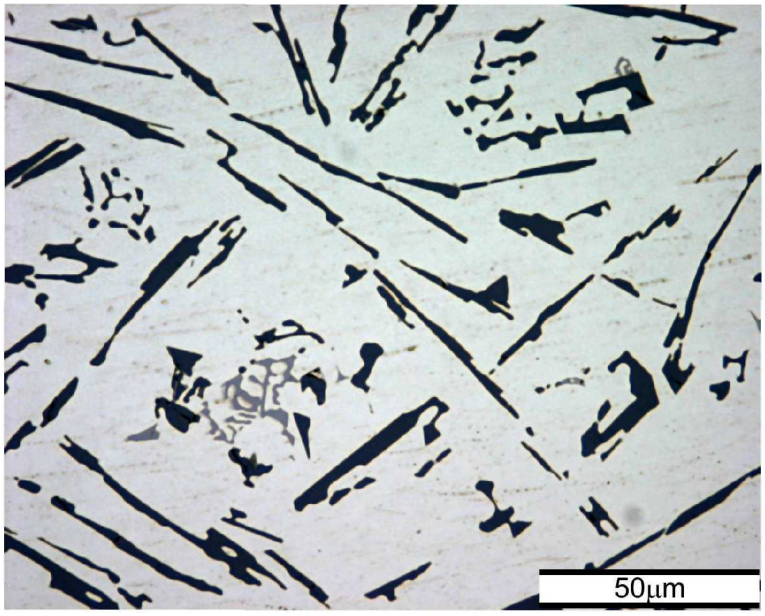

(c) Sand cast 0.02% Sr modified 0.02% Ti refined Al12Si eutectic alloy. As polished, 500x magnification.

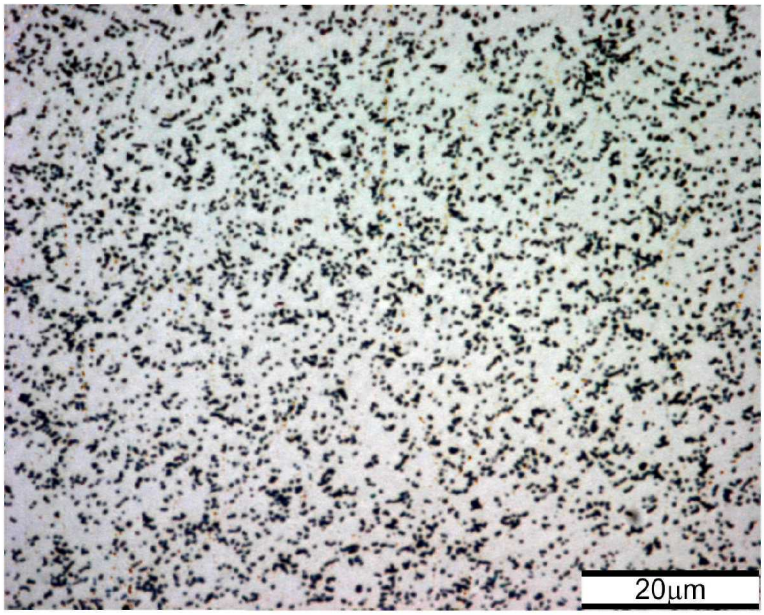

(d) Squeeze cast 0.02% Sr modified Al12Si eutectic alloy. As polished, 1000x magnification. Typical structure of homogenised eutectic.

Figure 5.21 continued.

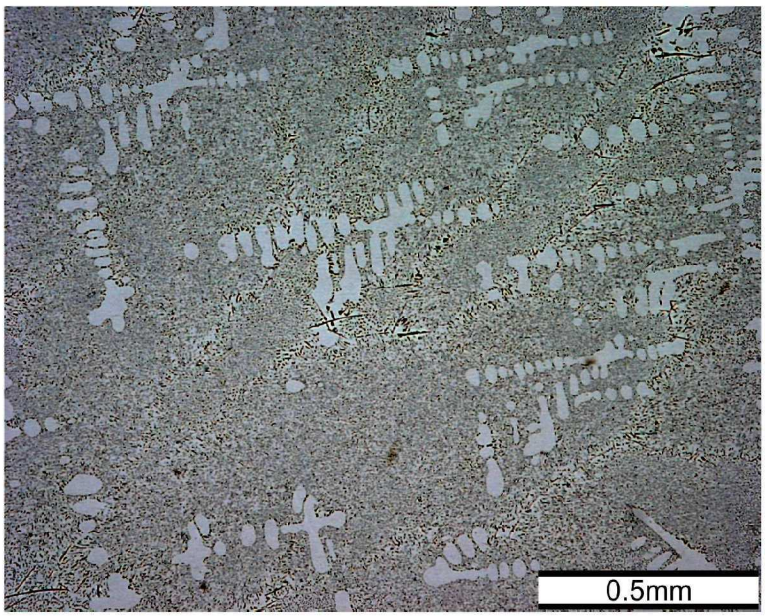

(a) Sand cast 0.06% Sr modified Al12Si eutectic alloy. As polished, 50x magnification. Typical structure towards the edge of the casting.

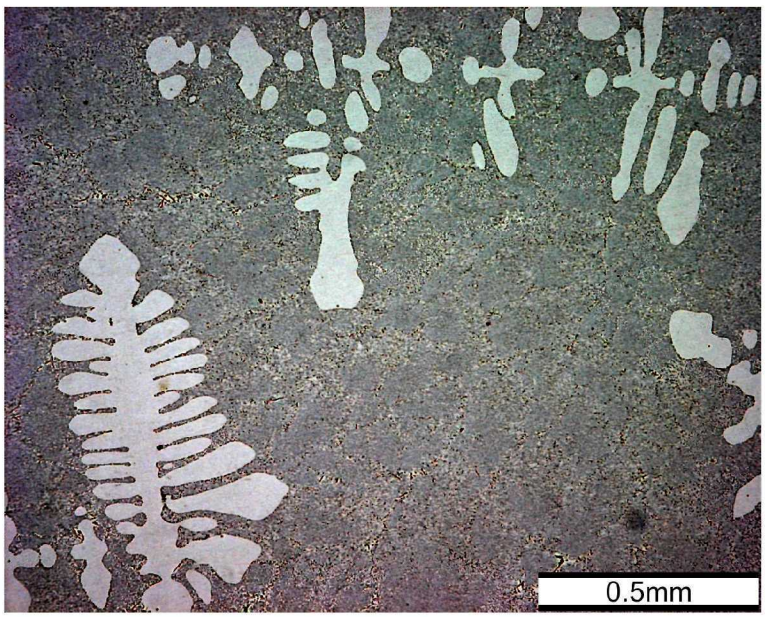

(b) Sand cast 0.06% Sr modified Al12Si eutectic alloy. As polished, 50x magnification. Typical structure towards the centre of the casting.

Figure 5.22 Experiment 5 - addition of 0.06% strontium, sand cast and squeeze cast at 100 MPa.

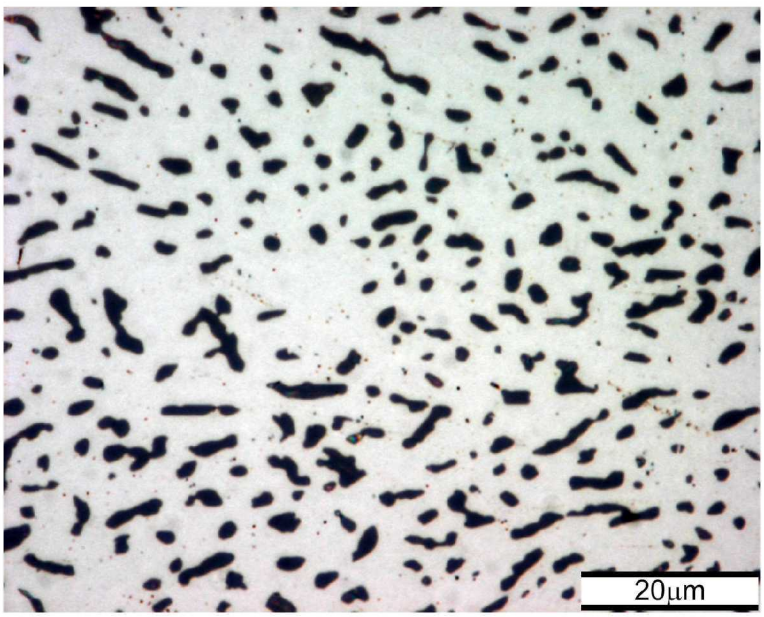

(c) Sand cast 0.06% Sr modified Al12Si eutectic alloy. As polished, 1000x magnification. Typical eutectic structure towards the edge of the casting.

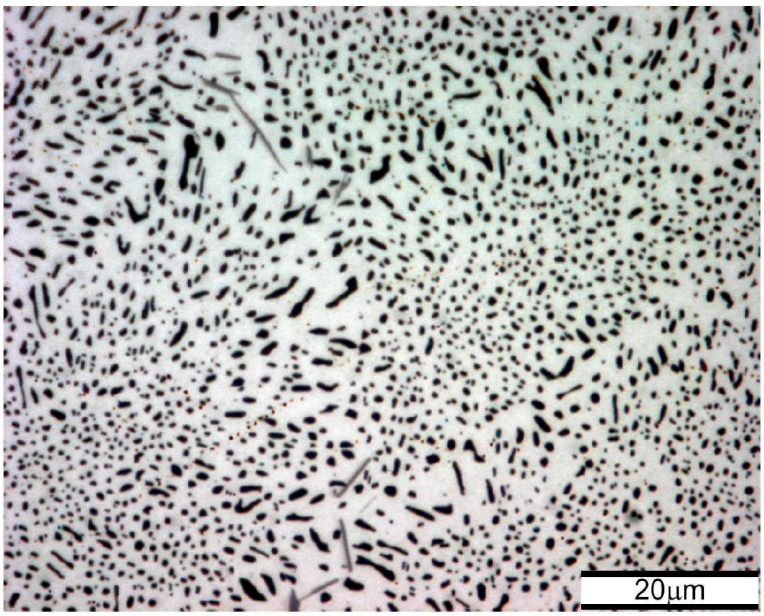

(d) Sand cast 0.06% Sr modified Al12Si eutectic alloy. As polished, 1000x magnification. Typical structure towards the centre of the casting.

Figure 5.22 continued

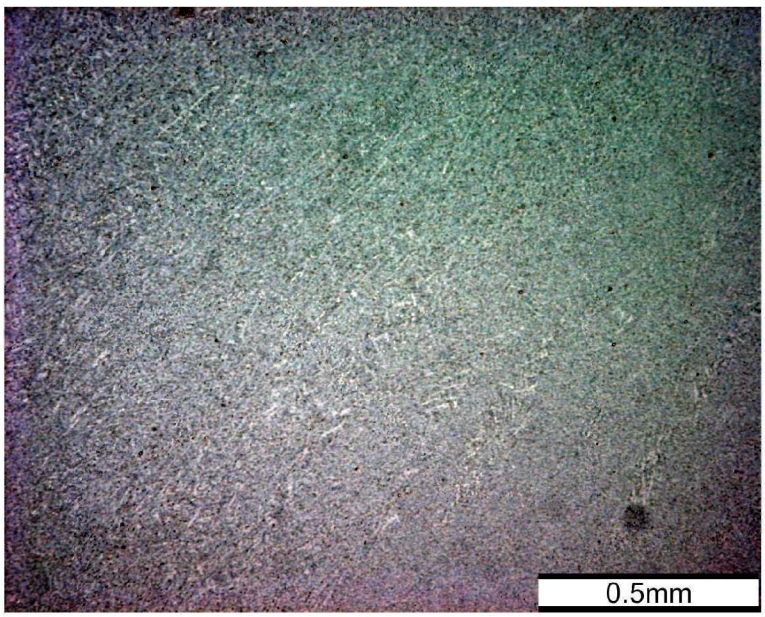

(e) Squeeze cast 0.06% Sr modified Al12Si eutectic alloy. As polished, 50x magnification. Typical structure towards the edge of the casting.

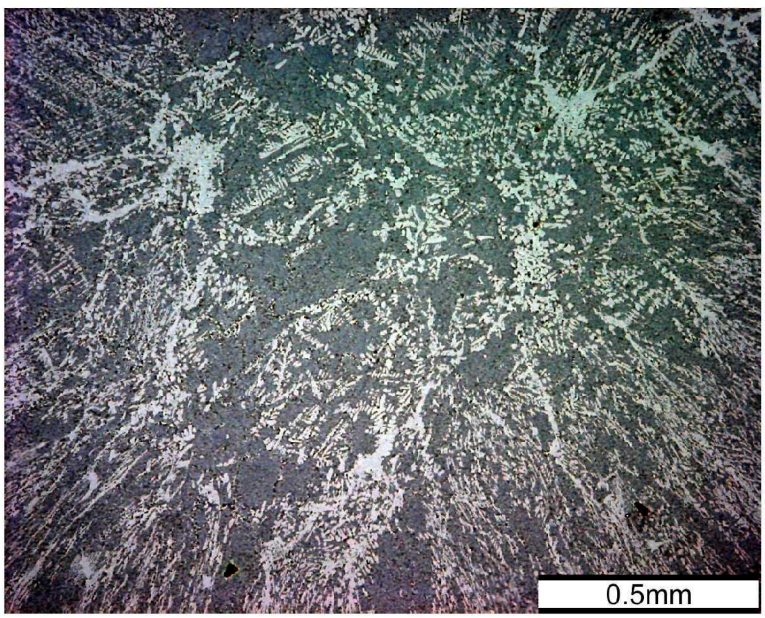

(f) Squeeze cast 0.06% Sr modified Al12Si eutectic alloy. As polished, 50x magnification. Structure at the centre of the casting.

Figure 5.22 continued

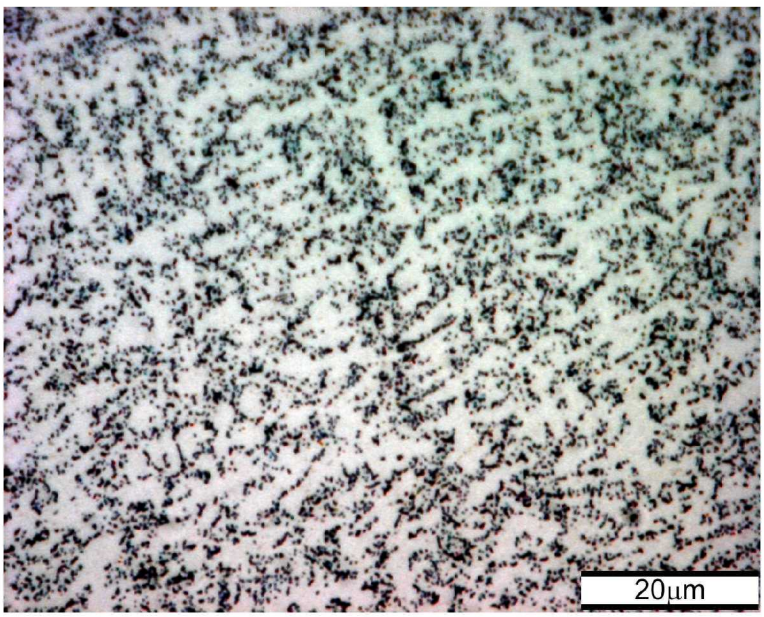

(g) Squeeze cast 0.06% Sr modified Al12Si eutectic alloy. As polished, 1000x magnification. Typical structure through the bulk of the casting.

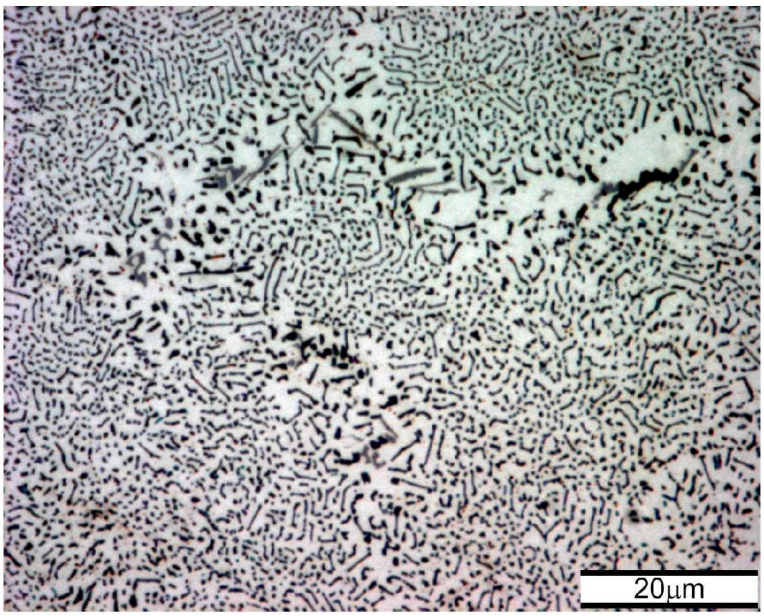

(h) Squeeze cast 0.06% Sr modified Al12Si eutectic alloy. As polished, 1000x magnification. Eutectic structure at the centre of the casting.

Figure 5.22 continued.

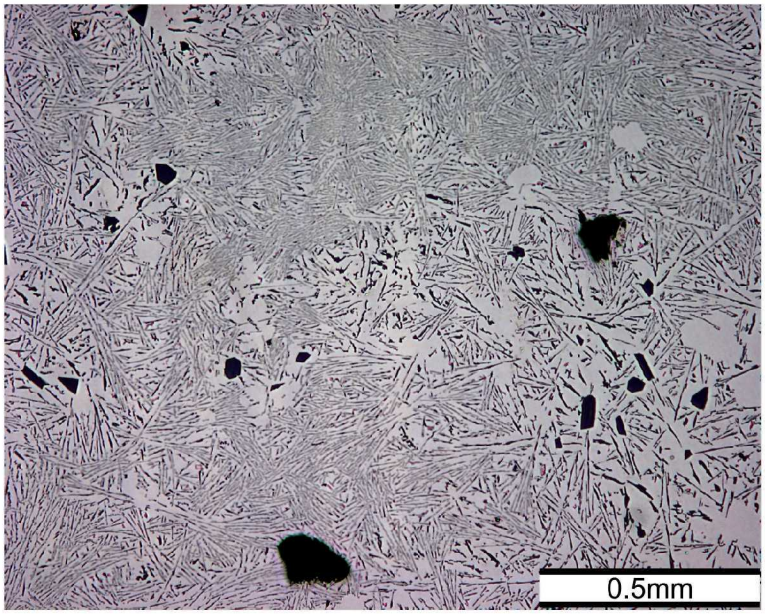

(a) Sand cast 0.05% Ti refined Al12Si eutectic alloy. As polished, 50x magnification. Typical structure through the bulk of the casting.

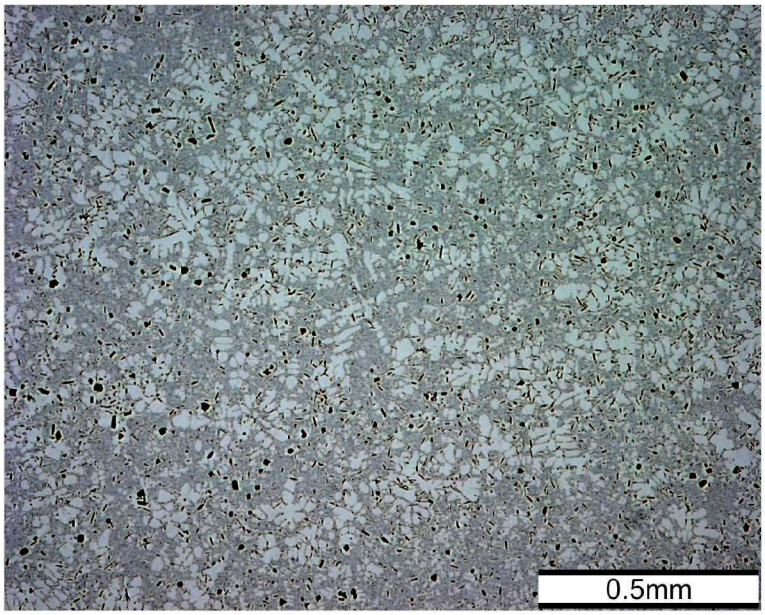

(b) Squeeze cast 0.05% Ti refined Al12Si eutectic alloy. As polished, 50x magnification. Typical structure through the bulk of the casting.

Figure 5.23 Experiment 6 - addition of 0.05% titanium, sand cast and squeeze cast at 100 MPa.

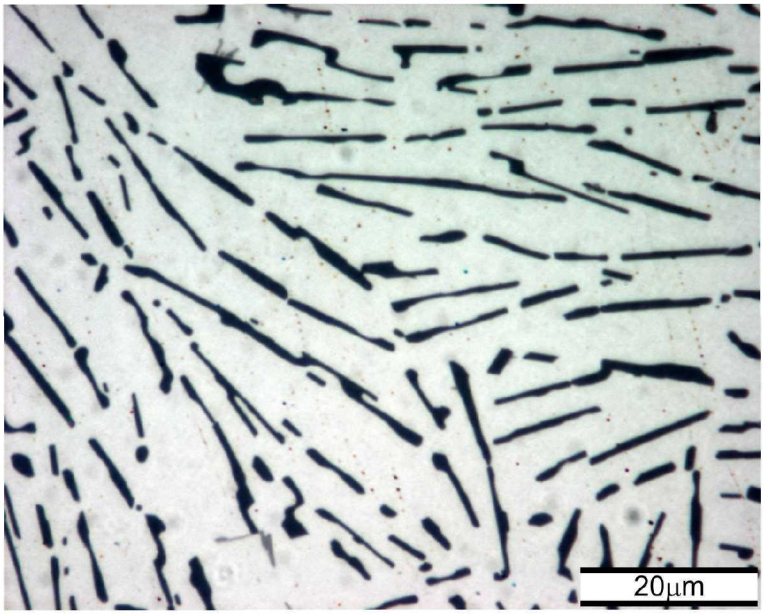

(c) Sand cast 0.05% Ti refined Al12Si eutectic alloy. As polished, 1000x magnification. Fine, unmodified eutectic structure towards the centre of the casting.

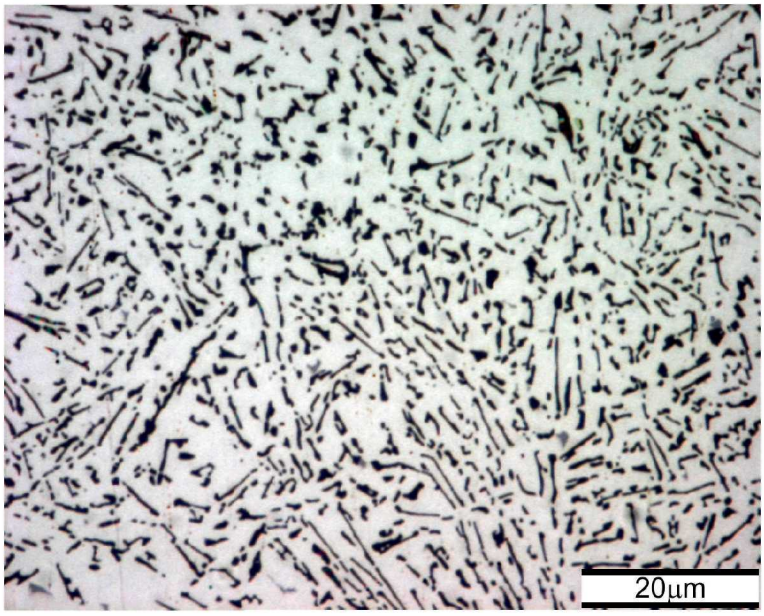

(d) squeeze cast 0.05% Ti refined Al12Si eutectic alloy. As polished, 1000x magnification. Typical structure of the eutectic in the bulk of the casting.

Figure 5.23 continued.

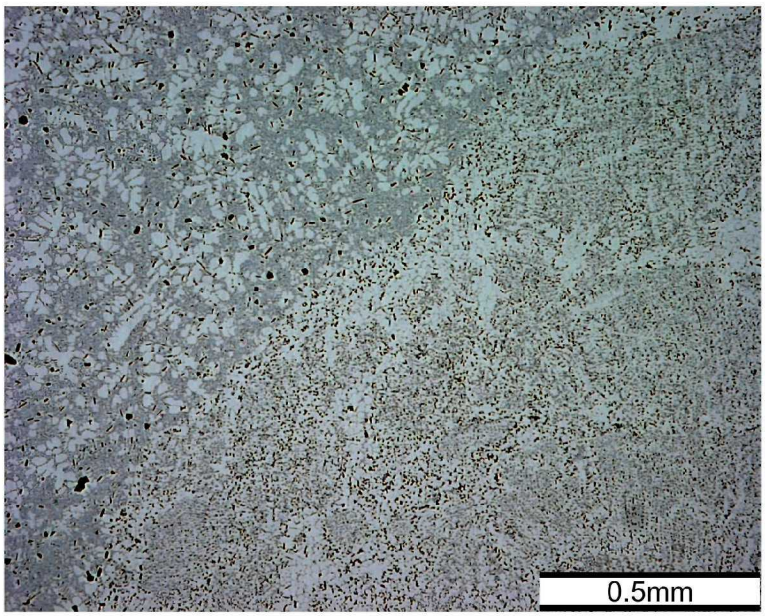

(e) Squeeze cast 0.05% Ti refined Al12Si eutectic alloy. As polished, 50x magnification. Boundary of central segregation. Centre of casting towards lower right.

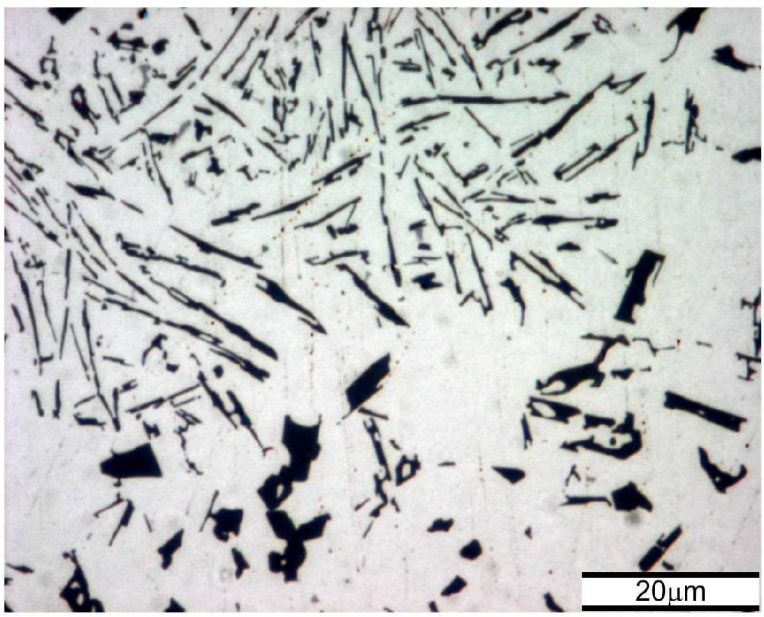

(f) squeeze cast 0.05% Ti refined Al12Si eutectic alloy. As polished, 1000x magnification. Detail of segregation boundary (runs from lower left to upper right).

Figure 5.23 continued.

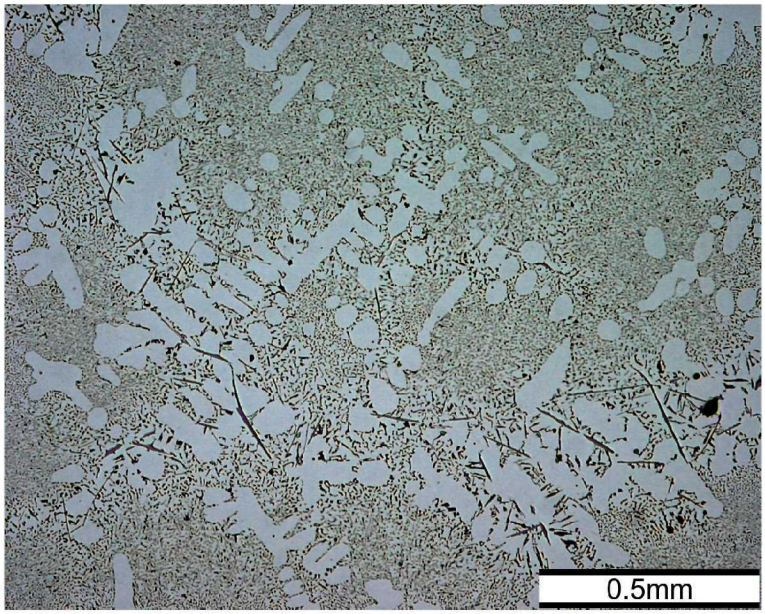

(a) Sand cast 0.06% Sr Modified, 0.05% Ti refined Al12Si eutectic alloy. As polished, 50x magnification. Typical cast structure.

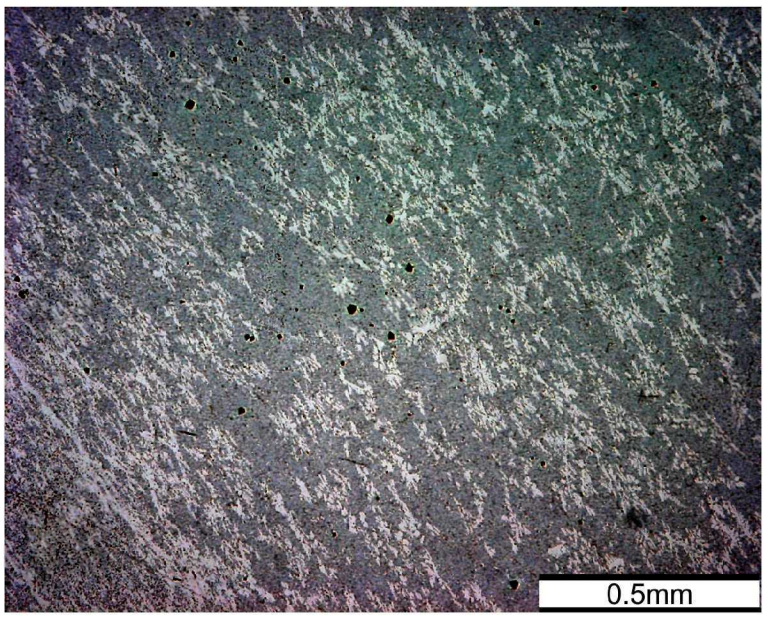

(b) Squeeze 0.06% Sr Modified, 0.05% Ti refined Al12Si eutectic alloy. As polished, 50x magnification. Typical cast structure.

Figure 5.24 Experiment 7 - addition of 0.06% strontium, 0.05% titanium, sand cast and squeeze cast at 150 MPa.

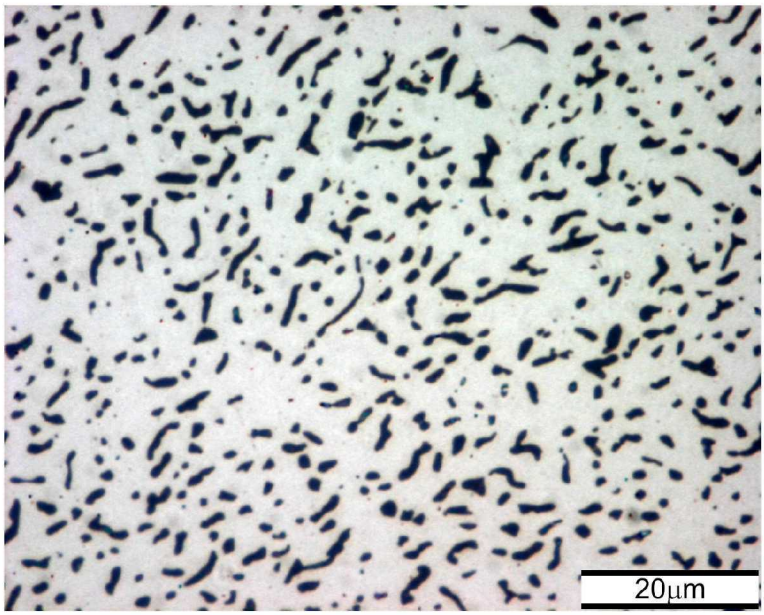

(c) Sand cast 0.06% Sr Modified, 0.05% Ti refined Al12Si eutectic alloy. As polished, 1000x magnification. Eutectic structure at centre of casting

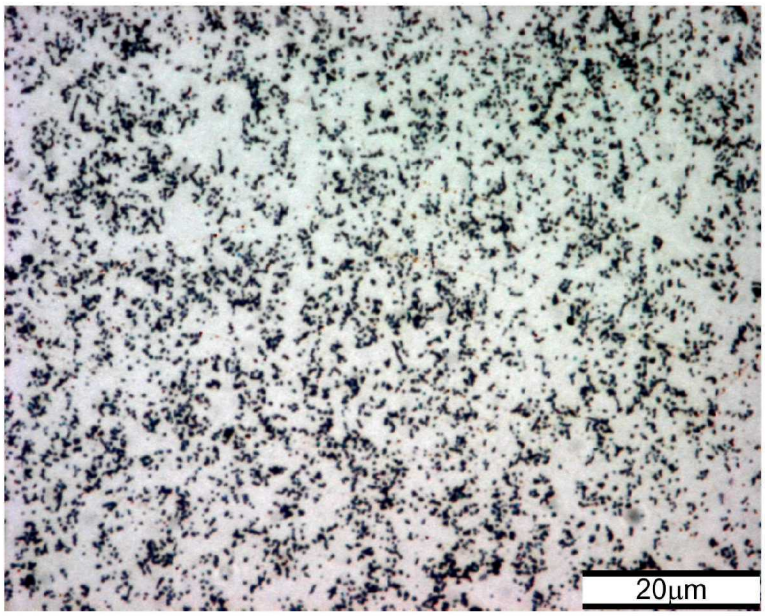

(d) Squeeze 0.06% Sr Modified, 0.05% Ti refined Al12Si eutectic alloy. As polished, 1000x magnification. Typical eutectic structure.

Figure 5.24 continued

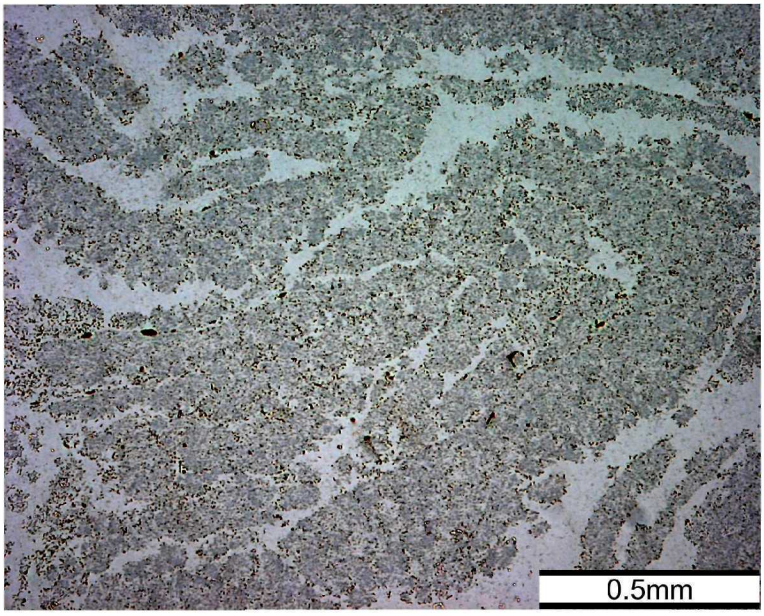

(e) Squeeze cast 0.06% Sr Modified, 0.05% Ti refined Al12Si eutectic alloy. As polished, 50x magnification. Central segregation.

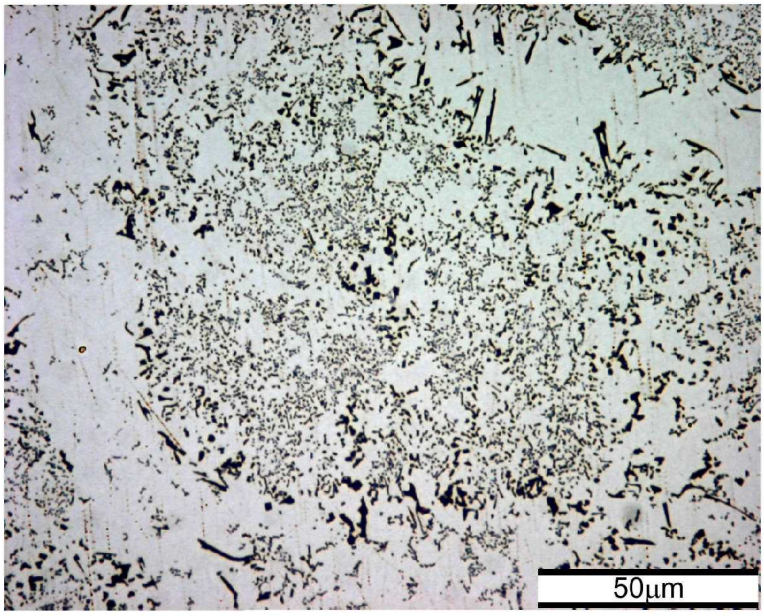

(f) Squeeze 0.06% Sr Modified, 0.05% Ti refined Al12Si eutectic alloy. As polished, 500x magnification. Central segregation.

Figure 5.24 continued

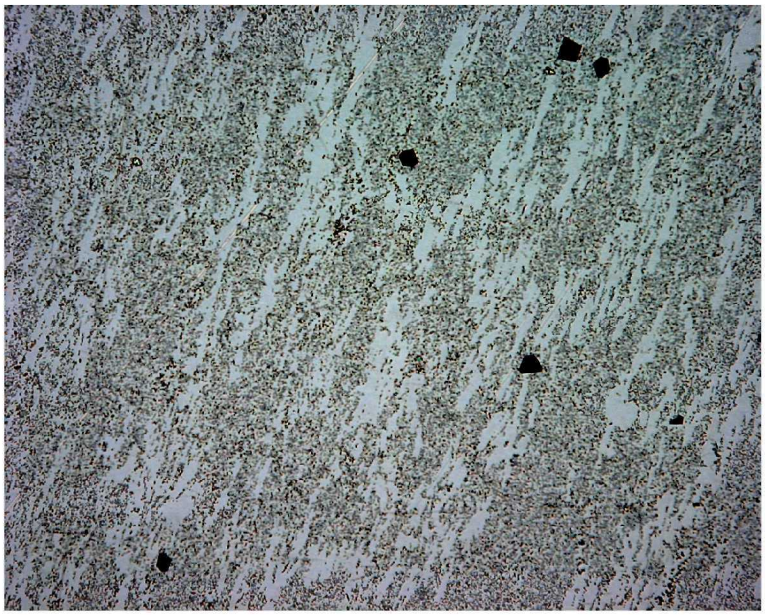

(g) Squeeze cast 0.06% Sr Modified, 0.05% Ti refined Al12Si eutectic alloy. As polished, 200x magnification. Non-eutectic silicon in altered microstructure.

Figure 5.24 continued.

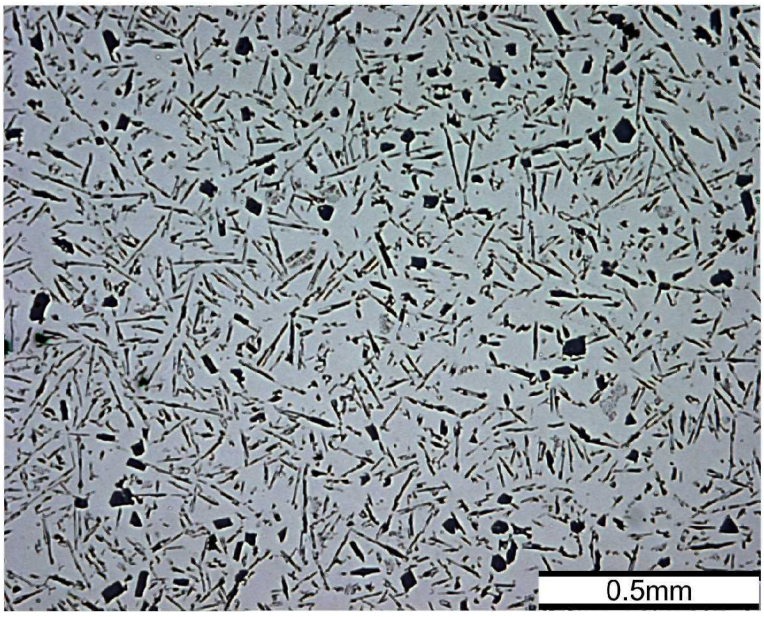

(a) Sand cast 0.02% Ti refined Al12Si eutectic alloy. As polished, 50x magnification. Typical structure.

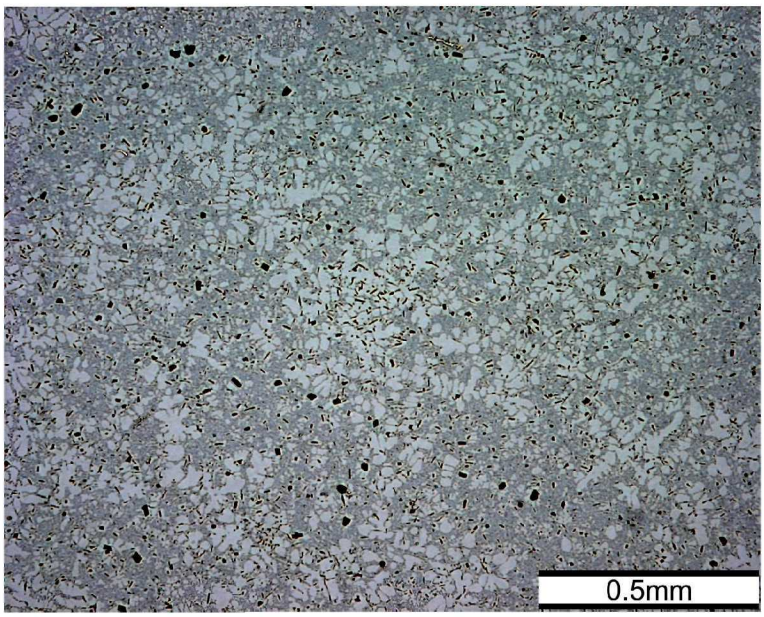

(b) Squeeze cast 0.02% Ti refined Al12Si eutectic alloy. As polished, 50x magnification. Typical structure.

Figure 5.25 Experiment 8 - addition of 0.02% titanium, sand cast and squeeze cast at 150 MPa.

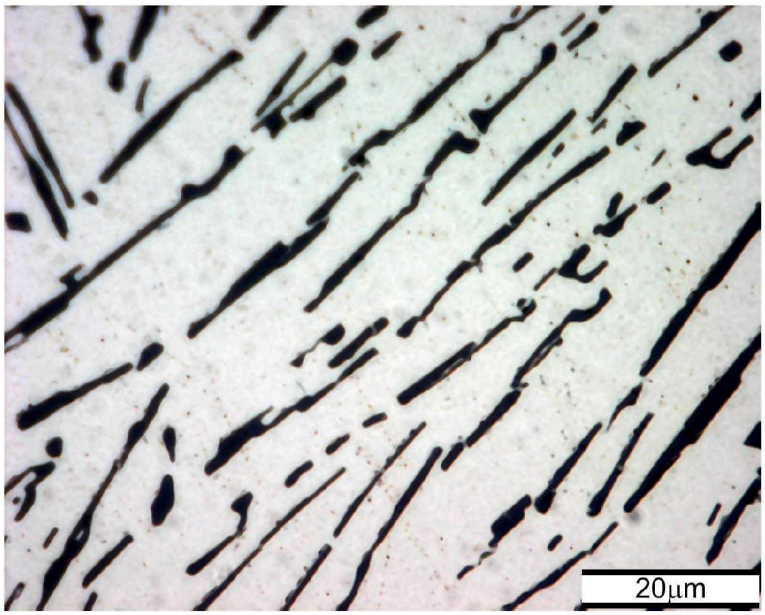

(c) Sand cast 0.02% Ti refined Al12Si eutectic alloy. As polished, 1000x magnification. Fine eutectic structure.

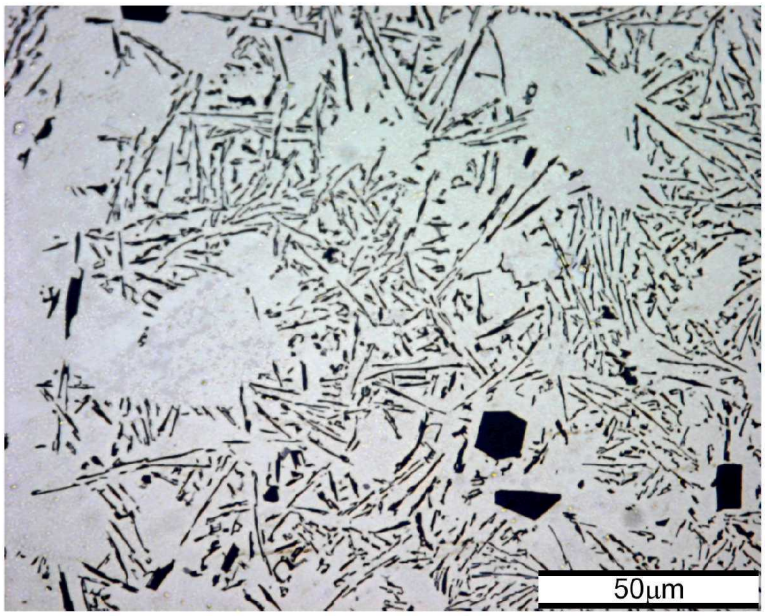

(d) Squeeze cast 0.02% Ti refined Al12Si eutectic alloy. As polished, 500x magnification. Typical structure of squeeze cast eutectic.

Figure 5.25 continued.

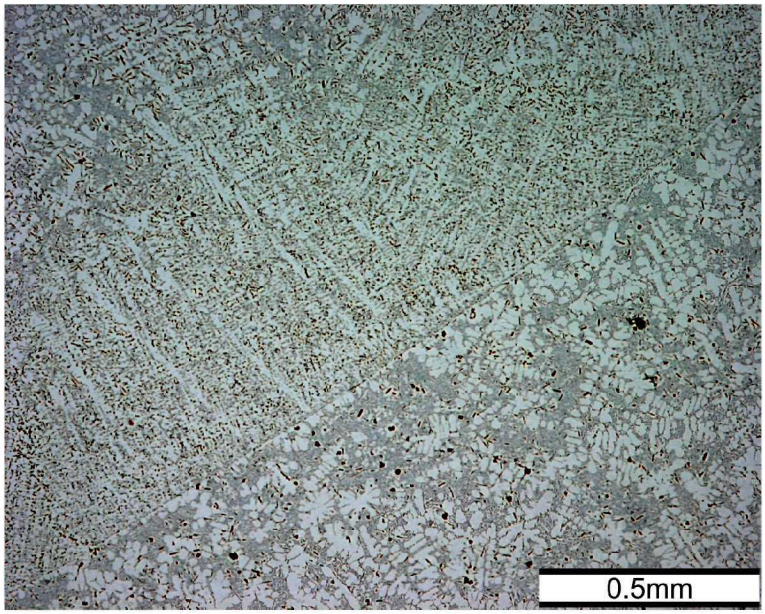

(e) Squeeze cast 0.02% Ti refined Al12Si eutectic alloy. As polished, 50x magnification. Dislodged chill solidified material which has moved into the bulk of the melt during the feeding of molten metal into the die.

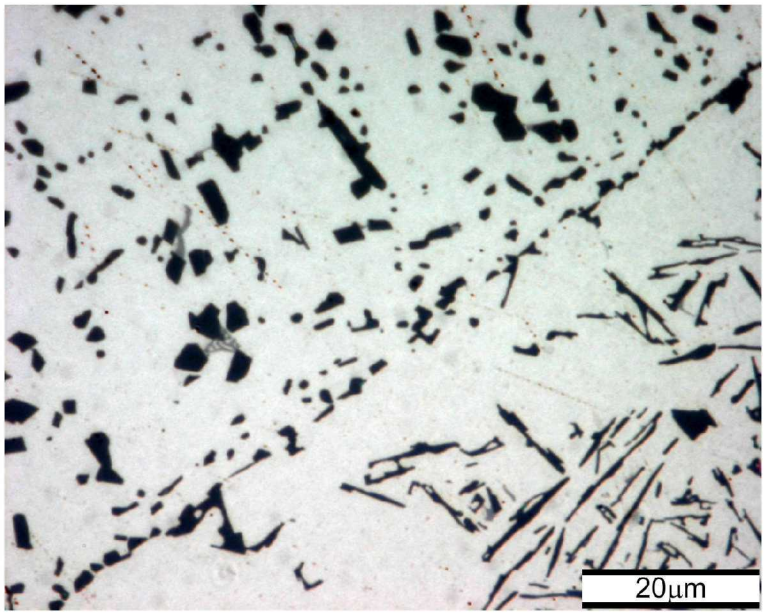

(f) Squeeze cast 0.02% Ti refined Al12Si eutectic alloy. As polished, 1000x magnification. Detail of boundary between dislodged chill solidified material (upper left) and bulk structure (lower right).

Figure 5.25 continued.

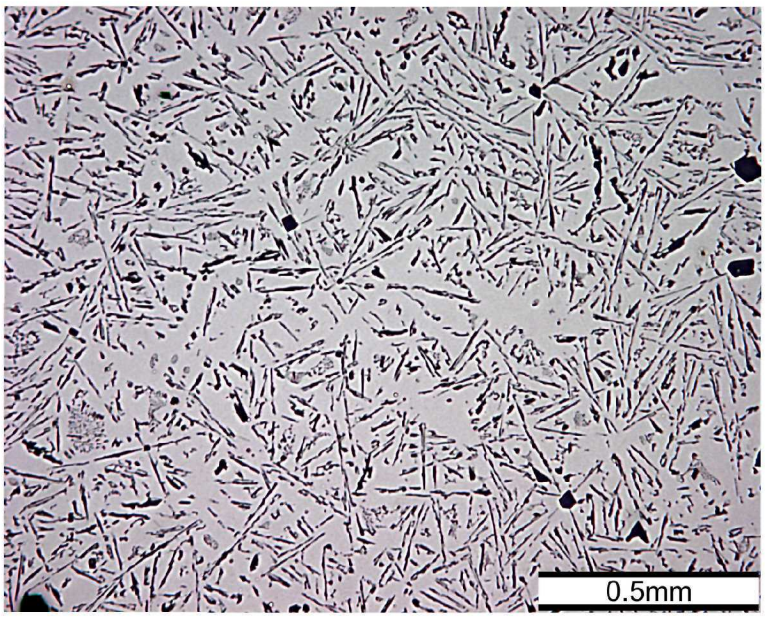

(a) Sand cast 0.02% Sr modified, 0.002% Ti refined Al12Si eutectic alloy. As polished, 50x magnification.

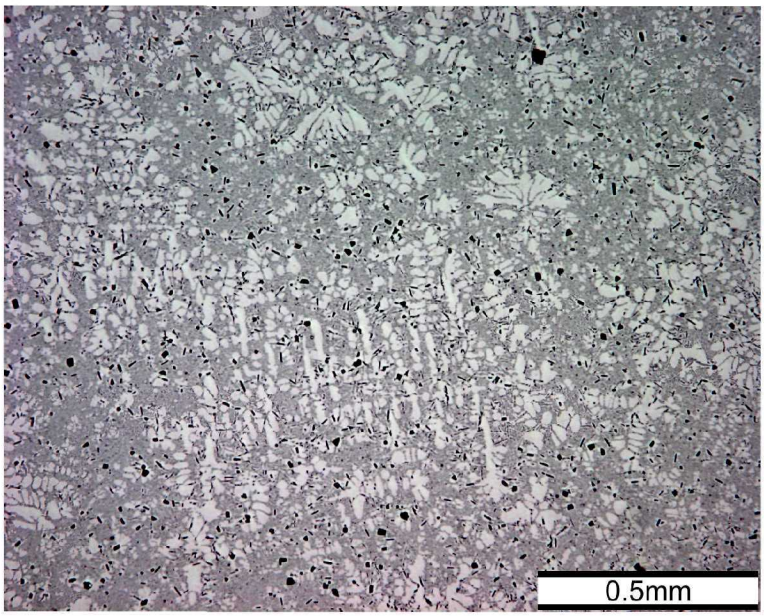

(b) Squeeze cast 0.02% Sr modified, 0.002% Ti refined Al12Si eutectic alloy. As polished, 50x magnification.

Figure 5.26 Experiment 9 - addition of 0.02% strontium, 0.02% titanium, sand cast and squeeze cast at 150 MPa.

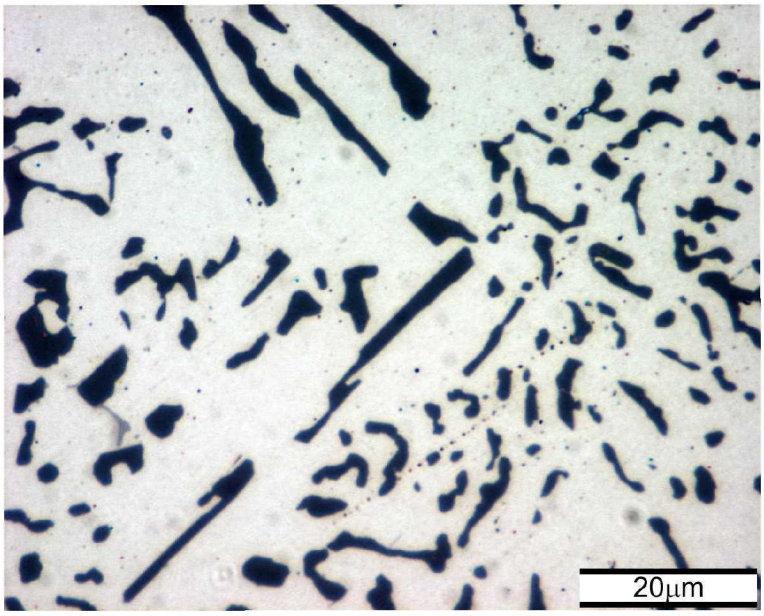

(c) Sand cast 0.02% Sr modified, 0.002% Ti refined Al12Si eutectic alloy. As polished, 1000x magnification. Typical eutectic structure.

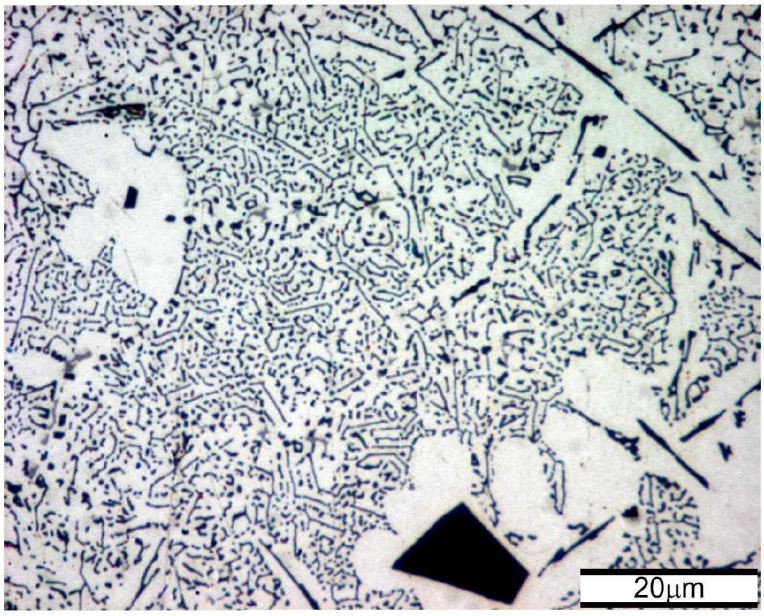

(d) Squeeze cast 0.02% Sr modified, 0.002% Ti refined Al12Si eutectic alloy. As polished, 1000x magnification. .

Figure 5.26 continued.

5.6 MICRO-INDENTATION TESTING

The aluminium silicon eutectic can be regarded as a composite of the two phases. Therefore the hardness of the eutectic can be a function of the hardness of the two phases and their relative proportions. Measuring the hardness of silicon is problematical, as crystalline silicon is brittle, and can crack during an indentation test. Therefore if hardness testing is limited to large scale indentations, then the behaviour under the indenter of any silicon is averaged. Small indentations can be placed to avoid large silicon crystals or coarse eutectic silicon. As a large scale indentation would be affected by the gross segregation seen in the experimental castings produced in this work, this would result in variations in properties across the width of the indentation. using a small, micro-indentation was the obvious choice. Multiple indentations were desirable to obtain a statistically significant value for the sections under examination.

Indentations were taken away from the chill zone and away from any central segregation. This would keep the results indicative of the bulk effect of pressure only. The sand cast eutectic hardness indentations were taken in randomly selected regions exhibiting the greatest local modification. Depending on the the amount of strontium addition, this was either fine flake eutectic silicon or the fibrous rod eutectic silicon. In the coarsest eutectics sampled, the spacing of the silicon in the eutectic meant that only a small number of particles were within the indentation. This resulted in the indentation being distorted. It was also observed that the silicon flakes could also fracture. Figure 5.27(a) gives an example of an indentation in a coarse, unmodified eutectic. In modified areas, the indentation was regular, and the morphology of the silicon had no obvious effect on the resulting shape of the indentation. For the squeeze cast specimens, regardless of the changes in the morphology of the eutectic, i.e. whether or not it had a conventional appearance or had been altered by the squeeze casting process, the local areas of finest eutectic silicon was sampled.

The aluminium hardness measurements were taken in a region of primary aluminium of suitable size immediately adjacent to the eutectic hardness measurements. If there were no suitable dendrites in the region ad-

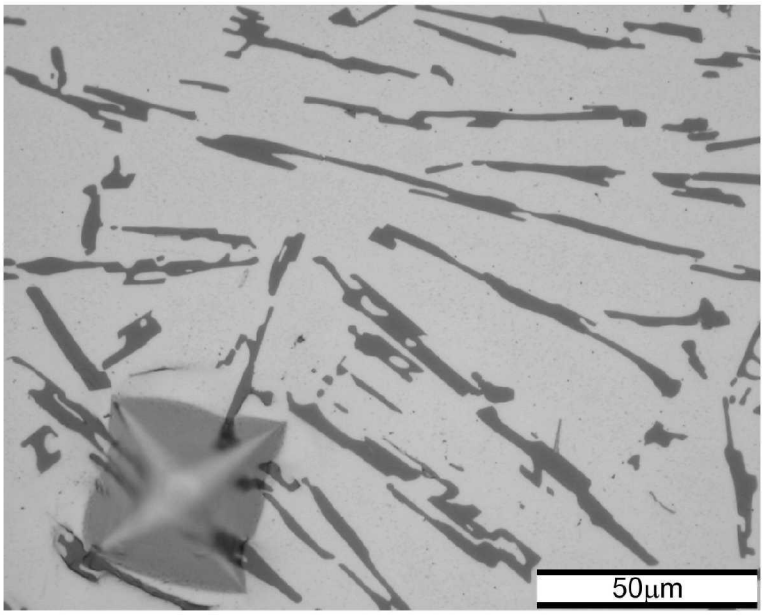

(a) Hardness indentation in coarse, unmodified eutectic structure.

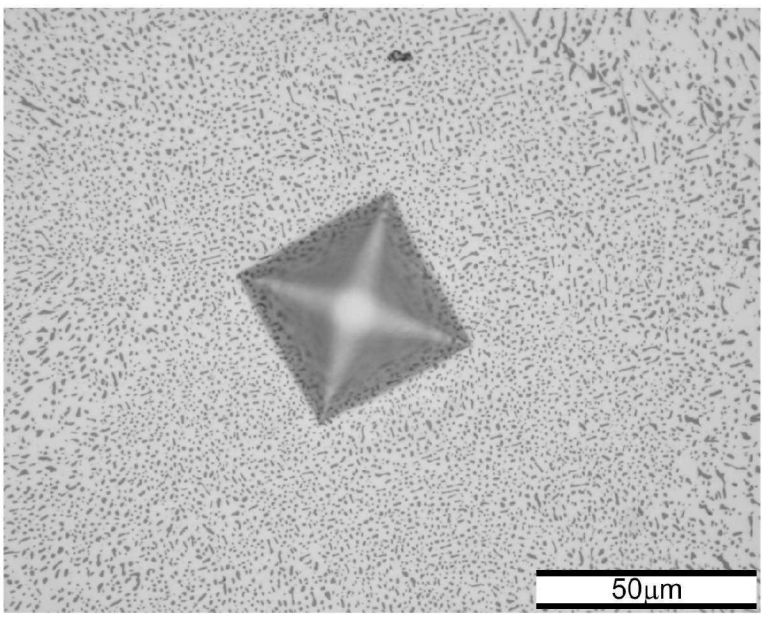

(b) Hardness indentation in fully modified eutectic structure.

Figure 5.27 Hardness indentations in sand cast specimens.

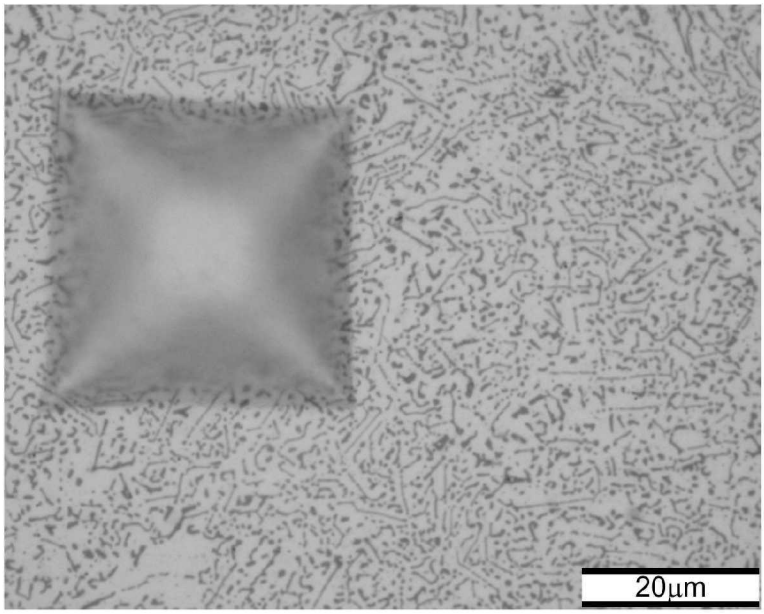

(a) Hardness indentation in conventional eutectic structure.

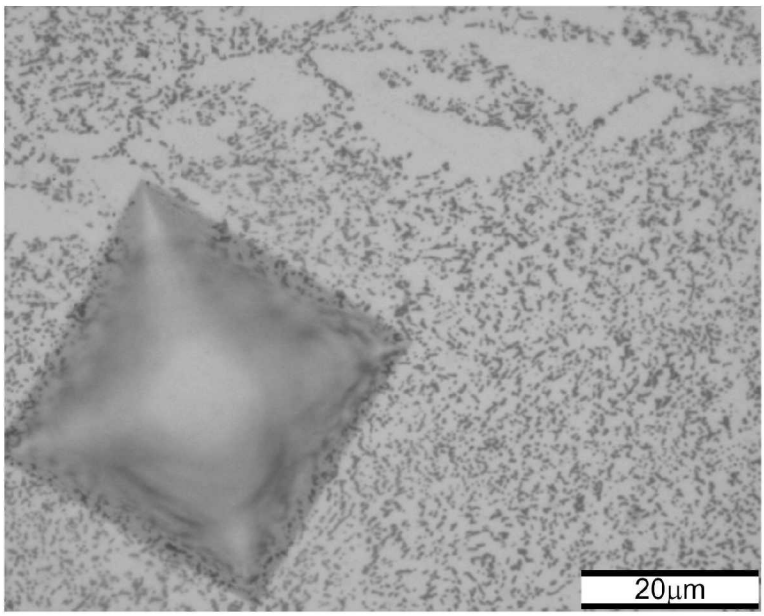

(b) Hardness indentation in altered eutectic structure.

Figure 5.28 Hardness indentations in squeeze cast specimens.

jacent to the eutectic measurements then any suitable area of aluminium present in the centre of the casting was used.

5.6.1 Quantitative Results

Analysis of the hardness testing showed that for the sand cast eutectic, the hardness is affected by the strontium content, with a decrease in hardness with increasing strontium content, especially at the higher strontium levels where full modification was observed. This is shown in Figure 5.29. Hardness readings taken in eutectic regions where the form of the silicon is flake-like were higher than hardness readings taken in regions, modified by the addition of strontium, where the form of the silicon was small and fibrous. The larger, flake silicon has a higher rigidity and strength than the fibrous silicon, and may transfer the applied load such that there is less plastic deformation in the surrounding structure. This is seen in the distorted shape of the hardness indentation next to the silicon structure, which is indicative of elastic springback[57]. The hardness indentations in modified eutectic, with the small, rounded, fibrous silicon had no such effect, and the hardness reading was lower when measured.

In contrast to the sand castings, the average hardness values for the squeeze cast specimens showed very little variation with strontium addition. The average hardness values recorded for the squeeze castings were consistently higher than the sand castings hardness values, approximately 16% higher at 0% strontium to 30% higher at 0.06% strontium addition by weight.

As would be expected, strontium content had no significant effect on the measured hardness of the primary aluminium. The micro-hardness of the aluminium would be a function of substitutional strengthening and micro-defects (arising from non-equilibrium solidification or plastic deformation) within the structure of the primary aluminium. Grain/dendrite refinement strengthening was not considered to be a mechanism affecting the hardness of the aluminium phase. This was due to the indentation being smaller than area of the dendrites tested. As Figure 5.30 shows, the hardness of the aluminium in the squeeze castings was, on average, 26% higher than the

hardness of the aluminium in the sand castings. This increase in strength could be a significant factor in the increase and maintenance of the hardness of the eutectic.

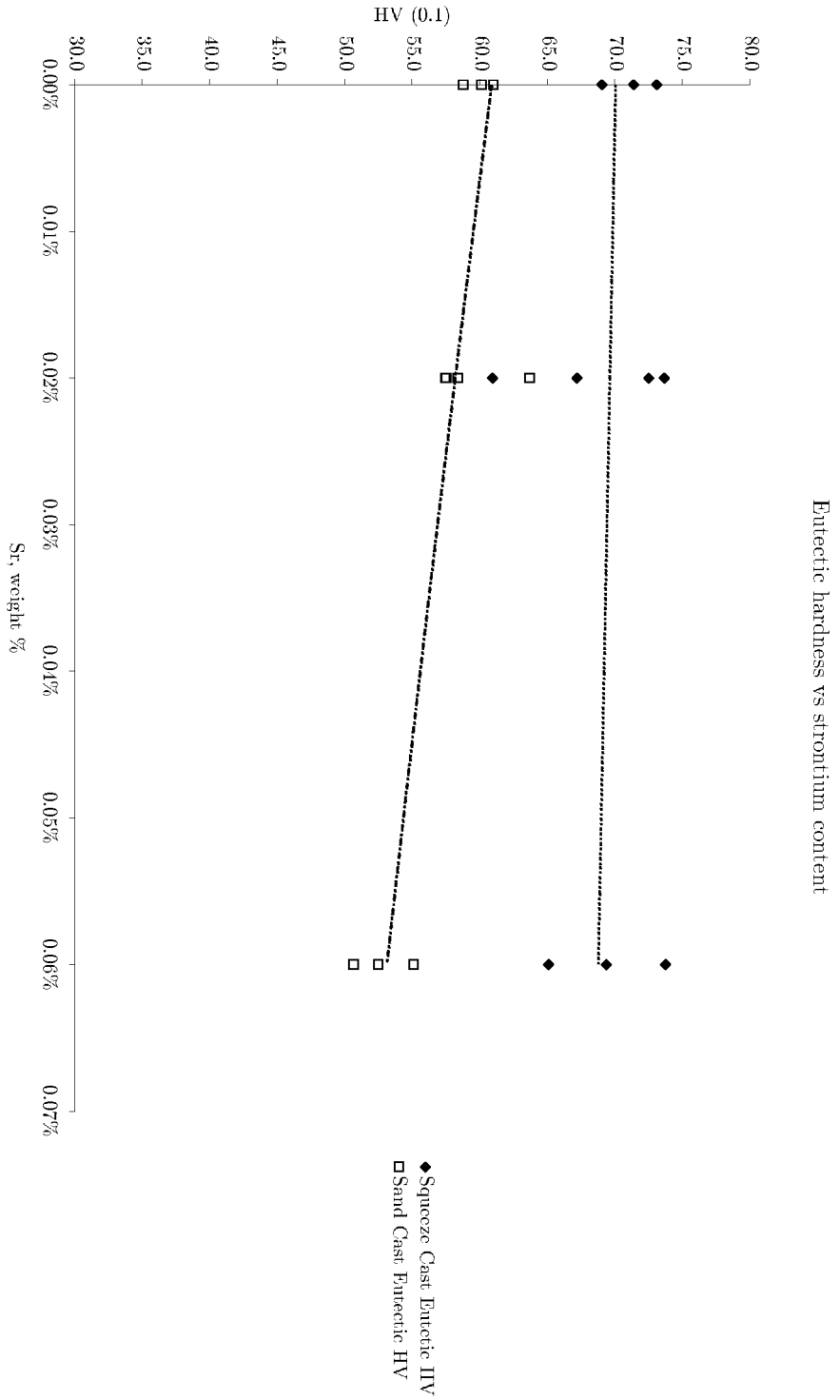

Figure 5.29 Effect of strontium on the hardness of the eutectic.

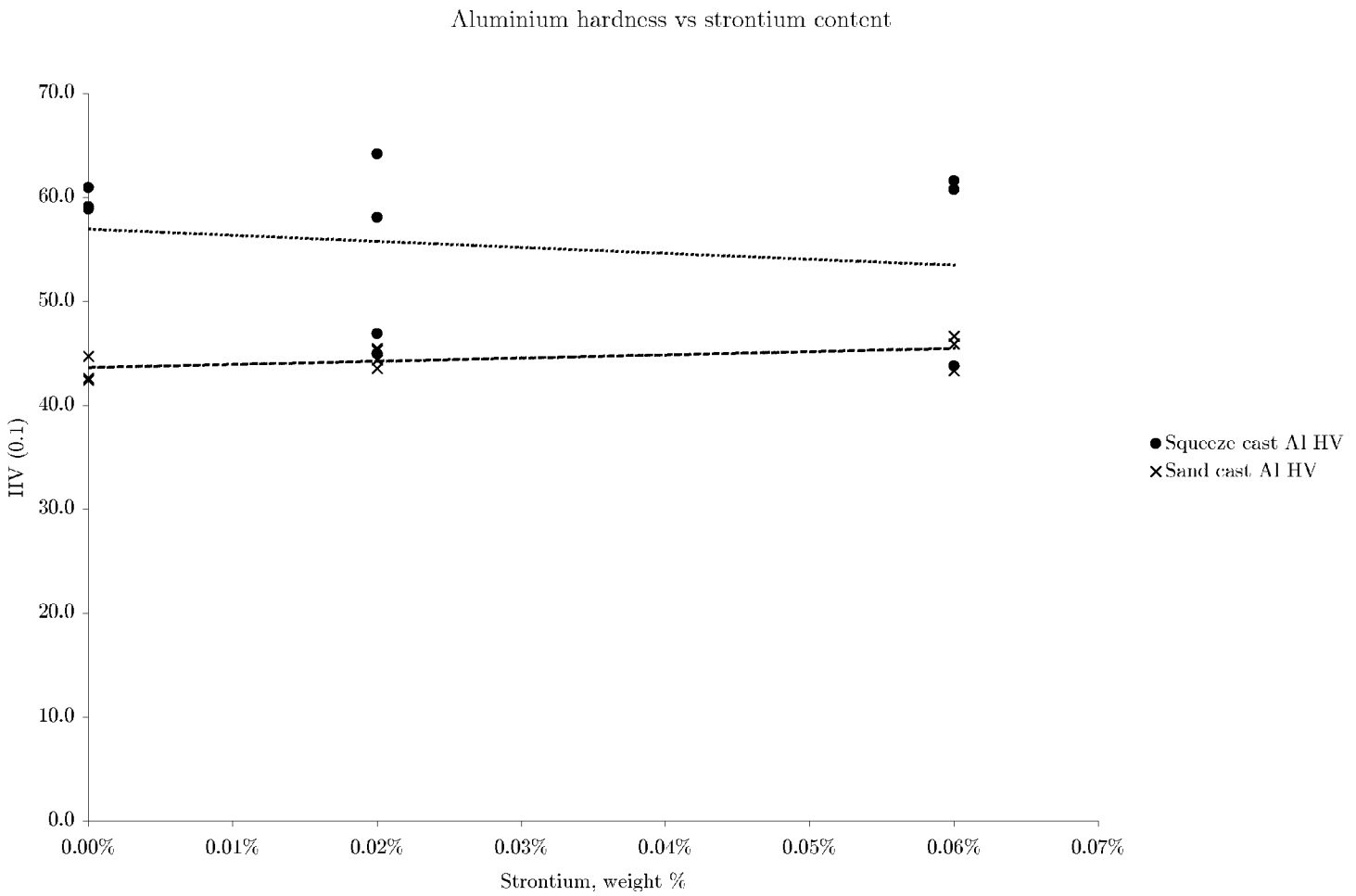

Figure 5.30 Effect of strontium on the hardness of primary aluminium.

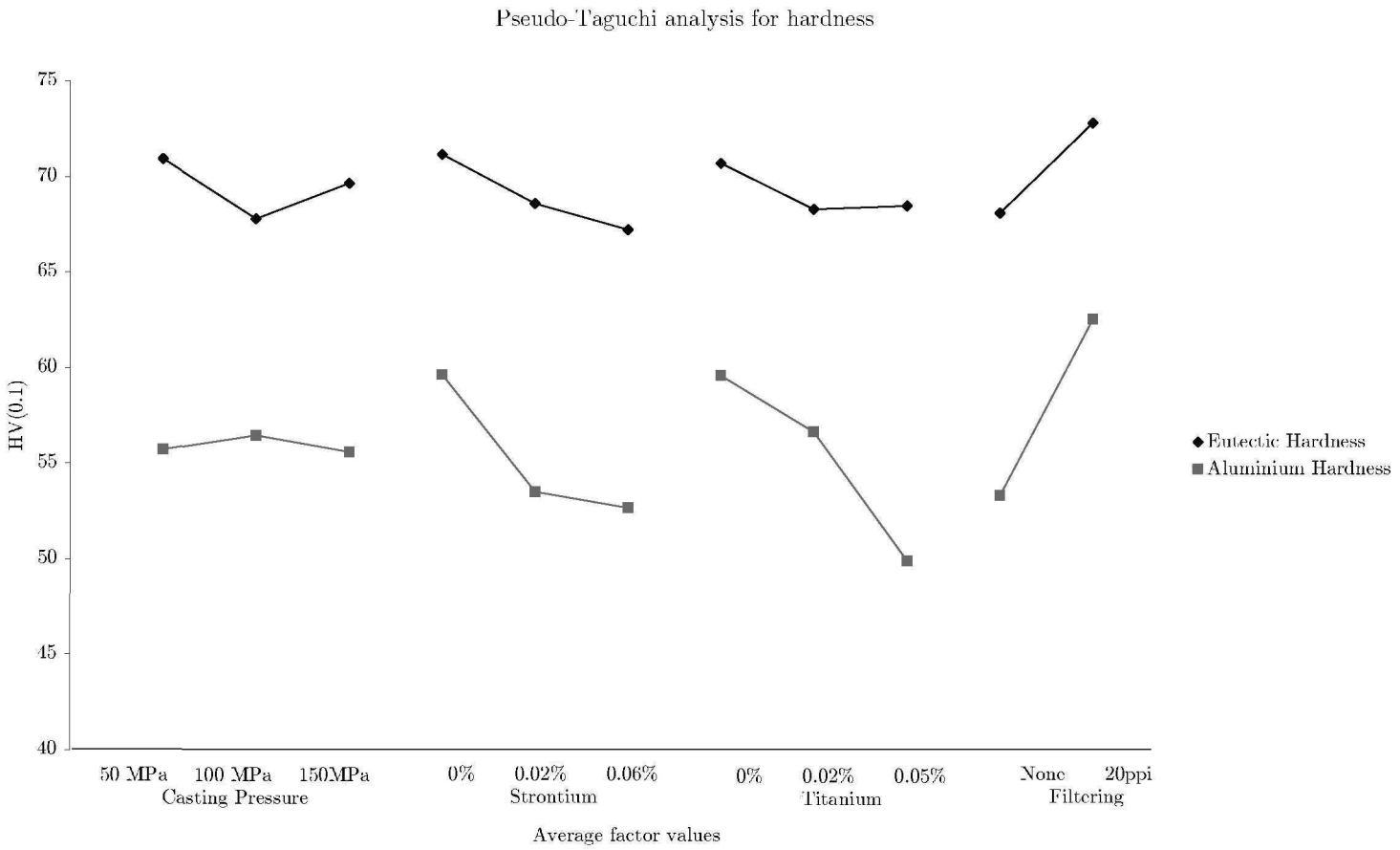

Figure 5.31 Average factor effects on measured hardness of squeeze castings.

5.7 ELECTRON MICROSCOPY

To complement the optical microscopy work and to help in the identification of intermetallic phases, analysis on specimens was carried out using scanning electron microscopy. The method was essentially the same as described by Kral et al[10] - precipitates were identified using either the secondary electron image or the back scattered electron image to obtain atomic number contrast. The appearance of the type and distribution of intermetallics are shown in Figures 5.32(a) and 5.32(b). The distribution and size of the precipitates are finer in the squeeze cast specimen than the sand casting. Individual precipitates are shown in Figures 5.33(a) and 5.33(b).

Once an intermetallic of interest was found, energy dispersive spectroscopy (EDS) analysis was used to identify the elements present in the intermetallic phases. Electron backscatter diffraction (EBSD) patterns from the intermetallics were compared against simulated patterns of possible compounds identified from the EDS data and cross referenced to crystallographic data[61]. This provided a reliable way to identify the crystal structure and the stoichiometry of the intermetallics.

The EDS data for the βAlFeSi was as expected, showing aluminium, silicon and iron peaks. The EDS data for the αAlFeSi was essentially identical, showing the same peaks. This made identification using EBSD harder, as αAlFeSi is generally held to contain manganese, although iron, manganese chromium and possibly copper, have been suggested as interchangeable in the intermetallic[1, pp490-491] . Therefore, crystallographic data of the most likely compounds were re-entered with iron substituting for manganese.

The intermetallic tentatively identified as Al_2SrSi_2 showed the expected strontium peak. A titanium peak occurred at the centre of the intermetallic, which was not unexpected, having been reported by Kral[62]. This would be explained by the precipitate nucleating on a titanium compound arising from the addition of grain refiner to the melt. There was also a strong calcium peak, which was unexpected. This may have arisen from contamination of the strontium master alloy, or more likely, contamination in the melt from particles of refractory insulation containing calcium (e.g.

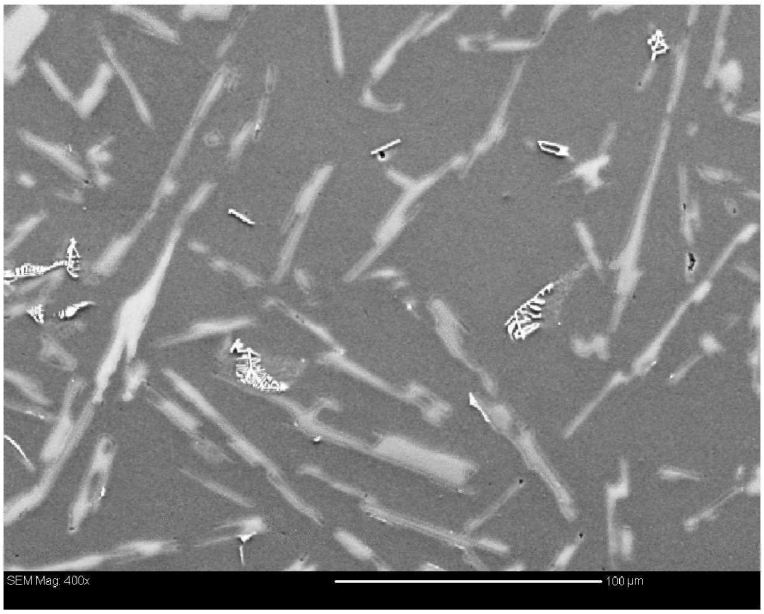

(a) Precipitate field in sand casting 8

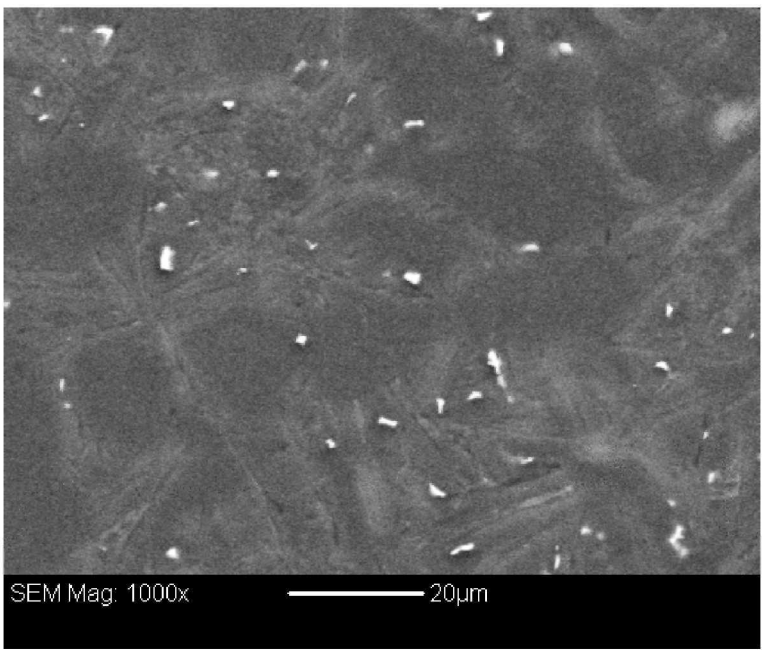

(b) Precipitate field in squeeze casting 8

Figure 5.32 Back-scatter electron images of intermetallic fields present in castings.

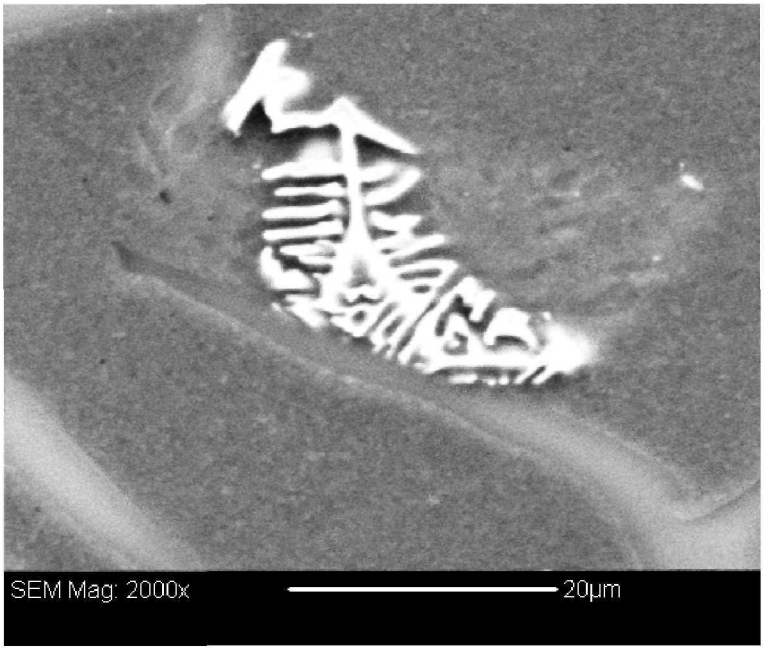

(a) Individual α intermetallic in sand casting 8

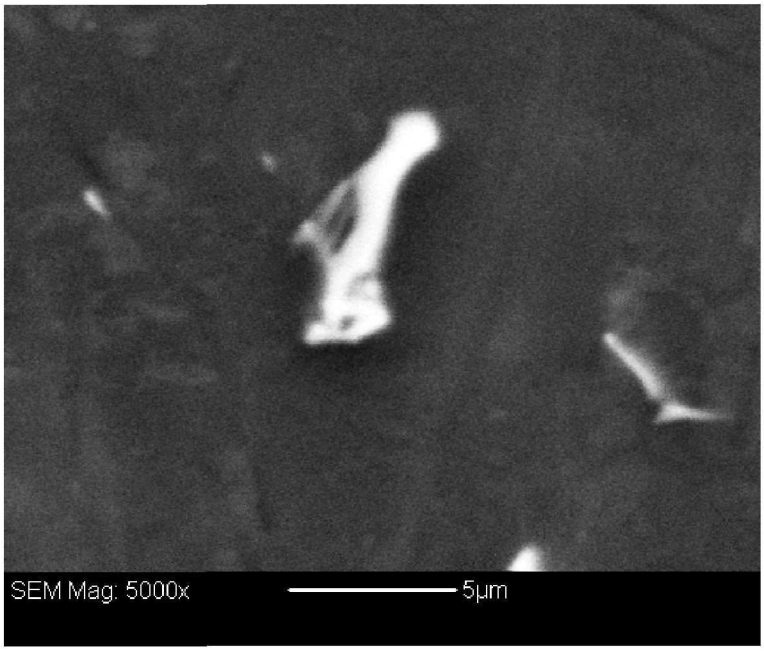

(b) Individual α intermetallic in squeeze casting 8

Figure 5.33 Back-scatter electron images of single intermetallics present in castings.

calcium carbonate) falling into, and reacting with, the melt. The presence of calcium in the intermetallic is easy to explain, as it has the same valency as strontium, and having a slightly smaller atomic radius (1.97 Angstroms) than strontium (2.15 Angstroms), can feasibly substitute for strontium in a crystal structure. Indeed, this mechanism is considered responsible for the undesirable uptake of radioactive strontium 90 in bone, e.g. [63, 64]. No $Al_2(Sr,Ca)Si_2$ was noted in any squeeze castings, being only present in strontium rich sand castings.

The results of the EBSD analysis confirmed the findings of Kral et al[10, 62], in that the needle-like βAlFeSi was resolved as Al_3FeSi_2, and the blocky strontium rich intermetallic was identified as $Al_2(Sr,Ca)Si_2$, based on a Al_2SrSi_2 prototype. The αAlFeSi script was identified as $Al_{19}Fe_5Si_2$, based on an $Al_{19}Fe_4MnSi_2$ prototype. It could be more generally described as an $Al_{19}M_5Si_2$ compound, where "M" is any mixture of Fe and Mn, depending what is present in the alloy. Avoiding the addition of manganese may be desirable, as it has been shown that at the low iron levels allowed in commercial aluminium silicon eutectic alloys, manganese has a detrimental effect on ductility, and at or below the same iron levels, the effect of iron-induced embrittlement is low and the strengthening associated with iron is not compromised[2, pp233-237].

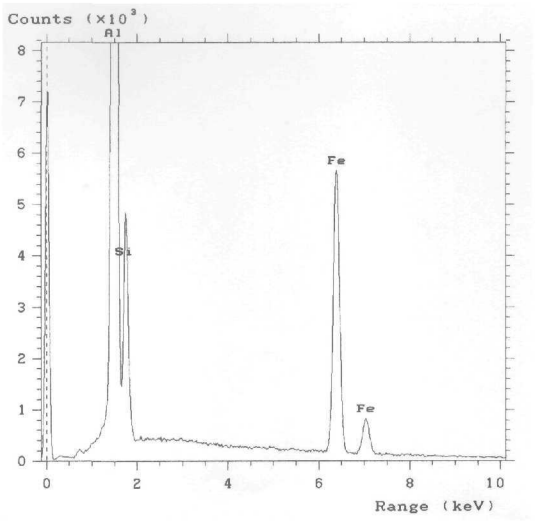

(a) EDS Data from intermetallic

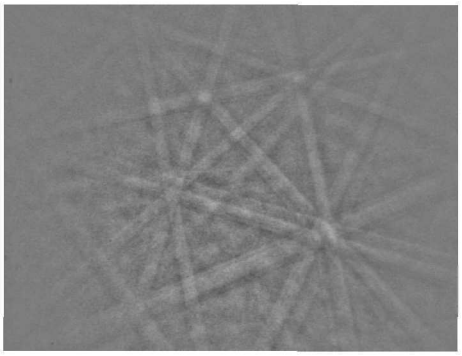

(b) EBSD pattern obtain from intermetallic

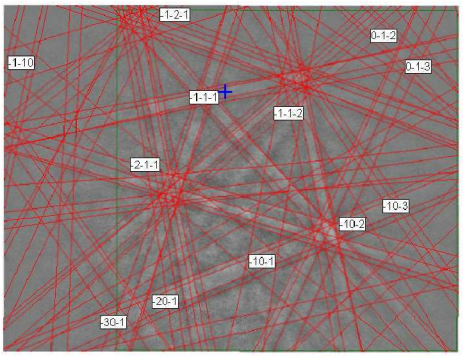

(c) Simulated EBSD solution for intermetallic

Figure 5.34 Typical EDS and EBSD data for an intermetallic identified as αAlFeSi, $Al_{19}M_5Si_2$.

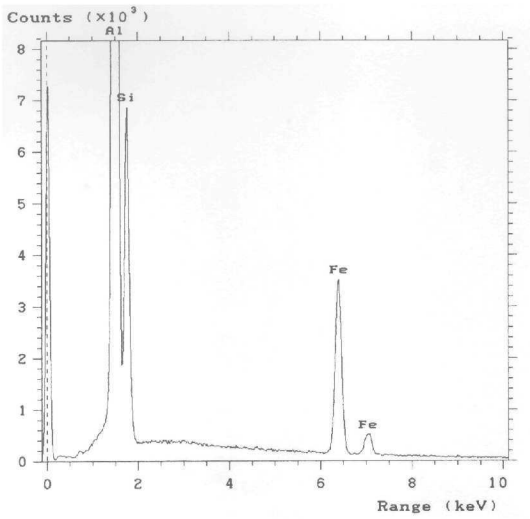

(a) EDS Data from intermetallic

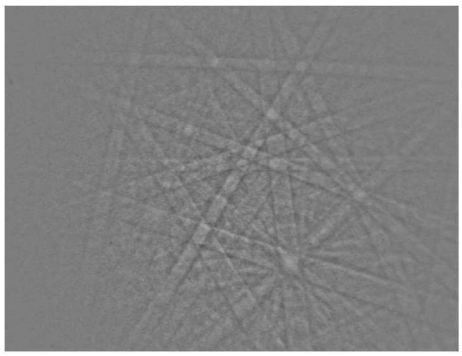

(b) EBSD pattern obtain from intermetallic

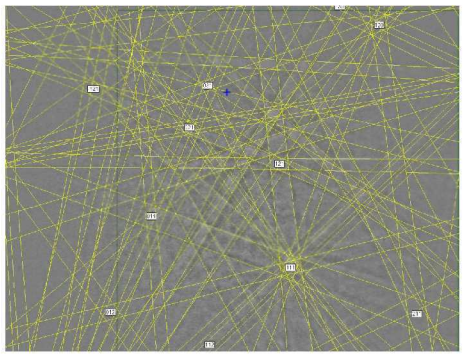

(c) Simulated EBSD solution for intermetallic

Figure 5.35 Typical EDS and EBSD data for an intermetallic identified as βAlFeSi, Al_3FeSi_2.

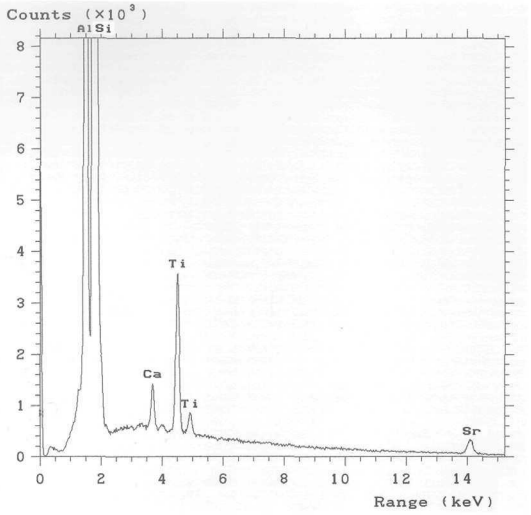

(a) EDS Data from centre of the intermetallic, showing titanium and calcium peaks The EDS data from bulk of the intermetallic showed very small or no titanium peaks

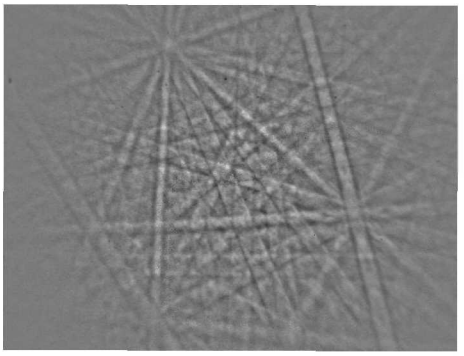

(b) EBSD pattern obtain from intermetallic

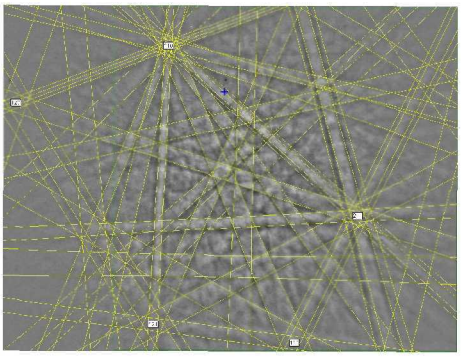

(c) Simulated EBSD solution for intermetallic

Figure 5.36 Typical EDS and EBSD data for an intermetallic identified as $Al_2(Ca,Sr)Si_2$.

Chapter 6

CONCLUSIONS AND RECOMMENDATIONS

6.1 CONCLUSIONS

This research has resulted in the successful design and construction of a bottom fed, bottom tapped squeeze casting machine . It has been used to produce squeeze castings of a commercial aluminium silicon eutectic alloy at a range of pressures and with a range of common micro-alloying additions. Quantitative and qualitative examination of the squeeze castings, compared to conventional sand castings of the same composition, led to the following conclusions:

- The macrostructure of the small volume castings produced by the casting machine were affected significantly by the combination of chill solidification and movement of the solidifying structure during the application of pressure. This would be a source of variability in the overall mechanical behaviour of small squeeze castings unless eliminated through careful melt handling and control of melt volume.

- Squeeze casting eliminated macro-porosity associated with the addition of strontium and titanium (TiBor) master alloys, as well as decreasing porosity to minimal levels in unalloyed castings. There was a small reduction in the measured porosity when the applied casting pressure went from 50MPa to 100Mpa, but no significant change in porosity between the casting pressures of 100MPa and 150 MPa.

- The secondary dendrite arm spacing of squeeze castings was significantly reduced compared to the conventional sand castings. A small measured increase in secondary dendrite arm spacing of the sand cast specimens when 0.05% by weight of titanium grain refiner was added was changed to a small decrease in secondary dendrite arm spacing in the squeeze castings with the same addition of titanium. The size of primary silicon present in any amount in the castings was reduced, although primary silicon formation was not eliminated. Primary aluminium dendrite proportions increased with squeeze castings.

- Squeeze casting increased the measured Vickers hardness of both the primary aluminium and the eutectic. A decrease in hardness of the eutectic in sand castings, associated with the addition of strontium modifier, was eliminated in the squeeze cast specimens.

- Squeeze casting eliminated the formation of $Al_2(Sr,Ca)Si_2$ precipitates associated with excess strontium addition, at the concentrations examined. The size and structure of two common AlFeSi intermetallics was reduced in the squeeze cast specimen. Manganese was not required to promote the growth of αAlFeSi script in the squeeze castings. This form of AlFeSi intermetallic was observed in both sand cast and squeeze cast specimens, but was rare in sand castings with strontium additions of 0.06% by weight, where the undesirable plate-like βAlFeSi was the dominant intermetallic.

- To achieve complete modification of squeeze castings, a modifier addition is still required. Complete modification was not seen at intermediate modifier levels, and the structure of the squeeze eutectic silicon remained flake-like (although much finer than the sand cast specimens) when no modifier was added, regardless of casting pressure.

- Care must be taken to control the atmosphere, especially with respect to humidity, when melting and feeding aluminium in a sealed environment. Avoiding hydroscopic refractories which degas significant amounts of water vapour near the melting temperatures is recommended.

- Ceramic foam filters with a density of 20 pores per inch provided no obstacle to the feeding system, given an extra 10°C superheat.
- The quantitative analytical techniques adapted in this research performed well, within the limitations discussed, especially the quantification of porosity via an inexpensive and common flatbed scanner.

6.2 RECOMMENDATIONS FOR FURTHER WORK

The time taken to develop the squeeze casting rig, and iron out the operational difficulties meant that a large portion of the work envisaged could not be performed in time. Other avenues of investigation revealed themselves as the various analyses were carried out. Recommendations for further work are as follows:

- Develop the squeeze casting machine as laid out in section 3.8, especially in relation to melt control and handling. Further work using this equipment would require more efficient and reliable casting, allowing more significant casting runs to be produced and analysed. The effect of ceramic foam filtration (which is only easily measured via mechanical testing) on the tensile and fatigue properties of the alloy would be a significant area of research.
- One area that has also come from concurrent research[10] in the Department of Mechanical Engineering at the University of Canterbury, is the role of manganese in the morphology of iron-rich precipitates in aluminium silicon alloys. It appears from this body of work that cooling rate or pressure and modifier addition has a significant effect on the preferential form of precipitation, independent of manganese content, and that reducing or eliminated the manganese additions may be desirable for alloys with a low, but non-zero, iron content.
- Combined modifier additions of strontium and sodium has also been investigated recently in the Department of Mechanical Engineering[9]. This reduces the fade effect of sodium, so it may be able to be utilised

as a modifier, via re-melt, in squeeze cast specimens produced by the existing equipment, and to see if the stronger modification of sodium affects the properties of the squeeze casting.

- The design of the hydraulic pressure power pack precluded the use of casting pressure lower than 50MPa. For the alloy and geometry examined, this pressure may be too high for intermediate effects on the casting properties to have occurred. The application of lower pressure and subsequent examination may help the identification of trends within the casting properties.

- Measurement of the thermal behaviour of the melt during casting would reveal much information about the heat transfer rates and solidification behaviour under pressure.

- Further examination of the macro-structure, in the longitudinal direction, will further reveal any possible plastic behaviour during and/or after solidification.

REFERENCES

[1] J.R. Davis, editor. *ASM Specialty Handbook: Aluminium and Aluminium Alloys.* ASM International, 1993.

[2] W. D. Shilvock. *The Effect of Alloy and Impurity Variation on the Treatment, Casting and Physical Properties of Aluminium-Silicon Eutectic Alloys.* PhD thesis, University of Canterbury, 1995.

[3] M. S. Brown. Design and build squeeze casting apparatus. Technical report, Department of Mechanical Engineering, University of Canterbury, 1995.

[4] G. R. Wakefield. *The Effect of Hot Isostatic Pressing (HIPing) on the Properties of Al-10%Mg Castings.* PhD thesis, University of Auckland, 1993.

[5] S. Chatterjee and A.A. Das. Some observations on the effect of pressure on the solidification of Al-Si eutectic alloys. *British Foundryman*, 66, 1973.

[6] S. Chatterjee and A. A. Das. Effects of pressure on the solidification of some commercial aluminium base casting alloys. *British Foundryman*, 65, November 1972.

[7] D.R. Askland. *The Science and Engineering of Materials.* Chapman and Hall, London, 2nd S.I. edition, 1990.

[8] I. J. Polmear. *Light Alloys: Metallurgy of the Light Metals.* Arnold, London, 3rd edition, 1995.

[9] H. R. McIntyre, J. Looij, and M. V. Kral. Effects of simultaneous na and sr additions in an eutectic al-si casting alloy. In Men G. Chu, D. A. Granger, and Qingyou Han, editors, *Solidification of Aluminum Alloys, TMS Annual Meeting*, pages 111–120, Charlotte, NC, 2004. The Metal, Minerals & Materials Society.

[10] M. V. Kral, H. R. McIntyre, and M. J. Smillie. Identification of intermetallic phases in a eutectic Al-Si casting alloy using electron backscatter diffraction pattern analysis (EBSD). *Scripta Materialia*, 51(3):215–219, 2004.

[11] G.A. Chadwick and T. M. Yue. Principles and applications of squeeze casting. *Metals and Materials*, Jan 1989.

[12] G. Williams and K. M. Fisher. Squeeze forming of aluminium-alloy components. *Metals Technology*, October 1981.

[13] *British Standard 1490: Specification for Aluminium and Aluminium Alloy Ingots and Castings*. British Standards Institution, London, 1977.

[14] *Australian Standard 1874:Aluminium and Aluminium Alloys - Ingots and Castings*. Standards Association of Australia, North Sydney, 1988.

[15] S. Rajagopal. Squeeze casting: A review and update. *Journal of Applied Metalworking*, 1(4), 1981.

[16] J.R. Franklin and A.A. Das. Squeeze casting - a review of the status. *British Foundryman*, 77:150–158, 1984.

[17] S. Suzuki. Vertical squeeze casting of aluminium components. *Modern Casting*, October 1989.

[18] Y. Kaneko, H. Murakami, K. Kuroda, and S. Nakazaki. Squeeze casting of aluminium. *Die Casting Engineer*, 22(3), May-June 1979.

[19] R.F. Lynch, R. P. Olley, and P. C. J. Gallagher. Squeeze casting of aluminium. *AFS Transactions*, 75(122), 1975.

[20] J. X. Dong, P. A. Karnezis, G. Durrant, and B. Cantor. The effect of sr and fe additions on the microstructure and mechanical properties of

a direct squeeze cast Al-7Si-0.3Mg alloy. *Metallurgical and Materials Transactions A*, 30A:1341–1356, 1999.

[21] S. Suzuki. Product quality by vertical filling casting machine. *Light Metal Age*, October 1993.

[22] P. V. Evans, R. Keyte, and R. A. Ricks. Squeeze casting of aluminium alloys for near net shape manufacture. *Materials and Design*, 14(1), 1993.

[23] S. Okada, N. Fuji, A. Goto, S. Morimoto, and T. Yasuda. Development of a fully automatic squeeze casting machine. *AFS Transactions*, 82(16), 1982.

[24] C.P. Hong, H.F. Shen, and I.S. Cho. Prevention of macrosegregation in squeeze casting of an Al-4.5 Wt Pct Cu alloy. *Metallurgical and Materials Transactions A*, 29A:339–349, January 1998.

[25] C. P. Hong, H. F. Shen, and S. M. Lee. Prevention of macrodefects in squeeze casting of an Al-7 Wt Pct Si alloy. *Metallurgical and Materials Transactions B*, 31B:297–305, 2000.

[26] S. M. Lee, H. Shen, and C. P. Hong. Formation criterion of macrosegregation in a squeeze-cast Al-7mass%Si alloy. *ISIJ International*, 39:1160–1168, 1999.

[27] Y. Nishida and H. Matsubara. Effect of pressure on heat transfer at the metal mould-casting interface. *British Foundryman*, 69, November 1976.

[28] J. A. Sekhar, G. J. Abbaschian, and R. Mehrabian. Effect of pressure on metal-die heat transfer coefficient during solidification. *Materials Science and Engineering*, 40:105–110, 1979.

[29] S. Rajagopal and W.H. Altergott. Quality control in squeeze casting of aluminium. *AFS Transactions*, 85(16), 1985.

[30] T.H Thiemen and M. Thiemen. Die casting goes vertical. *Die Casting Engineer*, 38(3), 1994.

[31] J. A. Cornie, Y Chiang, D. R. Uhlmann, A. Mortensen, and J. M Collins. Processing of metal and ceramic matrix composites. *American Ceramic Society Bulletin*, 65(2), 1986.

[32] ASM Handbook Committee. *ASM Handbook Vol. 15, Casting.* ASM International, Materials Park, Ohio, 9th edition, 1989.

[33] ASM Handbook Committee. *ASM Handbook Vol. 2, Properties and Selection: Nonferrous Alloys and Special-Purpose Materials.* ASM International, Materials Park, Ohio, 1990.

[34] T. W. Clyne and P. J. Withers. *An Introduction to Metal Matrix Composites.* Cambridge University Press, Cambridge, 1993.

[35] G. Durrant and P. S. Grant. *Metal Matrix Composites Part 1: Application and Processing*, chapter The Manufacture of Squeeze Cast and Spray Formed Al MMC's, pages 155–174. Trans Tech Publications, 1995.

[36] A. C. Street, editor. *The Diecasting Book. (2nd Ed.).* Porticullis Press, Redhill, England, 1986.

[37] B. Upton. *Pressure Diecasting Part 1: Metals - Machines - Furnaces.* Permagon Press, Oxford, England, 1982.

[38] D. F. Allsop and D. Kennedy. *Pressure Diecasting Part 2: The Technology of the Casting and the Die.* Permagon Press, Oxford, England, 1983.

[39] A. J. Clegg. *Precision Casting Processes.* Permagon Press, Oxford, England, 1991.

[40] S. Nourbakhsh, F. L. Liang, and H. Margolin. An apparatus for pressure casting of fibre-reinforced high-temperature metal-composites. *J. Phys. E: Sci Instrum.*, 21:898–902, 1988.

[41] J. E. Shigely. *Mechanical Engineering Design - 1st Metric Edition.* McGraw-Hill, New York, 1986.

[42] J. R. Brown. *Foseco Foundryman's Handbook.* McGraw-Hill, Oxford, 10th edition, 1994.

[43] R. B. Goodman. *A Primer on Pneumatic Valves and Controls.* Krieger Publishing Company, Malabar, Florida, 1997.

[44] I. C. Turner. *Engineering Applications of Pneumatics and Hydraulics.* Arnold, London, 1996.

[45] F. D. Yeaple. *Hydraulic and Pneumatic Power and Control: Design, Performance, Application.* McGraw-Hill, New York, 1966.

[46] A. Barber. *Pneumatic Handbook.* Trade and Technical Press Limited, Surrey, England, 7th edition, 1989.

[47] A. H. Hehn. *Fluid Power Handbook Volume 1: System Design, Maintenance and Troubleshooting.* Gulf Publishing, Houston, Texas, 1993.

[48] A. H. Hehn. *Fluid Power Handbook Volume 2: System Application and Components.* Gulf Publishing, Houston, Texas, 1993.

[49] Fletcher Steel. Mild steel.

[50] Fletcher Steels. Bright bar alloy steels and engineering steels.

[51] Unbrako Pty Ltd. Technical catalogue 5928.

[52] ASM Handbook Committee. *ASM Handbook Vol. 1, Properties and Selection : Irons, Steels, and High Performance Alloys.* ASM International, Materials Park, Ohio, 1990.

[53] *BS5500 Unfired Fusion Welded Pressure Vessels.*

[54] J. Looj. Furnace comments. Private communication, 2004.

[55] G. Vander Voort. Tech-notes: Preparation of cast aluminum-silicon alloys. Technical Report Vol 3, Issue 2, Buehler Ltd., 1999.

[56] ASM Handbook Committee. *ASM Handbook Vol. 9, Metallography and Microstructures.* ASM International, Materials Park, Ohio, 9th edition, 1989.

[57] G.F. Vander Voort. *Metallography, Principles and Practice*. McGraw-Hill, New York, 1984.

[58] A. B. Lintott. Fitting multi-modal distributions. Private communication, 2001.

[59] ABAQUS Inc. Abaqus 6.5-1, 2005.

[60] B. Hu and H. Li. Grain refinement of din226s alloy at lower titanium and boron addition levels. *Journal of Materials Process Engineering*, 74:56–60, 1998.

[61] P. Villars and L. D. Calvert. *Pearson's Handbook of Crystallographic Data for Intermetallic Phases*, volume 1. ASM International, Materials Park, Ohio, 2nd edition, 1991.

[62] M. V. Kral. EBSD identification of strontium precipitates. Private communication, 2004.

[63] K. C. Stamoulis, P. A. Assimakopoulos, K. G. Ioannides, E. Johnson, and P. N. Soucacos. Strontium-90 concentration measurements in human bones and teeth in Greece. *The Science of The Total Environment*, 229(3):165–182, May 1999.

[64] H. Spencer, L. Kramer, J. Samachson, E. P. Hardy, and J. Rivera. Strontium-90 Calcium interrelationships in man. *Health Phys.*, 24(5):525–533, May 1973.

Appendix A

EXPERIMENTAL DATA

Experiment	**1**	**2.1**	**2**	**3**	**4**	**5**	**6**	**7**	**8**	**9**
Initial Mass of Melt (g)	5500	5624	5500	5320	5365	5485	5400	5310	5265	5415
Total Mass of Melt (g)	5500	5637	5574	5374	5400	5523	5463	5402	5289	5450
% Sr Required	0.00%	0.02%	0.02%	0.06%	0.02%	0.06%	0.00%	0.06%	0.00%	0.02%
Sr Required (g)	0.00	1.13	1.11	3.22	1.08	3.31	0.00	3.24	0.00	1.09
Master alloy addition (g)	0.00	11.27	11.15	32.25	10.80	33.14	0.00	32.41	0.00	10.90
Al mass added (g)	0.00	10.03	9.92	28.70	9.61	29.49	0.00	28.84	0.00	9.70
% Ti Wanted	0.000%	0.000%	0.050%	0.020%	0.020%	0.000%	0.050%	0.050%	0.020%	0.020%
%Ti Present	0.000%	0.002%	0.002%	0.006%	0.002%	0.006%	0.000%	0.006%	0.000%	0.002%
% Ti Required	0.000%	0.000%	0.048%	0.014%	0.018%	0.000%	0.050%	0.044%	0.020%	0.018%
Ti addition (g)	0.00	0.00	2.68	0.75	0.97	0.00	2.73	2.38	1.06	0.98
Ti master alloy addition (g)	0.00	0.00	53.51	15.05	19.44	0.00	54.63	47.53	21.16	19.62
Al mass added (G)	0.00	0.00	50.30	14.14	18.27	0.00	51.35	44.68	19.89	18.44
Total Al mass added	0.00	10.03	60.22	42.84	27.88	29.49	51.35	73.53	19.89	28.14
Original % Si	12.70%	12.70%	12.70%	12.70%	12.70%	12.70%	12.70%	12.70%	12.70%	12.70%
Mass Si (g)	698.5	714.248	698.5	675.64	681.355	696.595	685.8	674.37	668.655	687.705
New % Si	12.70%	12.67%	12.53%	12.57%	12.62%	12.61%	12.55%	12.48%	12.64%	12.62%
Required % Si	0.00%	0.03%	0.17%	0.13%	0.08%	0.09%	0.15%	0.22%	0.06%	0.08%
Required Mass Si (g)	0.00	1.64	9.41	6.88	4.40	4.82	7.95	11.63	3.08	4.44
Total Added Mass (g)	0.00	12.91	74.07	54.17	34.64	37.96	62.57	91.57	24.23	34.96
% Added mass	0.0%	0.2%	1.3%	1.0%	0.6%	0.7%	1.1%	1.7%	0.5%	0.6%

Table A.1 Alloy additions to experimental castings.

Experiment	Casting Pressure (MPa)	% Sr	% Ti	% alloy	Filtration	Sand cast porosity %	Squeeze cast porosity %
1	50	0.00%	0.000%	0.000%	0	0.92	0.15
2.1	50	0.02%	0.002%	0.022%	0	2.27	0.02
2	50	0.02%	0.050%	0.070%	0	1.97	0.05
3	50	0.06%	0.020%	0.080%	20	1.81	1.46
4	100	0.02%	0.020%	0.040%	0	1.31	0.02
5	100	0.06%	0.006%	0.066%	0	2.01	0.02
6	100	0.00%	0.050%	0.050%	20	1.53	0.04
7	150	0.06%	0.050%	0.110%	0	2.74	0.02
8	150	0.00%	0.020%	0.020%	0	2.16	0.01
9	150	0.02%	0.020%	0.040%	20	1.33	0.02

Table A.2 Measured porosity of specimens.

Factor Number	Factor	Sand cast porosity %	Squeeze cast porosity %
1	50 MPa	N/A	0.05
2	100 MPa	N/A	0.03
3	150 MPa	N/A	0.02
4	0% Sr	1.54	0.07
5	0.02% Sr	1.72	0.03
6	0.06% Sr	2.37	0.02
7	0% Ti	1.63	0.07
8	0.02% Ti	1.60	0.02
9	0.05% Ti	2.18	0.03
10	No Filtering	N/A	0.04
11	20ppi Filtering	N/A	0.03

Table A.3 Average Kakuchi factors for porosity.

Experiment	Pressure (MPa)	% Sr	% Ti	% alloy	Filtration	Squeeze cast average DAS (μm)	Sand cast average DAS (μm)
1	50	0.00%	0.020%	0.020%	0	14.0	50.4
2.1	50	0.02%	0.006%	0.026%	0	11.1	46.9
2	50	0.02%	0.050%	0.070%	0	5.6	46.5
3	50	0.06%	0.050%	0.110%	20	14.7	38.6
4	100	0.02%	0.020%	0.040%	0	9.9	49.1
5	100	0.06%	0.020%	0.080%	0	4.7	39.3
6	100	0.00%	0.000%	0.000%	20	11.2	46.4
7	150	0.06%	0.000%	0.060%	0	5.0	49.4
8	150	0.00%	0.000%	0.000%	0	11.4	49.6
9	150	0.02%	0.000%	0.020%	20	7.9	38.0

Table A.4 Measured secondary dendrite arm spacing for castings.

Factor Number	Factor	Squeeze cast average DAS (μm)	Sand cast average DAS (μm)
1	50 Mpa	7.7	N/A
2	100 MPa	8.6	N/A
3	150 MPa	8.1	N/A
4	0% Sr	12.2	48.8
5	0.02% Sr	8.6	45.1
6	0.06% Sr	8.1	44.4
7	0% Ti	9.9	45.5
8	0.02% Ti	9.7	45.5
9	0.05% Ti	7.3	47.4
10	No Filtering	8.8	N/A
11	20ppi Filtering	9.5	N/A

Table A.5 Average Kakuchi factors for secondary dendrite arm spacing.

Experiment	Eutectic HV1	Eutectic HV2	Eutectic HV3	Average Eutectic HV	Al HV1	Al HV2	Al HV3	Average Al HV
1	63.1	61.6	58.3	61.0	43.4	41.3	42.6	42.4
2.1	55.2	55.2	62.1	57.5	43.2	42.7	44.7	43.5
2	51.0	61.1	63.0	58.4	41.0	48.5	46.3	45.3
3	55.1	55.5	54.7	55.1	44.6	40.4	44.9	43.3
4	59.0	65.0	67.1	63.7	43.1	45.6	47.7	45.5
5	48.7	49.0	59.7	52.5	47.4	46.5	43.8	45.9
6	63.9	53.7	62.8	60.1	48.9	39.9	45.4	44.7
7	50.8	48.9	52.3	50.7	46.5	50.8	42.7	46.7
8	51.9	63.2	61.2	58.8	44.3	44.3	39.2	42.6
9	53.0	58.7	60.6	57.4	45.4	43.2	44.5	44.4

Table A.6 Measured Vickers microhardness for sand castings.

		Distribution Analysis					
Casting Run	**Threshold Si %**	***Al proportion***	***Si proportion***	***Si+Noise proportion***	***Al %***	***Si %***	**Eutectic HV**
1	14.6%	0.71880	0.13347		84%	16%	63.1
1	17.5%	0.72808	0.15395		83%	17%	61.6
1	15.2%	0.75631	0.12306		86%	14%	58.3
2	16.1%	0.72887	0.13391		84%	16%	55.2
2	17.5%	0.67352	0.14940		82%	18%	55.2
2	17.3%	0.72469	0.15032		83%	17%	62.1
2	16.6%	0.68250		0.31750	68%	32%	51.0
2	18.9%	0.66018		0.33982	66%	34%	61.1
2	14.9%	0.68329		0.31672	68%	32%	63.0
3	19.0%	0.66564		0.33436	67%	33%	55.1
3	14.3%	0.75478		0.24522	75%	25%	55.5
3	16.1%	0.71506		0.28494	72%	28%	54.7
4	18.0%	0.72234	0.16532		81%	19%	59.0
4	15.7%	0.69141	0.15184		82%	18%	65.0
4	18.5%	0.63370	0.18075		78%	22%	67.1
5	15.7%	0.70624	0.11952		86%	14%	48.7
5	14.7%	0.70234	0.11902		86%	14%	49.0
5	16.2%	0.61306		0.38694	61%	39%	59.7
6	16.1%	0.74307		0.13006	74%	13%	63.9
6	15.3%	0.72145		0.14683	72%	15%	53.7
6	17.0%	0.70759		0.14693	71%	15%	62.8
7	16.9%	0.74814		0.11973	75%	12%	50.8
7	15.4%	0.70364		0.29636	70%	30%	48.9
7	14.5%	0.70647		0.29354	71%	29%	52.3
8	15.0%	0.74870	0.14276		84%	16%	51.9
8	18.0%	0.72780	0.16469		82%	18%	63.2
8	15.4%	0.79078	0.13648		85%	15%	61.2
9	15.0%	0.70769		0.29231	71%	29%	53.0
9	16.5%	0.72452		0.13014	72%	13%	58.7
9	16.6%	0.70886		0.13759	71%	14%	60.6

Table A.7 Areal analysis of sand cast eutectic silicon with associated hardness.

Experiment	Eutectic HV1	Eutectic HV2	Eutectic HV3	Average Eutectic HV	Al HV1	Al HV2	Al HV3	Average Al HV
1	70.4	68.1	68.7	69.1	59.0	59.5	58.8	59.1
2.1	77.3	69.7	74.0	73.7	57.2	56.1	60.9	58.1
2	64.5	71.6	65.5	67.2	43.1	44.4	47.4	45.0
3	76.3	71.2	73.8	73.8	60.9	56.8	64.6	60.8
4	61.7	59.4	61.8	61.0	46.5	47.6	46.5	46.9
5	72.2	69.0	66.9	69.4	53.0	65.4	66.4	61.6
6	72.6	72.2	74.5	73.1	62.4	58.3	62.1	60.9
7	66.5	66.8	62.0	65.1	46.1	42.0	43.2	43.8
8	73.6	69.8	70.8	71.4	60.7	53.7	62.2	58.9
9	73.6	71.6	72.4	72.5	66.0	65.9	60.6	64.2

Table A.8 Measured microhardness for squeeze castings.

		Distribution Analysis				
Casting Run	**Threshold Si %**	***Al proportion***	***Si+Noise proportion***	***Al %***	***Si %***	**Eutectic HV**
1	21%	0.68349	0.31652	68%	32%	70.4
1	18%	0.72029	0.27972	72%	28%	68.1
1	19%	0.71836	0.28164	72%	28%	68.7
2a	20%	0.62398	0.37602	62%	38%	77.3
2a	18%	0.67259	0.32741	67%	33%	69.7
2a	16%	0.69166	0.30834	69%	31%	74.0
2	22%	0.70807	0.29193	71%	29%	64.5
2	16%	0.75498	0.24502	75%	25%	71.6
2	14%	0.72529	0.27471	73%	27%	65.5
3	16%	0.58899	0.41101	59%	41%	76.3
3	18%	0.69665	0.30335	70%	30%	71.2
3	16%	0.71520	0.28480	72%	28%	73.8
4	15%	0.71278	0.28722	71%	29%	61.7
4	15%	0.61392	0.38608	61%	39%	59.4
4	13%	0.63472	0.36528	63%	37%	61.8
5	16%	0.58928	0.41073	59%	41%	72.2
5	15%	0.76434	0.23566	76%	24%	69.0
5	13%	0.61923	0.38077	62%	38%	66.9
6	18%	0.63865	0.36136	64%	36%	72.6
6	23%	0.61025	0.38976	61%	39%	72.2
6	19%	0.69473	0.30527	69%	31%	74.5
7	16%	0.67916	0.32085	68%	32%	66.5
7	19%	0.73328	0.26672	73%	27%	66.8
7	16%	0.65504	0.34496	66%	34%	62.0
8	15%	0.58244	0.41756	58%	42%	73.6
8	22%	0.57657	0.42343	58%	42%	69.8
8	19%	0.62839	0.37161	63%	37%	70.8
9	21%	0.55326	0.44674	55%	45%	73.6
9	21%	0.73225	0.26776	73%	27%	71.6
9	22%	0.66849	0.33151	67%	33%	72.4

Table A.9 Areal analysis of squeeze cast eutectic silicon with associated hardness.

Appendix B

OPERATING INSTRUCTIONS FOR SQUEEZE CASTING RIG

B.1 FURNACE SECTION

B.1.1 Introduction

The furnace is an electrical resistive element furnace that can be pressurised to a maximum of 1 bar gauge pressure. A Kanthal spiral pinned into a refractory cement lining provides the heating. The refractory cement and a layer of Kaowool blanket insulation provide thermal and electrical insulation.

B.1.2 Power Supply

The furnace is powered by single phase 240V AC. The furnace maximum power rating is 2.4 kW. This requires a power outlet with at least 10 amps capacity. Another outlet is required to power the metal level sensing circuit.

B.1.3 Temperature Control

Temperature control can be supplied by two methods. One is a simple voltage control - using a solid-state voltage limiter to limit the current flowing through the heating element. This is simple but the control over temperature variation is limited to manual adjustment.

A solid state temperature controller can also be used to control the furnace temperature. The use of this can be limited as there may be current surge when the supply is switched on and off. Make sure the power outlet used has sufficient protection and capacity if this is the case. The temperature controller can also be used in conjunction with the voltage controller to reduce the maximum power going into the furnace.

B.1.4 Sealing and Pressurisation

A copper o-ring sitting between the top flange and the lid of the furnace seals the furnace. The lid is nominally attached by 12 M6 cap screws. Note that one has been replaced by a M8 cap screw. Also note, the lid has slightly buckled during fabrication and sealing can be difficult to obtain. Any small areas of leakage can be temporarily sealed with a high-temperature silicone sealant. This would have to be replaced each time the lid is opened.

A graphite gland seal is used to seal the central feed stalk. It is tightened by a large hex gland nut. The graphite seal may need to be replaced at irregular intervals due to degradation at high temperatures.

The furnace is pressurised by inert gas (Nitrogen or Argon) up to a maximum of 1 bar. **The safety valve is set to 1 bar or less and should never be altered, unless to set to a lower pressure. The operating pressure has been set at 0.15 bar for the casting performed to date.** The supply pressure is regulated by a precision regulator. This can be set so the furnace does not exceed a certain value. The supply pressure can be increased to increase flow through the flow control valve to make up for leakage.

B.1.5 Electrical Safety

The heating element is isolated from earth by the surrounding thermal insulation. If the heating element fails or touches the metal crucible, an earthing wire connects the crucible to the body of the furnace, which is earthed. **Never operate the furnace with this wire unattached.** The heating element is not exposed when the furnace lid is open, being covered

by Kaowool. However, **never operate the furnace when the lid is open and the elements exposed to touch.**

B.1.6 Thermal Safety

At operating temperature the body of the furnace is hot enough to burn. A Kaowool layer wrapped around the body of the furnace provides some protection. When the furnace is at its operating temperature, the inside of the furnace can be at 700 degrees Celsius. **Always use protection, such as gloves and aprons when working with the furnace open.** If the lid is raised after the furnace is operational, the lid, lid insulation and the melt transfer stalk will be hot. Be aware of this.

B.1.7 Furnace Operation - Step by Step

1. Check electrical safety.
2. Check insulation for wear or gaps.
3. Check connections to earth.
4. Check suitable power supply.
5. Check inside of furnace.
6. Re-coat furnace, stalk or thermocouple if necessary.
7. Install melt filters in stalk if required.
8. Place small pieces of the aluminium alloy in the crucible, up to the mass required. Space any alloying additions amongst the aluminium pieces.
9. Leave a space for the transfer stalk - a steel pipe can be used as a spacer.
10. Seal furnace lid.
11. Check pressurisation.

12. Place temporary plate over stalk lid and pressurise furnace to check the seal. Once the furnace is satisfactorily sealed, release pressure and remove plate.

13. Move furnace and attach to angled transfer stalk leading to die.

14. Switch on temperature controller and set temperature (usually 700 degrees Celsius).

15. Wait for operating temperature to be reached. This should be between 3 and 5 hours, dependant on the amount being melted. It may be prudent to set the temperature to below the melting point of the alloy being melted and check operation of the furnace before melting occurs. If the furnace is operating satisfactorily, set the furnace temperature to the required melt temperature.

16. To remove moisture and/or smoke from water and oil contamination, cycle the furnace pressurisation circuit to flush them out via the exhaust. **This needs to be done at temperatures below the melting point of the alloy (570°C) otherwise pressure transients may force the melt up the transfer stalk, where it will solidify and block the feeding of metal into the die.**

17. Commence casting operation.

B.2 DIE SECTION

B.2.1 Introduction

The squeeze casting die has two arrangements: a direct pressure application via a vertically mounted 10 tonne hydraulic ram, applying pressure to the end of a cylindrical specimen, and direct pressure application to the four long sides of an rectangular specimen via four horizontally mounted 50 tonne hydraulic rams. Molten metal is fed via a pressurised furnace into a sleeve, from which it is injected into the preheated die by the vertical ram and pressurised by either the vertical ram or 4 horizontal rams.

B.2.2 Power Supply

The die requires 4 power supplies. Three phase AC is required to power the hydraulic pump. Note that even though the rated current is 14 amps, current surge on startup requires at least a 20 amp capable power supply. Single phase, 240V AC is required to power the cooling fan on the hydraulic power pack, the control switches, and the die heaters. The last item requires its own 10 amp capable outlet.

B.2.3 Hydraulics Operation

The hydraulic power pack incorporates a high flow, high pressure capability with an accumulator, a cooling fan, and a 150 litre reservoir. Two pressure switches that control the hydraulic pump operation can be adjusted to alter the hydraulic pressure between 300 and 3000 psi (10kN to 100kN force from the vertical ram). 12V solenoid valves within a manifold block on the power pack control the operation of the die. Control is via a switch box with three switches - one to turn the unit on, one to move the vertical ram up or down and one to move the horizontal rams in or out.

B.2.4 Die Operation

B.2.4.1 Uniaxial (Vertical) Pressure Application

- Ensure die is firmly in place and closed firmly. Check top plug is held down firmly.
- Check the die heating elements wires are not shorted out.
- Place protective cover over die.
- Turn power on.
  - Hydraulic power pack.
  - Oil cooler, if necessary.
  - Hydraulic control switches.

– Die heaters.

Note: Never operate die heaters without the protective cover. This protects from electric shock. The die heaters heat the die to a steady state temperature of approximately 300 degrees Celsius after 30 minutes of operation. The steady state temperature is controlled via a solid state variac. The variac setting should be calibrated for each particular die configuration and desired temperature. After melt and die temperature are suitable, inject melt into die sleeve.

Method 1 (melt volume not important)

1. Turn off die heaters.
2. Pressurise furnace until 0.13 bar is reached. This will ensure the melt fills the entire die. Note further pressure may be required if a ceramic filter is used, but this has not been observed in practice.
3. Quickly activate the vertical die. This will force metal back down the tube as the injector seals off the die, possible increasing the pressure inside the furnace.
4. Once the vertical ram is static, immediately depressurise the furnace. Excess melt should return to the furnace.
5. Wait until melt is solid (dependant on die temperature, casting temperature and casting pressure, but should be less than three minutes) and remove the protective covers, slightly open die, and remove the top plug. Use the remaining travel of the plunger to push the casting up out of the die. In practice, this takes anywhere from 10 minutes to hours, if die soldering has taken place. In practise, during the solidification and cooling of the casting specimen, the furnace was opened and excess melt was poured into various molds for reuse or analysis.
6. Remove casting, clean and lubricate die, close and cover die in readiness for next casting. In practice, casting was limited to one specimen a day, with a day of cleanup and preparation for casting again, two days after the last cast.

Method 2 (Melt volume control) This method has not been tried, as the risk of solidification during the wait periods (e.g. step 3) was too high, due to both lack of heating/insulation and leakage of pressure (and therefore a drop in melt height) in the furnace. This method needs an accurate, electronic pressure reading to allow precise control of the melt delivery. The casting equipment was designed to allow such automated control, but as currently exists, manual control, as described previously, is the only option.

1. Activate level sensor unit.
2. Pressurise furnace. Melt level sensor unit will stop pressurisation when the metal level is at the sensor level.
3. Noting the furnace pressure, increase by 4 to 5kPa. This represents a melt height increase of approximately 150mm i.e.

   Height (m) = pressure (Pa) / (g * density (kg/m^3))

   0.145 = 4000 / (9.81 * 2800)
4. Quickly activate the vertical die. Once the vertical ram is static, immediately depressurizes the furnace. Excess melt should return to the furnace.
5. Turn off die heaters.
6. Wait until melt is solid (dependant on die temperature, casting temperature and casting pressure) and remove the protective covers, slightly open die, and remove the top plug. Use the remaining travel of the vertical ram to push the casting up out of the die.
7. Remove casting, clean and lubricate die, close and cover die in readiness for next casting.
8. Repeat casting procedure until all melt has been used.
9. Turn off power to the die heaters, furnace and hydraulics to allow cooling.

10. Remove any solidified aluminium from the furnace and transfer stalk (May require some disassembly and localised heating).

11. Ready furnace and die for next set of castings.

B.3 MAINTENANCE AND TROUBLESHOOTING

B.3.1 Maintenance

Generally, the squeeze casting rig needs little regular maintenance. Replacement parts would be used as required. Consideration should be given to the following:

Corrosion To prevent the build up of rust, a light spray of oil (e.g. CRC5.56, WD40 or LPS) should be used on all bare metal parts when the equipment is not in use.

Insulation Torn or ragged insulation should be replaced.

Seals The O-rings are custom items, fabricated from annealed copper wiring. Either use a suitable diameter wire or slightly flatten a wire to form an elongated cross section.

Heating element The furnace element was obtained from Argus Heating Ltd, Christchurch. It should only be replaced if it is burnt out and not able to be repaired.

Hydraulic Powerpack Check the level of the hydraulic oil in the powerpack. Check operation of controller box.

Hydraulic lines Check for leaks at the joins.

Die parts Keep moving die parts well lubricated with graphite powder.

B.3.2 Troubleshooting

There is power going into the furnace but the temperature is falling! The furnace element has burnt out. Repair or replace element after furnace has cooled down.

The furnace controller is not working! Check that power is being supplied - check connections, fuses, power supply circuit breakers.

I can't get the furnace to pressurise! Check the seals on the furnace - look for notches in the O-ring. Feel for leaks and tighten the lid bolts around the leaks. Check to see the pressure supply line is not blocked by debris or twisted shut. Increase supply pressure to account for small leakage - do not increase to more than 1.0 bar.

The furnace is not getting past 570 to 580 °C. The alloy in the furnace is in the process of melting. The energy supplied by the furnace is going into melting the metal, rather than increasing the temperature. Wait approximately 10 minutes per kg of aluminium.

Where is all that water coming from? The refractory used in insulating the furnace is hydroscopic. Ensure the furnace is preheated before melting to drive out any moisture. Use dry (Laboratory grade) inert gases to pressurise the furnace. If there is moisture/water present at any stage during the casting process, a molten aluminium/steam reaction will occur.

The injection ram won't go down! The flow from the pump seems to swamp one of the hydraulic valves. To retract the injection ram, open the manual valve at the base of the ram. Do not operate the ram while this valve is open, as the tubing is not rated for operational pressure. The small amount of flow/pressure in the system when the hydraulic power-pack is active is sufficient to lower the ram slowly when the valve is released.

There is solidified aluminium in the feed system! This may occur on a regular basis after a casting run. The two feed tubes can be removed from the casting die and placed in a furnace to melt the majority of the metal out. To remove solidified metal from the injection block, remove as much as possible from the inlet via drilling and use the injection ram to punch the remaining metal out through the top.

Appendix C

SELECTED MANUFACTURING DRAWINGS

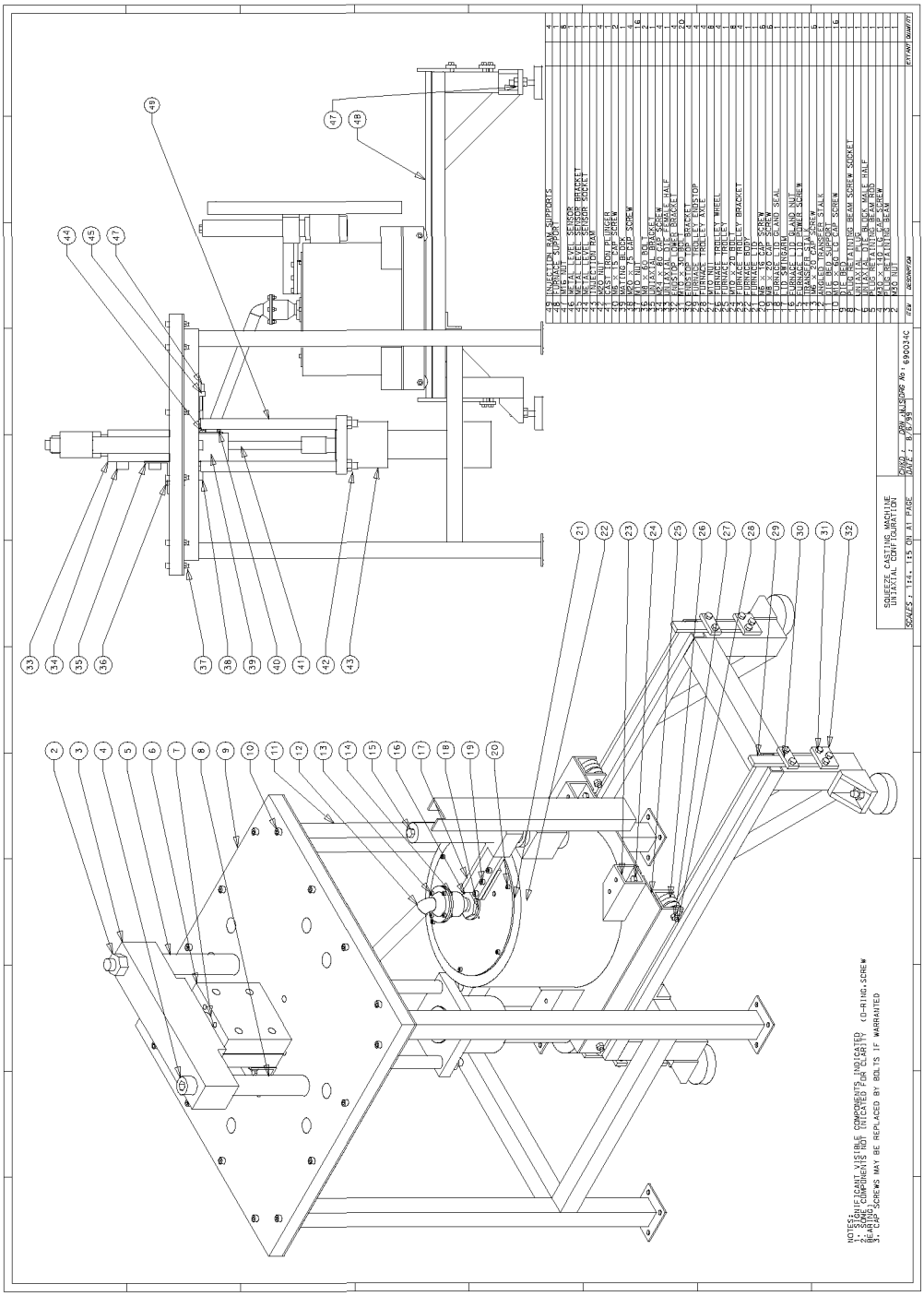

Figure C.1 Uniaxial die and furnace assembly.

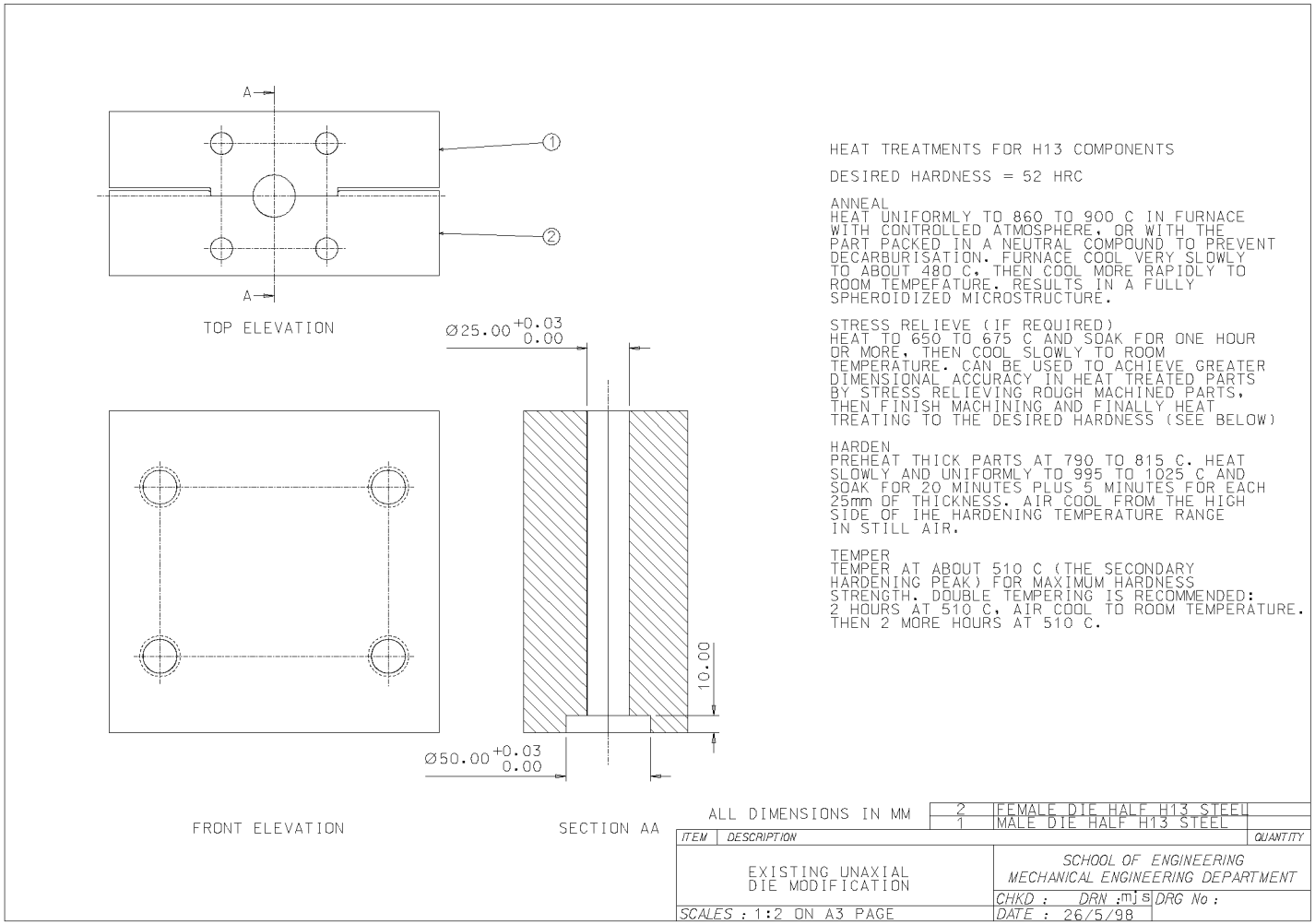

Figure C.2 Uniaxial die detail.

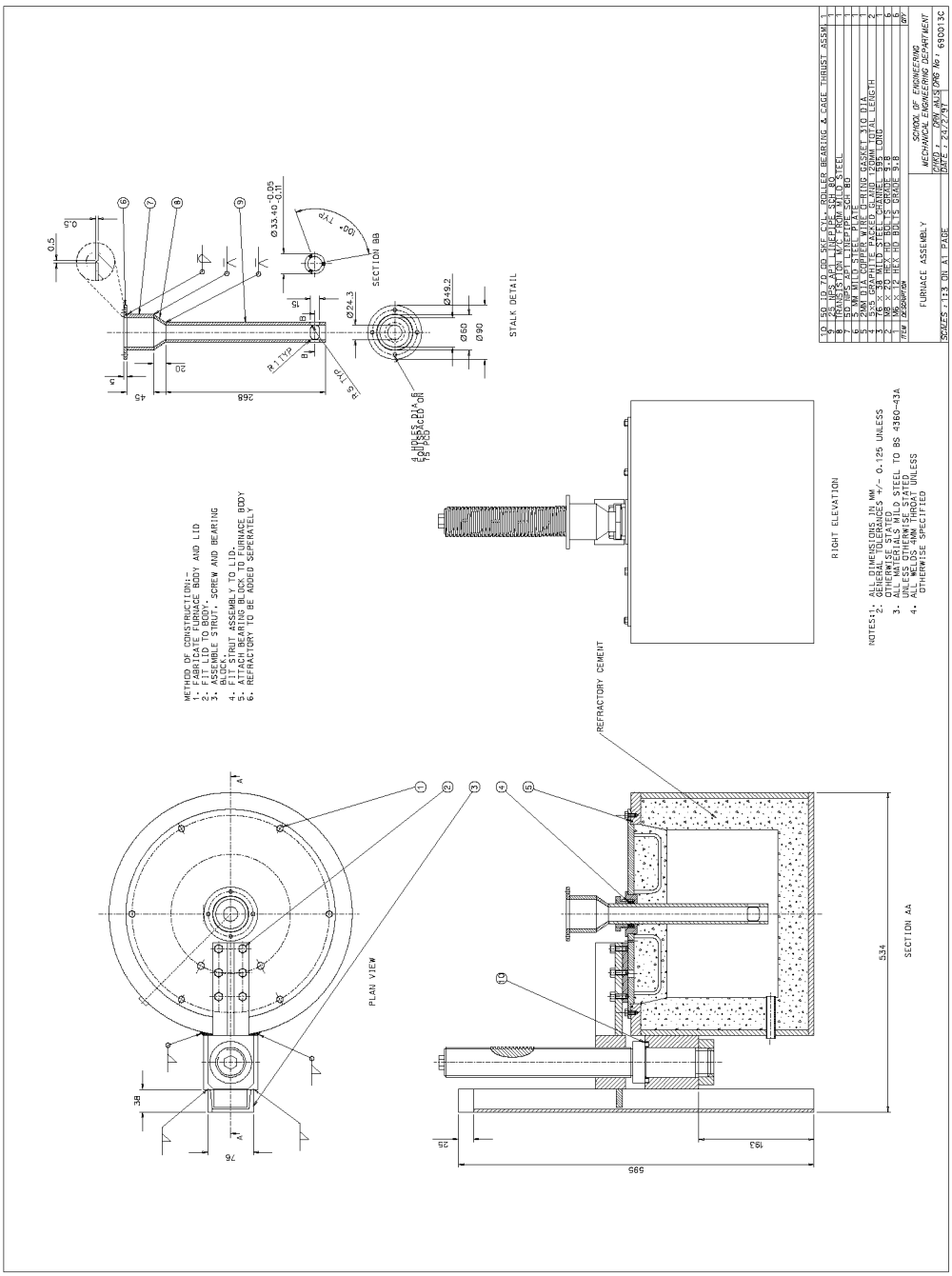

Figure C.3 Furnace design.

Appendix D

IMAGE ANALYSIS MATLAB^{TM} SOURCE CODE

The following source code is run as a MATLAB^{TM} script file, called from the MATLAB^{TM} command interpreter. Such code can be easily converted into a MATLAB^{TM} function. The file input/output as shown varies according to the way files were analysed: individually or in batches.

Lines prefixed with a % are comments within the MATLAB^{TM} code.

D.1 POINT COUNTER

```
% point_count.m
% Display an image with an equispaced grid of n^2 points.
% Used for metallographic point counting.
% Uses .bmp images
% Version 040620 Author: Matt Smillie
    clf;
    clc;
    clear;
% Read and display the image
    cd('c:\image_path\');
    current_image='image_file.bmp';
    image=imread(current_image);
    image_size=size(image);
% Set the number of points: total number is point_root squared.
% Note that the image dimension is divided by point_root+1 to get
% equispaced points _inside_ the image.
    point_root=8;
    big_dimension=max(image_size)*.9;
```

```
    small_dimension=min(image_size)*.9;
    point_spacing=small_dimension/(point_root+1);
    points=[min(point_spacing):point_spacing:small_dimension-point_spacing];
    points=round(points);
% Randomise the placement of the grid inside the image
    offset1=-min(points)+rand*(max(image_size)-max(points)
        -(min(points)/2));
    offset2=-min(points)+rand*(min(image_size)-max(points)
        -(min(points)/2));
% Store the position of each point in points_data
    points_data=[];
        for i=1:length(points);
            for j=1:length(points);
                points_data=[points_data ;
                points(i), points(j)];
            end;
        end;
    [n,p]=size(points_data);
% Show the grid of points over the image
    figure(1);
    axis tight;
    axis off;
    hold on;
    colormap(gray);
    imagesc(flipud(image));
    h=plot(points_data(1:n,1)+offset1,points_data(1:n,2)+offset2,'+r');
% Loop, picking up the points.
    disp('Left mouse button picks inside points.')
    disp('Hit return to finish')
    but=1;
    ones=0;
    halves=0;
        while ~isempty(but)
            [xones,yones,but] = ginput(1);
            plot(xones,yones,'bo');
            ones=ones+1;
        end;
%take into account the extra "one" when finishing due to return key
%- kludge, but it works
    ones=ones-1;
    disp('Left mouse button picks boundary points.')
```

```
    disp('Hit return to finish')
    but=1;
        while ~isempty(but)
            [xhalves,yhalves,but] = ginput(1);
            plot(xhalves,yhalves,'b+');
        end
%take into account the extra "half" when finishing due to return key
% - kludge, but it works
    halves=halves-1;
    point_count_percentage=(ones+halves/2)/(point_root)^2;
    percentage=point_count_percentage(1)*100
```

D.2 GRAIN SIZE MEASUREMENT

```
% grain_count.m
% Overlays concentric circles on a metallographic image to allow a
% manual count of grain boundaries using the Heyn (Intercept) method.
% Requires an image with a clear micron marker.
% May require functions from the image analysis toolbox
% Author: Matt Smillie Version 040327
    clear all;
    clc;
    clf;
% Read the image
    cd('c:\image_path\');
    dir *.bmp;
    current_image=input('Enter file name to analyse>> ','s');
    image=imread(current_image);
    [image,imagemap]=rgb2ind(image,256);
    image=flipud(image);
    image_size=size(image);
% Size the circles
% Relative sizes
    big=79.58;
    mid=53.05;
    small=26.53;
% Scale to image in pixels
    diameter_big=min(image_size)-0.1*min(image_size);
    diameter_med=diameter_big*(mid/big);
    diameter_small=diameter_big*(small/big);
% plot circles on figure
    figure(1);
    axis off;
    hold on;
    colormap(imagemap);
    imagesc(image);
    axis image;
    centrex=max(image_size)/2;
    centrey=min(image_size)/2;
    r=[diameter_big,diameter_med,diameter_small]/2;
    N=256;
    t=(0:N)*2*pi/N;
```

```
        for n=1:length(r)
           plot( r(n)*cos(t)+centrex, r(n)*sin(t)+centrey);
        end
% Find the scale of the image from the micron marker
    disp('Pick ends of micron marker');
    [markerx,markery]=ginput(2);
    marker_pixel_length=sqrt((markerx(2)-markerx(1))^2
        +((markery(2)-markery(1)))^2);
    marker_micron_length=input('Enter length of marker in microns >> ');
    pixels_per_mm=1000*marker_pixel_length/marker_micron_length
% Initialise the counts.
    but=1;
    ones=0;
    halves=0;
    triples=0;
% Loop, picking up the points.
    disp('Left mouse button picks single intercepts')
    disp('Hit return to finish')
        while ~isempty(but)
            [xones,yones,but] = ginput(1);
            plot(xones,yones,'yo');
            ones=ones+1;
        end
%take into account the extra "one" when finishing due to return key
%- kludge, but it works
    ones=ones-1;
    disp('Left mouse button picks triple points.')
    disp('Hit return to finish')
    but=1;
        while ~isempty(but)
            [xtriples,ytriples,but] = ginput(1);
            plot(xtriples,ytriples,'g^');
            triples=triples+1;
        end
%take into account the extra "half" when finishing due to return key
%- kludge, but it works
triples=triples-1;
disp('Left mouse button picks tangent points.')
disp('Hit return to finish')
but=1;
    while ~isempty(but)
```

```
        [xhalves,yhalves,but] = ginput(1);
        plot(xhalves,yhalves,'r+');
        halves=halves+1;
    end;
%take into account the extra "half" when finishing due to return key
%- kludge, but it works
    halves=halves-1;
% Find number of intersections divided by line length
    sum_points=ones+triples*1.5+halves*.5
% Total length in pixels
    line_length=pi*(diameter_big+diameter_med+diameter_small);
% Find points per length in pixels and scale to mm
    Pl=sum_points/line_length; %Points per pixel
    Pl=Pl*pixels_per_mm; %Points per mm
% Lineal intercept, in mm
    L3=1/Pl;
% ASTM grain size
    G=-6.646*log10(L3)-3.298
% Save data.  Format is: Date.time Filename Count Pl L3 "ASTM Grain Size"
    save_data=input('Accept these results? y/n?','s');
        if strcmp(save_data,'y') | strcmp(save_data,'Y') ;
            dateid=datestr(now,21);
            fileid=current_image;
            fid = fopen('grain_size.dat','a');
            fprintf(fid,'%24s %20s %7.1f %7.1f %7.3f %7.2f\n'
                ,dateid,fileid,sum_points,Pl,L3,G);
            fclose(fid);
            disp('Data saved');
        end;
```

D.3 CURVE FITTING ANALYSIS

D.3.1 Automated Bimodal Analysis

D.3.1.1 Image-histogram.m

```
% image_histogram.m
% A function to fit a greyscale image to two normal populations
% Uses the least squares non-linear optimisation function, LSQNONLIN
% found in the Matlab Optimisation toolbox.
% Uses matts_curve_fit.m as the model function
% Author: Matt Smillie Version: 010427
%
%Read in and display the image.
    cd('c:\image_path')
    current_image='image_file.bmp';
    image_matrix=imread(current_image);
    image_values=linspace(1,256,256);
% Fitting PDF of two normal populations (Bimodal Distrubution) to
% experimental data
% Obtain the distribution information from the grayscale values.
% Need to change from uint8 to double (+1 offset) and change from
% matrix to vector of values - (:)
    [n,xout]=hist(double(image_matrix(:))+1,image_values);
% Convert Y values to a percentage probability to allow comparison
% to the PDF
    percent_n=n/sum(n);
    X=xout;
    Y=percent_n;
% Set up the initial conditions.
% The final result is very sensitive to the initial conditions.
% Let us try fitting a smoothed spline and using differentiation
% to find the local max and mins.
    epsilon=max(diff(X))^3/16;  % Tolerance function, from Spline
                                % Toolbox docs
    spline_approx=csaps(X,Y,1/(1+epsilon*10000));
    spline_data=fnval(spline_approx,X);
% Working, groovy.
    dsdx_data=gradient(spline_data);% The (approx) first
                                    %derivative of the spline
    dsdxdsdx_data=gradient(dsdx_data);  % The (approx) second
```

```
                                        % derivative of the spline
%figure(2);
%plot(X,Y,'.',X,spline_data,X,dsdx_data*10,X,dsdxdsdx_data*30);
%grid on;
%axis tight;
% Finding the points at which the derivative of spline_approx intercepts
% the x-axis.  Checks for a change in sign of the data.
    intercepts=[];
    num_intercepts=0;
        for i=1:(length(dsdx_data)-1);
% Checking for a change in sign, and if so, storing the x value
            if (dsdx_data(i)>0 & dsdx_data(i+1)<0)
                | (dsdx_data(i)<0 & dsdx_data(i+1) > 0);
                    num_intercepts=num_intercepts+1;
                    intercepts(num_intercepts)
                        =find(dsdx_data==dsdx_data(i));
            end;
        end;
% Now, to check those intercepts are maxima.
    maxes=[];
    num_maxes=0;
        for i=1:length(intercepts);
            if dsdxdsdx_data(intercepts(i))<0;
                    num_maxes=num_maxes+1;
                    maxes(num_maxes)=intercepts(i);
            end;
        end;
% We are only interested in the largest two maxima
% - others may be artifacts of the spline approximation.
    two_max=sort(Y(maxes));
    two_max=fliplr(two_max);
    initialA=find(Y==two_max(1)); % The biggest maximum
    initialB=10; % Just a guess.  Still sensitive to this
    initialC=find(Y==two_max(2)); % The next biggest maximum
    initialD=10; % Just a guess.  Still sensitive to this
% Initial value of 'p' can be calculated from mean and initial conditions
    initialp=abs((mean(double(image_matrix(:))+1)
        -initialC)/(initialA-initialC));
% Initial condition coefficients matrix
    X0=[initialA initialB initialC initialD initialp];
    options=optimset('Largescale','on');
```

```
% Set the limits on the coefficients;
% LB - lower bounds
% UB - upper bounds
    LB=[ 1 1 1 1 0];
    UB=[ 256 50 256 50 1];
% Call the least squares non-linear solver, using 'matts_curve_fit.m',
% which returns the difference between the theoretical PDF and the
% experimental values, Y, along X, 1 to 256.
    xinitial=lsqnonlin('matts_curve_fit',X0,LB,UB,options,X,Y);
% I am considering using an interation at this point, by entering in
% the just obtained values for the co-efficients back into the
% non-linear solver, until the coeffcients match
% to within, say, 2 d.p.
    x=lsqnonlin('matts_curve_fit',xinitial,LB,UB,options,X,Y);
% Plot the fitted PDF against the measured data.
    fitted_PDF = (x(5)/(x(2)*sqrt(2*pi)))*exp(-0.5*((X-x(1))/x(2)).^2)
        + ((1-x(5))/(x(4)*sqrt(2*pi)))*exp(-0.5*((X-x(3))/x(4)).^2);
% Can now find the threshold - minimum between the two means, given
%by x(1) and x(3)
    threshold=find(fitted_PDF ==
        min(fitted_PDF(round(x(1)):round(x(3)))));
    p=1-x(5)
    threshold_p_data=sum(n(threshold:end))/sum(n)
    threshold_p_fittedPDF=sum(fitted_PDF(threshold:end))/sum(fitted_PDF)
% Output the results
    figure(1);
    plot(xout,percent_n,'+',X,fitted_PDF,'-r','LineWidth',1);
        hl=legend('Actual count','Theoretical PDF',2);
        LEG = findobj(hl,'type','text');
        set(LEG,'FontName','cmr10')
        label1(1)={['\mu = ',int2str(x(1))]};
        label1(2)={['\sigma = ',int2str(x(2))]};
        label1(3)={['p = ',int2str(x(5)*100),'%']};
        label2(1)={['\mu = ',int2str(x(3))]};
        label2(2)={['\sigma = ',int2str(x(4))]};
        label2(3)={['p = ',int2str((1-x(5))*100),'%']};
        text(round(x(1)*1.15),fitted_PDF(round(x(1)))
            ,label1,'FontName','cmr10');
        text(round(x(3)*1.15),fitted_PDF(round(x(3)))
            ,label2,'FontName','cmr10');
        box off;
```

```
        axis([0 255 0 Inf])
        ht=title('Grayscale image distribution.','FontName','cmr10');
        hx=xlabel('8 bit grey scale value. 0 = black
            , 255 = white.','FontName','cmr10');
        hy=ylabel('Pixel count percentage','FontName','cmr10');
% Now, to save the figure in an .eps file - making sure we add on the
% right extension. Messy, but safe!
    cd('c:\image_path\results\');
    current_image=strcat(current_image,'.eps');
    print('-depsc','-tiff',current_image);
```

D.3.1.2 Matts-curve-fit.m model function

```
function diff = matts_curve_fit(x,X,Y)
        % This function is called by lsqnonlin.
        % x is a vector which contains the coefficients of the
        % equation.  X and Y are the option data sets that were
        % passed to lsqnonlin.
        A=x(1);
        B=x(2);
        C=x(3);
        D=x(4);
        p=x(5);
        diff = ((p/(B*sqrt(2*pi)))*exp(-0.5*((X-A)/B).^2)
            + ((1-p)/(D*sqrt(2*pi)))*exp(-0.5*((X-C)/D).^2)) - Y;
```

D.3.2 Semi-automated Multi-peak Analysis

D.3.2.1 Multi-histogram.m

```
% multi_histogram.m
% Analyse a multi-peak greyscale .bmp - for 3 or more phases
% Uses multimodefn.m as the model function - Written by Andrew Lintott
% Uses bfgs.m as solver rountine - Written by Ian Coope
%                                  altered by Andrew Lintott
%
% Version 040405 Author: Matt Smillie, portions Andrew Lintott
    clear all;
    close all;
    clc;
    clf;
% Semi-automatiicaly batch process the files.  Commented code below
% manually selects the files
% Read the image
    %   cd('c:\users\matt\matlab\image_analysis\hv\samples\');
    %   dir *.*;
    %   current_image=input('Enter file name to analyse >> ','s');
cd('c:\image_path\');
files = dir('c:\image_path\*.bmp');
for file = 1:size(files);
    current_image=files(file).name
    image=imread(current_image);
    colormap(gray);
    figure(1);
    imagesc(image);
    radius=ceil(size(image)*0.005);
    filter=input('Filter image? Y/N >> ','s');
        if strcmp(filter,'y') | strcmp(filter,'Y') ;
             image=medfilt2(image,radius);
             imagesc(image);
        end;
    figure(2);
    hold on;
    image_values=linspace(1,256,256);
% Fitting PDF of populations to experimental data
% Obtain the distribution information from the grayscale values.
% Need to change from uint8 to double (+1 offset) and change from
% matrix to vector of values - (:)
```

```
    [n,xout]=hist(double(image(:))+1,image_values);
% Convert Y values to a percentage probability to allow comparison
% to the PDF
    percent_n=n/sum(n);
    X=xout;
    Y=percent_n;
% Set up the initial conditions.
% The final result is very sensitive to the initial conditions.
% Manually pick peaks - allows selection of number of peaks as
% well to allow the analysis
% of more than two phases.
    plot(xout,percent_n,'+');
    box off;
    axis([0 255 0 Inf])
% Manually select the data peaks
    disp('Left mouse button picks approximate data peaks')
    xypeaks = [];
    n = 0;
% Loop, picking up the points.
    disp('Right mouse button picks last point.')
    but = 1;
        while but == 1
            [xpeaks,ypeaks,but] = ginput(1);
            plot(xpeaks,ypeaks,'ro')
            n = n+1;
            xypeaks(:,n) = [xpeaks;ypeaks];
        end
    [m,n]=size(xypeaks);
    xpeaks=xypeaks(1,1:n);
% Entering the data into Andrew Lintotts general case bfgs solver.
% Initial is the estimated initial conditions from the picked data peaks.
    initial=[];
    j=1;
        for i=1:length(xpeaks);
            initial(j)=xpeaks(i);
            initial(j+1)=1;
            initial(j+2)=1/length(xpeaks);
            j=j+3;
        end;
% Calling the solver
    opt=bfgs;
```

```
    [xmin fmin]=bfgs('multimodefn',initial',opt,X,Y);
% Evaluate model using cost function
    [dum dum Model]=multimodefn(xmin,X,Y);
% Estimate sigma_k, the variance of the Gaussian noise
    plot(X,Model,'r');
% Parameters displayed as a vector made up of:
% mean1 sigma1 p1 mean2 sigma2 p2 ... meani sigmai pi
    disp('Estimated parameters')
    disp(xmin')
    remainder=0;
    if length(xpeaks)==1;
        disp('Estimated Silicon Remainder')
        remainder=sum(percent_n)-sum(Model);
        disp(remainder)
    end;
% Getting percentages from the model, rather than the data
    k=1:(length(xmin)/3);
    p_total=sum(xmin(k*3));
% Output the results
    hold off;
    clf;
    plot(xout,percent_n,'+',X,Model,'-r','LineWidth',1);
        hl=legend('Actual count','Theoretical PDF',2);
        LEG = findobj(hl,'type','text');
        set(LEG,'FontName','cmr10')
            for j=1:3:length(xmin);
                labelj(1)={['\mu = ',int2str(xmin(j))]};
                labelj(2)={['\sigma = ',int2str(xmin(j+1))]};
                labelj(3)={['p = ',int2str((xmin(j+2)/p_total)*100),'%']};
                text(round(xmin(j)*1.15),
                    Model(round(xmin(j))),labelj,'FontName','cmr10');
            end;
        box off;
        axis([0 255 0 Inf])
        ht=title('Grayscale image distribution.','FontName','cmr10');
        hx=xlabel('8 bit grey scale value. 0 = black
            ,255 = white.','FontName','cmr10');
        hy=ylabel('Pixel count percentage','FontName','cmr10');

% Now, to save the figure in an .eps file - making sure we add on
% the right extension. Messy, but safe!
```

```
    cd('c:\image_path\');
    current_image=strcat(current_image,'.eps');
    print('-depsc','-tiff',current_image);
    picture=strcat(current_image,'.eps');
    print('-depsc','-tiff',picture);
    %And finally, save the data.
    save_data=input('Accept these results? y/n?','s');
    if strcmp(save_data,'y') | strcmp(save_data,'Y') ;
        dateid=datestr(now,21);
        fileid=current_image;
        fid = fopen('phase_count.dat','at');
        points=length(xmin)/3;
        fprintf(fid,'\n %24s %20s %2f %2f %2f %2f %2f %2f %2f %2f'
            ,dateid,fileid,points,xmin,remainder);
        fclose(fid);
        disp('Data saved');
    end;
    clc;
    hold off;
    clf;
    clear n xout percent_n X Y;
    disp('Next image')
end;
```

D.3.2.2 Multimodefn.m Model Function

```
unction [f,J,F]=multimodefn(a,x,dat)
% Function: [f,J,F]=multimodefn(a,x,dat)
%
% Purpose:  Evaluates cost function for BFGS minimiser.
%
% Arguments:
%   a       Trial model parameters [mu1 sig1 A1 mu2 sig2 A2]'
%   x       Values of the abscissa of the distribution.
%   dat     Ordinates of the distribution.
%
% Returns:
%   f       The cost function sum(dat-F) where F is the model.
%   J       The Jacobian of the cost function. A 1x3n matrix where n is
%           the number of peaks in the model.
%   F       F the value of the model over x.
n=length(a)/3;
F=zeros(size(x));
J=zeros(3*n,length(x));
for i=1:n,
  mu=a(3*i-2);
  sig=a(3*i-1);
  A=a(3*i);
  v=x-mu;
  e=exp(-0.5*v.*v/(sig*sig));
  F=F+A/sig*e;
  if nargout>1,
    dmu=A/(sig*sig*sig)*v.*e;
    dsig=A*((v.*v-sig*sig)/(sig^4)).*e;
    dA=e/sig;
    J(i*3-2:i*3,:)=[dmu; dsig; dA];
  end
end
F=F/sqrt(2*pi);
dF=F-dat;
J=J*dF(:)/sqrt(2*pi);
f=dF*dF'/2;
```

D.3.3 BFGS.m Solver Routine

```
function   [xmin,fmin,itn,H] = bfgs(fg,x0,opt,varargin)
% Function: [xmin fmin itn H]=bfgs(fg,x0,opt,a,b,c...)
%
% Purpose:  Performs unconstrained minimization by a quasi-Newton
%           method using the BFGS updating formula and Wolfe conditions
%           line search.
%           If f(x) appears to be unbounded below or if the gradient
%           appears to have been mis-programmed a diagnostic is displayed.
%
% Arguments:
%   fg      Name of function to minimise. fg returns function and
%           gradient values.
%   x0      Starting point for minimisation.
%   opt     Various options to control the minimisation.
%     .acc  Accuracy parameter. A return is made when the condition
%           norm(g)<=acc. [1e-6]
%     .maxit Maximum number of iterations. [inf]
%     .c1   Wolfe condition parameter 1. [0.01]
%     .c2   Wolfe condition parameter 2. [0.9]
%     .H    Starting Hessian. [empty]
%     .verbose Prints out progress information if 1. [0]
%
% Returns:
%   xmin    Solution.
%   fmin    Function value at solution.
%   itn     Number of iterations required for solution.
%   H       Approximate inverse Hessian at the solution.
%
% Usage:    opt=bfgs;
%           [xmin,fmin]=bfgs('func',[0 0]',opt);
%
%           Minimizes 'f' from starting point [0 0]'. 'func' is the name
%           of a function that returns the function value and gradient
%           defined as
%           function [f,g]=func(x,a,b,c)
%
%           Try the following example:
%           [xmin,fmin] = bfgs('rosenfg',[-1.2;1])
%
% Author:  I.D. Coope, 19/2/91 altered by A Lintott (2000)
```

```
if nargin==0,
  xmin=struct(...
          'acc',1e-6,...
          'maxit',inf,...
          'c1',0.01,...
          'c2',0.9,...
          'H',[],...
          'verbose',0);
  return
end

x0 = x0(:); n=length(x0);
if isempty(opt.H),
  H=eye(n);
else
  H=opt.H;
end
if opt.c2<opt.c1 | opt.c2>=1 | opt.c1<=0,
  error('0 < c1 < c2 < 1, is required.');
end
itn=0;
[f0,g0]=feval(fg,x0,varargin{:}); nf=1; xmin=x0; fmin=f0;

while  norm(g0)>opt.acc,
  p = -H*g0; pg=p'*g0;
  if ~p, break; end    % zero gradient/search direction
  if pg>=0, break; end % must be rounding errors
  if pg>=-10*eps*abs(f0), break; end
  itn = itn + 1;
  normp=norm(p); normx=norm(x0); scale=1+normx;
  if normp>scale, step=scale/normp; else step=1; end
  l=0; u=-1;
  while step*normp>100*eps*normx,  % Wolfe condition line search
    xmin = x0 + step*p;
    % disp(sprintf('l=%g u=%g step=%g pg=%g',l,u,step,pg))
    [fmin,gmin] = feval(fg,xmin,varargin{:}); nf=nf+1;
    pgmin=p'*gmin;
    if  fmin > f0 + opt.c1*step*pg  % | pgmin> -c2*pg,
       u=step;  l=0;
    elseif pgmin<opt.c2*pg,
       l=step;
```

```
    else
       break;
    end
    if u<0, step=4*step;
    else
       step=(l+u)/2; if step<=l | step >=u, break; end
    end
  end
  if f0==fmin, break, end % Line search failed
  y=gmin-g0;  s=xmin-x0;  sy=s'*y;
  if sy>0, r=s-H*y; s=s/sy; H = H + ((r*s'+s*r') - ((r'*y)*s)*s'); end
  if opt.verbose>=1,
     str=sprintf('%4.0f BFGS: nf=%d\tf=%g\tstep=%g',itn,nf,fmin,step);
     disp(str)
  end
  if itn >= opt.maxit,
    if opt.verbose>=1, disp('BFGS: too many iterations!'); end
    break;
  end
  x0=xmin; f0=fmin; g0=gmin;
end

itn=[itn,nf];
```